Spring 5-1-2019

Parametric Amplification Study and Applications in Millimeter-Wave Transmitters

Sherry Huang
Southern Methodist University, sxhuang@smu.edu

PARAMETRIC AMPLIFICATION STUDY AND APPLICATIONS IN MILLIMETER-WAVE TRANSMITTERS

Approved by:

_____

Prof. Ping Gui
Professor of Electrical Engineering

_____

Prof. Mitchell Thornton
Professor of Electrical Engineering

_____

Prof. Jennifer Dworak
Associate Professor of Computer Science

_____

Prof. Joseph Camp
Associate Professor of Electrical Engineering

_____

Prof. Theodore Manikas
Clinical Professor of Computer Science

PARAMETRIC AMPLIFICATION STUDY

AND APPLICATIONS TO MILLIMETER-WAVE TRANSMITTERS

A Dissertation Presented to the Graduate Faculty of

Lyle School of Engineering

Southern Methodist University

in

Partial Fulfillment of the Requirements

for the degree of

Doctor of Philosophy

with a

Major in Electrical Engineering

by

Sherry Huang

May 18th, 2019

ACKNOWLEDGMENTS

I would like to thank Prof. Gui for the constant guidance and support throughout this work. I'm also forever grateful to my family for being so patient with me and my friends for supporting me.

Sherry Huang Ph.D., Electrical Engineering, Southern Methodist University, Dallas, 2019

Parametric Amplification Study
and Applications in Millimeter-wave Transmitters

Advisor: Professor Ping Gui

Doctor of Philosophy conferred: May 18th, 2019

Dissertation completed: May 18th, 2019

In wireless communication systems, the millimeter-wave frequency band has been gaining more interests recently, mainly due to its wide bandwidth and ability to support high data-rate. However, challenges come with the advantages. To transmit and receive complexed data, the quadrature amplitude modulation (QAM) scheme paired with orthogonal frequency-division multiplexing (OFDM) is used most commonly. In transmitter designs of such modulation schemes and frequency access schemes, two important requirements are high linearity and high efficiency. The building blocks of transmitters include power amplifiers (PA) and mixers. Nevertheless, traditional design techniques exhibit trade-offs between linearity and efficiency for PAs, and between conversion gain and linearity for mixers.

The nonlinear varactor-based parametric amplification theory can be applied to PA designs to improve both linearity and efficiency. Parametric amplification requires a pump waveform whose frequency is twice the operation frequency of the output waveform of the PA. The theory of parametric amplification is also applied to construct non-linear transmission lines, which is applied to mixer designs to improve both conversion gain and linearity.

The proposed PAs and mixers are designed and compared with conventional designs. For the PA, both power-added efficiency (PAE) and linearity are improved. For the mixer, both conversion gain and linearity are improved, and noise figure is lowered.

Previously, the theory of parametric amplification has been applied only to lower-frequency circuits, mainly due to the difficulty to generate a required pump signal, whose frequency needs to be twice of the signal frequency, at higher frequency ranges, such as the millimeter-wave (mm-Wave) frequency bands. This work demonstrates the feasibility of applying parametric amplification to circuits at mm-Wave frequency. In the PA design of this work, the pump is extracted from the second harmonic tone of the PA itself. As a result, the design complexity is simplified, the circuit area and DC power consumption are saved.

TABLE OF CONTENTS

LIST OF FIGURES

LIST OF TABLES

This is dedicated to my parents.

CHAPTER 1: WIRELESS COMMUNICATION

1.1 Introduction

In the electromagnetic spectrum, each frequency range is allocated to some certain applications. Figure 1 below [11] gives some examples. AM radio uses the frequency range from 600 kHz to 1.6 MHz. TV broadcast is from 54 to 700 MHz. Mobile phones are from 900 MHz to 2.4 GHz. Bluetooth technology is 2.45 GHz.

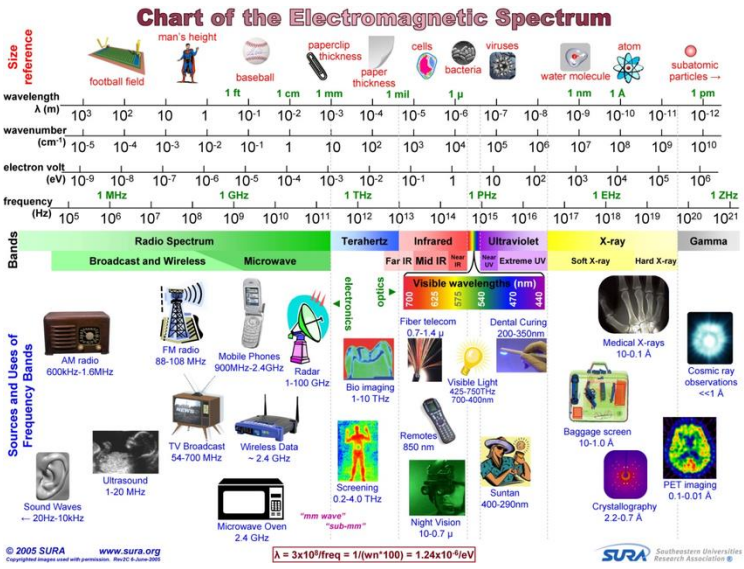

Figure 1. Examples of applications in various frequency bands.

As technologies are constantly developing, this spectrum is getting more and more crowded. For wireless communication systems, higher level modulation schemes (such as QPSK, 16-QAM, 64-QAM, 256-QAM, etc.) and multiple access schemes (FDMA, TDMA, CDMA, and OFDMA) are used to improve the spectrum efficiency.

Among these complex communication systems, OFDM paired with the QAM modulation, by far, is most popular due to the highest spectrum efficiency, but at a price of higher system complicity, latency, and cost [1]. One way to further increase the communication system throughput is to continue increasing modulation and multiplex levels. Nevertheless, given existing crowed multi-standard and multi-band scenario, there is limited room to improve system performance due to technologies and device performance limitations.

Another way is to explore higher frequencies, e.g., the RF bands and mm-Wave bands. Mm-Wave provides huge potential in Giga-bit communications and high-resolution sensing systems due to its wide spectrum (30 – 300 GHz). The demand for increasing data rate in wireless communication applications makes mm-Wave systems attractive due to their ability to accommodate wide bandwidths, high antenna array gain, and small form factor. Figure 2 shows some of these applications [12].

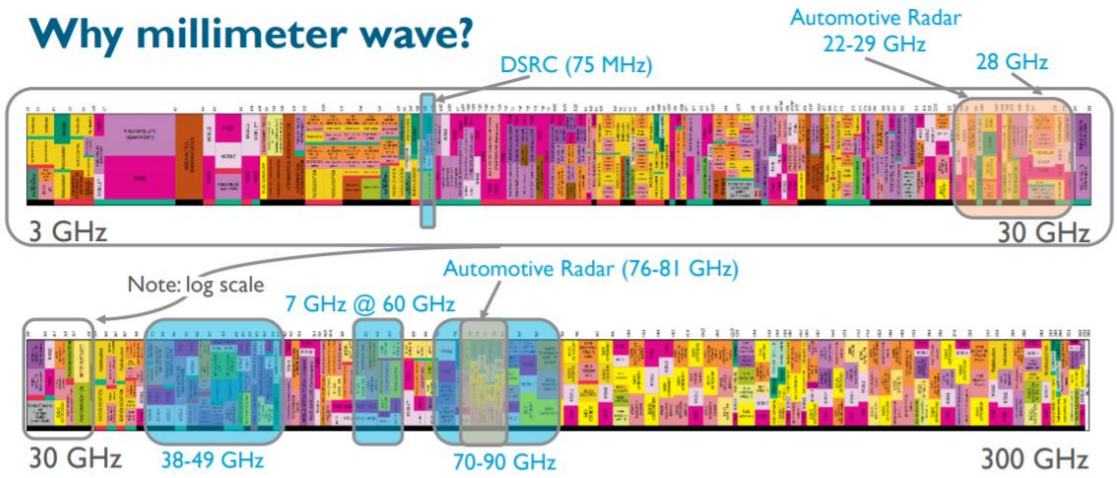

Figure 2. Application examples in RF and mm-Wave frequencies

The unlicensed band around 60 GHz, from 57 to 64 GHz provides Gbps data rate for short-distance data communication applications, and the FCC and industries are considering add another 7 GHz to this band to cover entire contiguous 14 GHz from 57 to 71 GHz. Communication protocols in this 60-GHz band include WiGig and WirelessHD. WiGig is a commercial name of the IEEE 802.11ad protocol. It utilizes the 60 GHz band from 57 to 64 GHz, and it can support a data rate up to 7 Gbps. WirelessHD specification utilized this 57-to-64 GHz band too. It is mainly used to transmit high-definition videos to consumer electronics products. It can stream uncompressed video (and related audio) up to 1080p 24-bit color at a 60-Hz refresh rate [13].

Figure 3 [14] shows that attenuation of mm-Wave signals in the atmosphere by oxygen and water. The top curve is at sea level and the lower curve is at an altitude of 9150 meters. The space we live is between these two altitudes. As can be seen, the attenuation around 60 GHz is especially high. This imposes difficulties in designing wireless communication systems around this frequency. The gain needs to be high enough to compensate this attenuation.

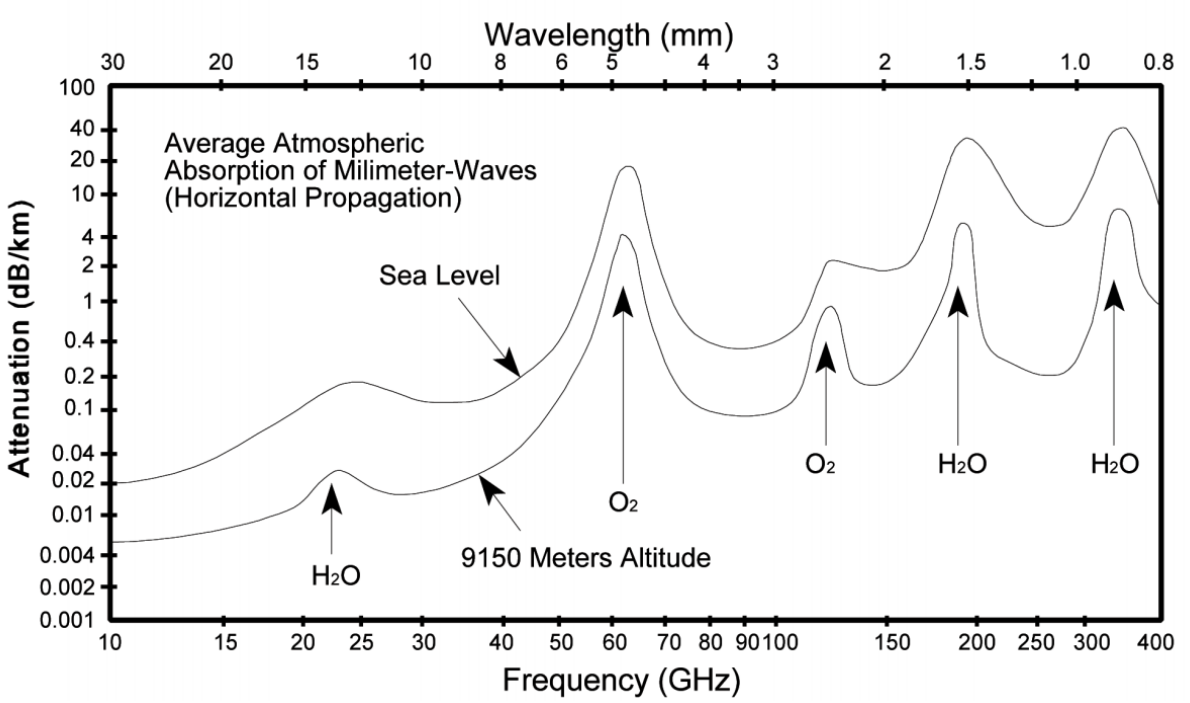

Figure 3. Attenuation of signals in the atmosphere by oxygen and water

Other popular millimeter wave bands are generally licensed [15]. The 71-to-76-GHz and 81-to-86-GHz bands are designated to point-to-point wireless communications, with the 71-76-GHz band for down-conversion and 81-to-86-GHz band for up-conversion. The 76-to-81-GHz band is designated to long-range radar applications. Recently, automotive radars have been developing in this band. The 94 and 140 GHz bands are designated for mm-Wave imaging applications.

1.2 CMOS mm-Wave Circuits

The mm-wave range was not popular previously, especially before the year of 2000. The main reason is that the technology at that time was not ready. III-V semiconductors were used to design circuitry at such high frequencies. These types of semiconductors mainly include GaAs, InP, GaN,

and GaP. Then SiGe semiconductor was introduced. These two generations of semiconductors are expensive, and thus are not good for massive production.

Since early 2000, advanced super-scaled CMOS technologies started to provide a new trend of mm-wave applications due to transistor speed, ubiquitous applications, and cost effectiveness of CMOS [2]. More importantly, CMOS RF front-ends can be integrated with digital CMOS circuitries for high integration level applications, for example, system-on-chip (SoC).

However, most of CMOS processes are optimized for low power digital circuit designs operated at low voltage supply (0.9V or lower) [3], which significantly limits the power handling capability and linearity of CMOS devices. Particularly, the low breakdown voltage of digitally oriented CMOS processes limits the output power, efficiency, and linearity of CMOS power amplifiers (PA), one of the critical building blocks in wireless transceivers. In addition, low voltage operation of CMOS considerably lowers its signal headroom, which in turn limits the PA's linearity[4]. For OFDM systems with high peak-to-average-ratio (PAPR) and other high-level modulation systems, high linearity is important [5].

Figure 4 [16] shows the comparison of output power and efficiency of a group of narrow band PAs designed in InP, GaAs, SiGe, GaN, and CMOS processes. Unfortunately, the PA designed in CMOS process has the lowest output power and the lowest efficiency. This is mainly due to the lossy substrate of silicon in CMOS process. In many scenarios, it is important to improve the power efficiency to save power.

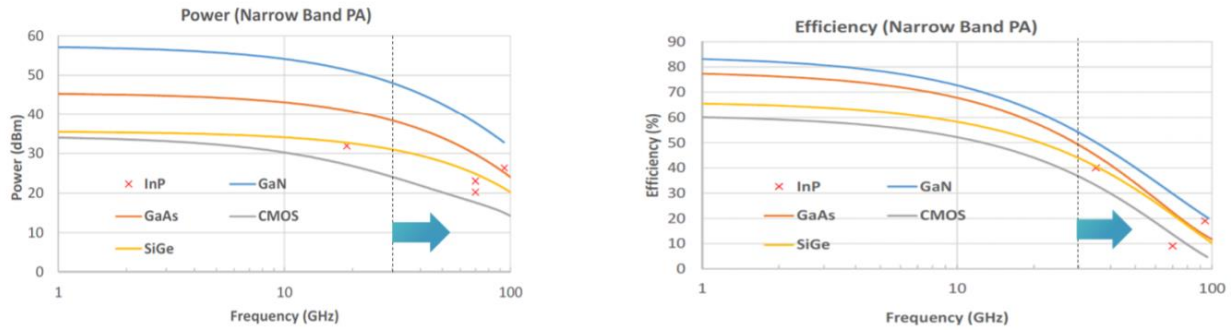

Figure 4. Comparison of power and efficiency among different processes

This work focuses on the wireless communication applications. Figure 5 below is a simple block diagram of a direct-conversion transceiver in wireless communication. The top part is called a receiver. It receives wireless signal through an antenna and transmits it to the digital baseband for signal processing. The bottom part is called a transmitter. It transmits a processed signal to an antenna to be propagated.

The power amplifier design is the main subject of study of this work. Mixer design is also explored.

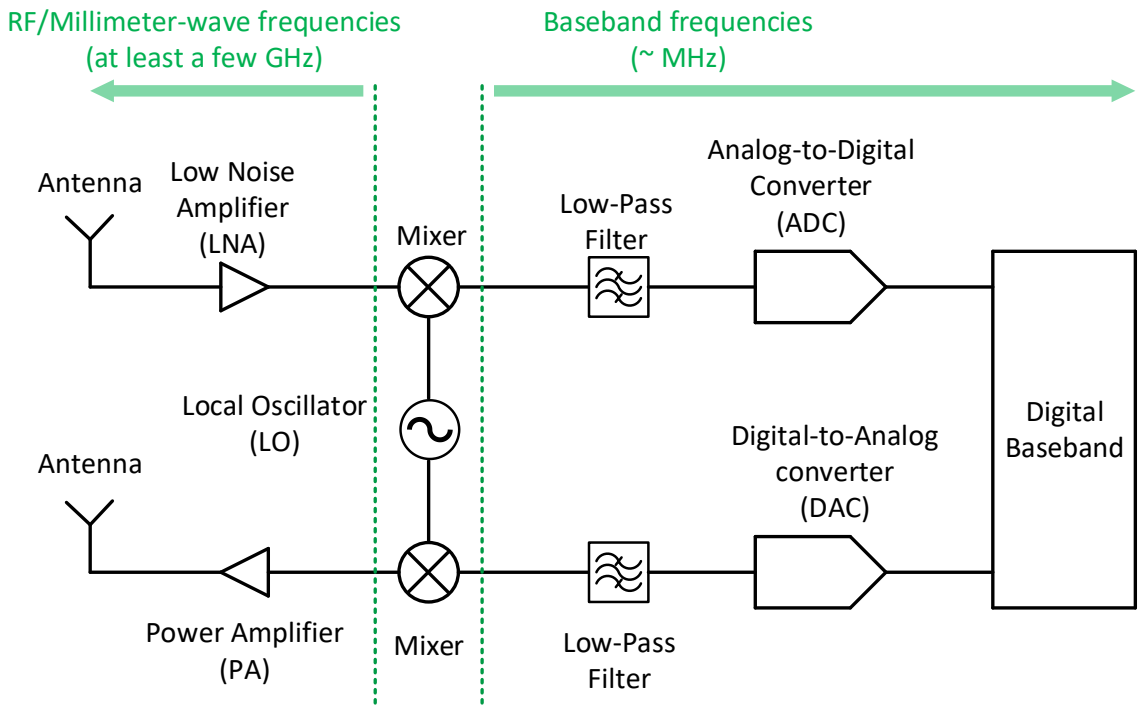

Figure 5. Block diagram of a typical direct-conversion wireless communication system

CHAPTER 2: POWER AMPLIFIERS

A power amplifier (PA) is an amplifier that is designed to deliver the maximum power output or maximum of power efficiency for a given selection of active device.

2.1 Background

In this section, basic concepts of power amplifiers [17] are explained.

P_{IN}: the input power of a PA. It is usually measured in dBm.

P_{OUT}: the output power of a PA. It is usually measured in dBm.

P_{DC}: the DC power supply needed for a PA to function. It is usually measured in dBm.

Power gain: the difference between input power and output power. It is usually measured in dB.

Efficiency (η): power efficiency, or simply efficiency. As shown in Equation (2.1) below, it is defined as the amount of power delivered to the load divided by the amount of DC power drawn from supply.

$$\eta = \frac{P_{OUT}}{P_{DC}} \tag{2.1}$$

PAE: power-added efficiency of a power amplifier. It is used to characterize if how efficiently the PA uses the DC power supplies to amplify its input signal. It can be calculated by the following equation:

$$PAE = \frac{P_{OUT} - P_{IN}}{P_{DC}} \tag{2.2}$$

P_{SAT}: the saturated output power of a PA. As the input power levels increases, the power gain drops. As a result, the output power increases more slowly, and it eventually saturates at a fixed power level. This fixed power level is the saturated power, which is abbreviated as P_{SAT}.

Linearity: in power amplifier design, the linearity measures the ability of the PA to amplify a range of input power levels. The criteria that characterize the linearity of a PA include gain compression points, intercept points, and intermodulation distortion.

If the input of a PA is a sinusoidal wave:

$$x(t) = A\cos\omega t \tag{2.3}$$

Where A is the amplitude and ω is the frequency, respectively, of the input waveform.

Ideally, if the PA is perfectly linear, then the output waveform should contain only the frequency component of ω. However, the transistors are nonlinear, causing the output waveform to have numerous frequency components. The output waveform is expressed as follows:

$$y(t) = \alpha_1 x(t) + \alpha_2 x^2(t) + \alpha_3 x^3(t) + \cdots \tag{2.4}$$

Substitute Equation. (2.3) into Equation (2.4):

$$y(t) = \frac{\alpha_2 A^2}{2} + \left(\alpha_1 A + \frac{3\alpha_3 A^3}{4}\right)\cos\omega t + \frac{\alpha_2 A^2}{2}\cos 2\omega t + \frac{\alpha_3 A^3}{4}\cos 3\omega t + \cdots \tag{2.5}$$

On the right-hand side of the Equation (2.5), the first term is the DC offset, which is caused by second-order nonlinearity. The second term is the fundamental tone, the third term is the second harmonic, the fourth term is the third harmonic, etc. As can be seen from Equation (2.5), the output waveform consists of a set of frequencies of DC, ω, 2ω, 3ω, etc. The output power is distributed

among these frequency components, but only the fundamental tone is desired. As the input power level increases, a larger amount of the output power is distributed among the frequency components other than the fundamental tone. Therefore, the gain of the fundamental tone drops. Typical plots of power gain vs. P_{IN} (left) and P_{OUT} vs. P_{IN} (right) are shown in Figure 6 below.

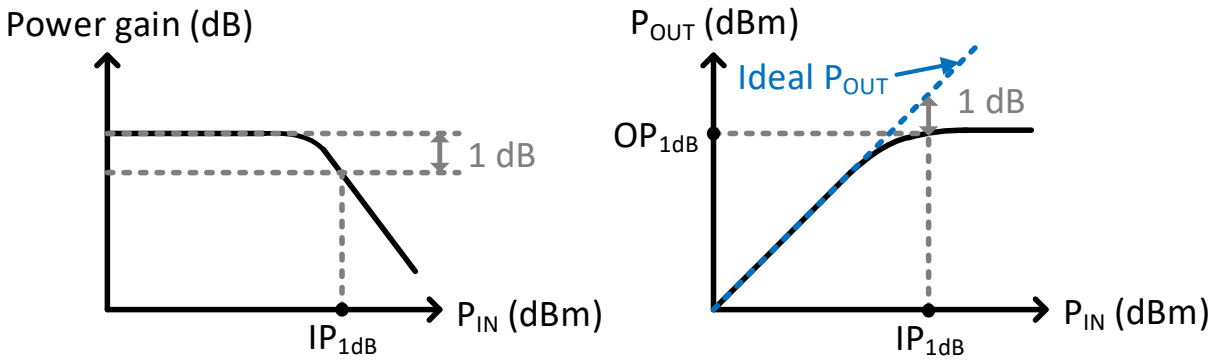

Figure 6. Typical plots of power gain and output power

Gain compression points: the points where the gain of the fundamental tone is compressed by certain dB from the ideal gain.

P_{1dB}: the gain compression point of 1 dB. The corresponding input power of this point is called **IP_{1dB}**, and the corresponding output of this point is called **OP_{1dB}**. The higher the IP_{1dB}, the better the linearity.

Among the all the harmonics, the third harmonic is of the most interest. For power amplifier designs, most designs are differential, which can cancel out the even harmonics at the output. For odd harmonics, the 3rd harmonic has the highest power and can degrade the performance of the entire transmitter. The power levels of higher odd harmonics are much lower and thus have

negligible effects on the performance of the transmitter. A typical plot of the fundamental tone and the 3rd harmonic of the output power vs. input power is shown below in Figure 7.

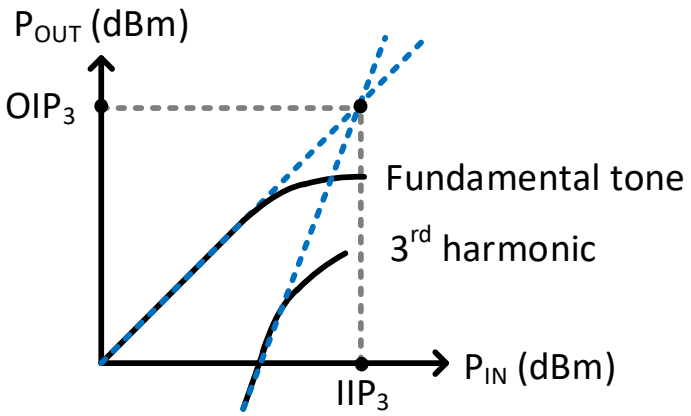

Figure 7. Typical plot of the fundamental tone and the 3rd harmonic of the output power

The gain of both the fundamental tone and the 3rd harmonic drops as input power increases.

Intercept point: the extrapolated point where the harmonic intercepts the fundamental tone.

IP_3: the extrapolated point where the 3rd harmonic intercepts the fundamental tone. The corresponding input power level of this point is called **IIP_3**, and the corresponding output power level of this point is called **OIP_3**. The higher the IIP_3, the better the linearity.

Intermodulation distortion: When the input of a PA consists of two frequencies, the output spectrum of the PA consists of a broad range of the products of the two frequencies. These products are called intermodulation distortion.

If the input contains frequencies ω_1 and ω_2, it can be expressed as follows:

$$x(t) = E_1 \sin \omega_1 t + E_2 \sin \omega_2 t \qquad (2.6)$$

Where E_1 and E_2 are the amplitude of each frequency component, respectively.

Then the output can be expressed as follows:

$$y(t) = \alpha_1(E_1 \sin \omega_1 t + E_2 \sin \omega_2 t) + \alpha_2(E_1 \sin \omega_1 t + E_2 \sin \omega_2 t)^2 + \alpha_3(E_1 \sin \omega_1 t + E_2 \sin \omega_2 t)^3 + \cdots \quad (2.7)$$

Expand the second term on the right-hand side of Equation (2.7):

$$\alpha_2 x^2(t) = \frac{K_2\left({E_1}^2 + {E_2}^2\right)}{2} - \frac{K_2}{2}\left({E_1}^2 \cos 2\omega_1 t + {E_2}^2 \cos 2\omega_2 t\right) + 2K_2 E_1 E_2[\cos(\omega_1 - \omega_2)\, t - \cos(\omega_1 + \omega_2)\, t] \quad (2.8)$$

In Equation (2.8), the $2\omega_1$ and $2\omega_2$ components are second harmonics, and the $\omega_1 - \omega_2$ and $\omega_1 + \omega_2$ components are called **second order intermodulation**.

Expand the third term on the right-hand side of Equation (2.7):

$$\begin{aligned} \alpha_3 x^3(t) = \frac{3K_3}{4}\big({E_1}^3 \sin \omega_1 t + {E_2}^3 \sin \omega_2 t + 2{E_1}^2 E_2 \sin \omega_2 t \\ + 2{E_2}^2 E_1 \sin \omega_1 t\big) \\ + \frac{K_3 {E_2}^3}{4}\left({E_1}^3 \sin 3\omega_1 t + {E_2}^3 \sin 3\omega_2 t\right) \\ + \frac{3K_3 {E_1}^2 E_2}{2}\left[\sin(2\omega_1 - \omega_2)t - \frac{1}{2}\sin(2\omega_1 + \omega_2)t\right] \\ + \frac{3K_3 {E_2}^2 E_1}{2}\left[\sin(2\omega_2 - \omega_1)t - \frac{1}{2}\sin(2\omega_2 + \omega_1)t\right] \end{aligned} \quad (2.9)$$

In Equation (2.9), the $3\omega_1$ and $3\omega_2$ components are third harmonics, and the $2\omega_1 - \omega_2$, $2\omega_1 + \omega_2$, $2\omega_2 - \omega_1$, $2\omega_2 + \omega_1$ components are called **third order intermodulation**.

A plot of the output spectrum in frequency domain is shown below in Figure 8.

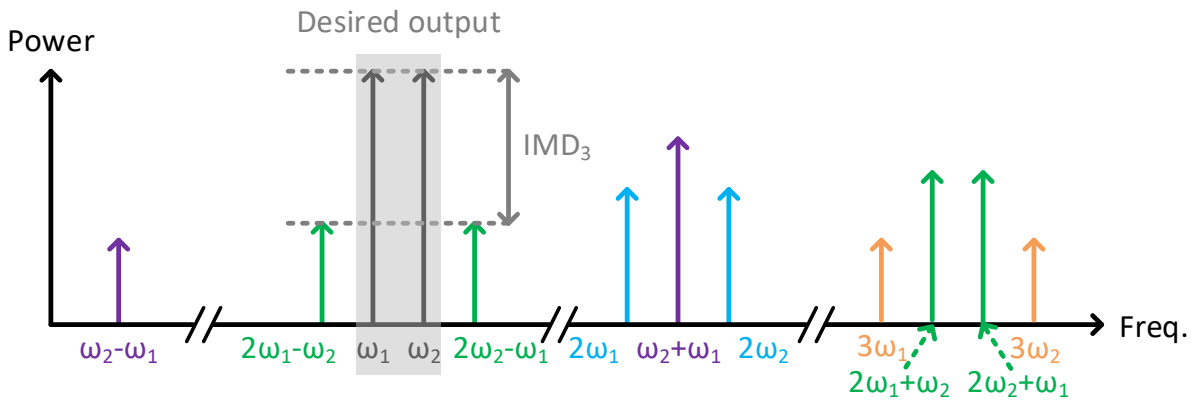

Figure 8. Output spectrum when the input has two frequency components

As shown in Figure 8, only the ω_1 and ω_2 components are the desired output components. Except the $2\omega_1 - \omega_2$ and $2\omega_2 - \omega_1$ components, all the other components are far away from the desired output, and thus can be easily filtered out through a bandpass filter. However, the $2\omega_1 - \omega_2$ and $2\omega_2 - \omega_1$ components are close to the desired output and are difficult to filter out. As a result, these two components affect the performance of the PA, and will affect the overall performance of the entire transmitter.

The difference of the power levels of the fundamental tone and the $2\omega_1 - \omega_2$ or $2\omega_2 - \omega_1$ components is called **IMD3**. The larger the IMD_3, the better the linearity.

AM-AM distortion and **AM-PM distortion**: the nonlinearity of PAs can also be shown through AM-AM distortion and AM-PM distortion. AM-AM distortion is the undesired modulation of amplitude in the output signal. It is measured in dB/dB. AM-PM distortion is the undesired modulation of phase in the output signal. It is measured in degree/dB.

If the input signal is expressed as:

$$v_{in}(t) = A(t)\cos[\omega t + \theta(t)] \tag{2.10}$$

And the output signal is expressed as:

$$v_{out}(t) = G[A(t)]\cos\{\omega t + \theta(t) + \psi[A(t)]\} \quad (2.11)$$

Then, $G[A(t)]$ is the AM-AM distortion curve and $\psi[A(t)]$ is the AM-PM distortion curve of the PA [19].

Constellation: in communication systems, the plot of possible symbols is called a constellation. More detailed explanations will be in Section 2.3.

Error vector magnitude (EVM): it measures how accurately the symbols are transmitted within its constellation. More detailed explanations will be in Section 2.3.

2.2 Amplifiers Classes

Amplifiers can be classified based on their circuit configuration and operating characteristics. Power amplifiers are classified into two basic categories: non-switching amplifiers and switching amplifiers [20].

The non-switching amplifiers are further categorized into different classes based on the conduction angle. For sinusoidal input signals, conduction angle means how much time the amplifier is turned on during one cycle, with a conduction angle of zero being completely turned off, and a conduction angle of 2π being completely turned on.

Table 1. Amplifier classes

Amplifier Classes	Conduction Angle
A	2π
AB	$(\pi, 2\pi)$
B	π
C	$(0, \pi)$

Switching amplifiers are non-linear. When operating, they are either fully turned on or fully turned off. The ideal efficiency of switching amplifiers is 100%.

2.2.1 Class-A Amplifiers

In a Class-A amplifier, the transistor is biased such that it is turned on for the entire cycle of each cycle of the input voltage. Figure 9 below shows its bias condition on the load line. The entire input voltage swing is above the threshold voltage of the transistor. The DC value of the output voltage is positioned at around half of the rail voltage to ensure the output voltage can have a maximum swing without distortion. Therefore, Class-A amplifier is the most linear one [9].

However, the power efficiency (η) of Class-A amplifiers is low. Equation 2.10 below shows the calculation of η. I_q in Equation 2.10 represents the quiescent current. Ideally, the maximum $I_{out} = I_D$, and $V_{out} = V_{DD}$. Thus, the ideal maximum η is 0.5, or 50%.

$$\eta = \frac{0.5 I_{out} V_{out}}{I_q V_{DD}} = 0.5 \tag{2.10}$$

In reality, η is typically below 30%.

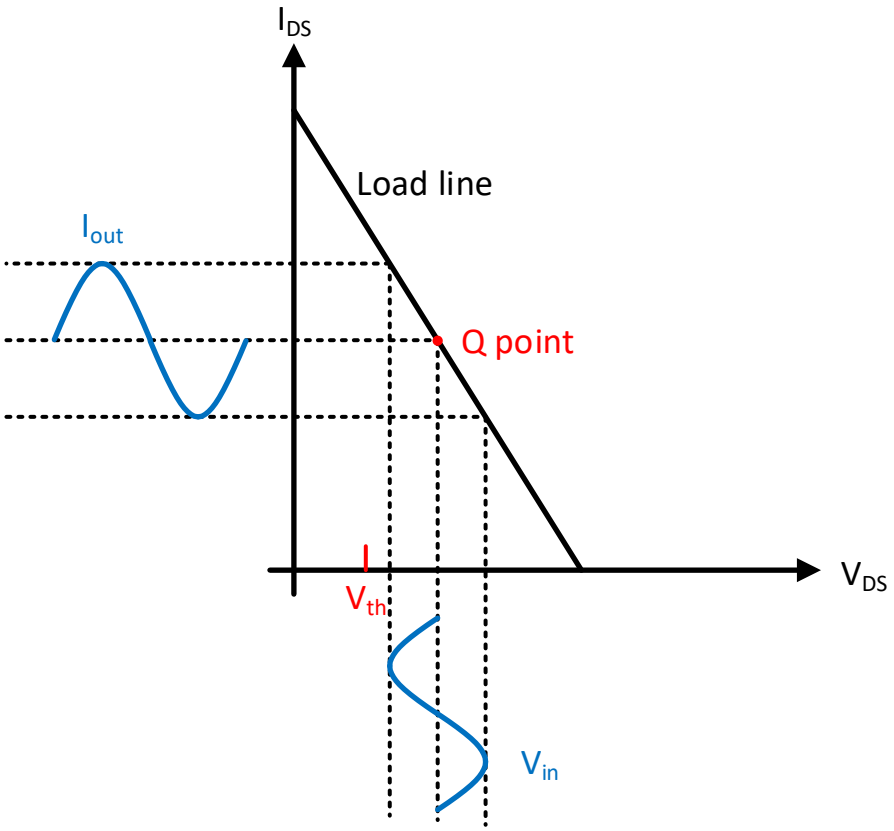

Figure 9. Class-A bias

2.2.2 Class-B Amplifiers

In a Class-B amplifier, the transistor is biased such that it is turned on for half cycle of each cycle of the input voltage. Figure 10 shows its bias condition on the load line.

The output current *i* can be written as a Fourier-series expansion, as shown in Equation (2.11).

$$i = I_0 + I_1 \cos \omega t + I_2 \cos 2\omega t + I_3 \cos 3\omega t + \cdots \qquad (2.11)$$

And I_0 (DC component) and I_1 (fundamental component) can be calculated by:

$$I_0 = \frac{1}{2\pi}\int_{-\theta}^{\theta} I(\cos\omega t - \cos\theta)\, d(\omega t) = I \cdot \gamma_0 \tag{2.12}$$

$$I_1 = \frac{1}{2\pi}\int_{-\theta}^{\theta} I(\cos\omega t - \cos\theta)\cos\omega t\, d(\omega t) = I \cdot \gamma_1 \tag{2.13}$$

Where

$$\gamma_0 = \frac{1}{\pi}(\sin\theta - \theta\cos\theta) \tag{2.14}$$

$$\gamma_1 = \frac{1}{\pi}(\theta - \sin\theta\cos\theta) \tag{2.15}$$

For Class-B amplifiers, θ is 90°, or π/2, the ideal maximum η can be calculated as follows

$$\eta = \frac{1}{2}\frac{\gamma_1}{\gamma_0}\frac{V_{out}}{V_{DD}} = \frac{\pi}{4} \approx 0.785, or\ 78.5\% \tag{2.16}$$

In reality, η of Class-B amplifier can reach 70%.

Two Class-B amplifiers can be connected in parallel to output a full sine-wave.

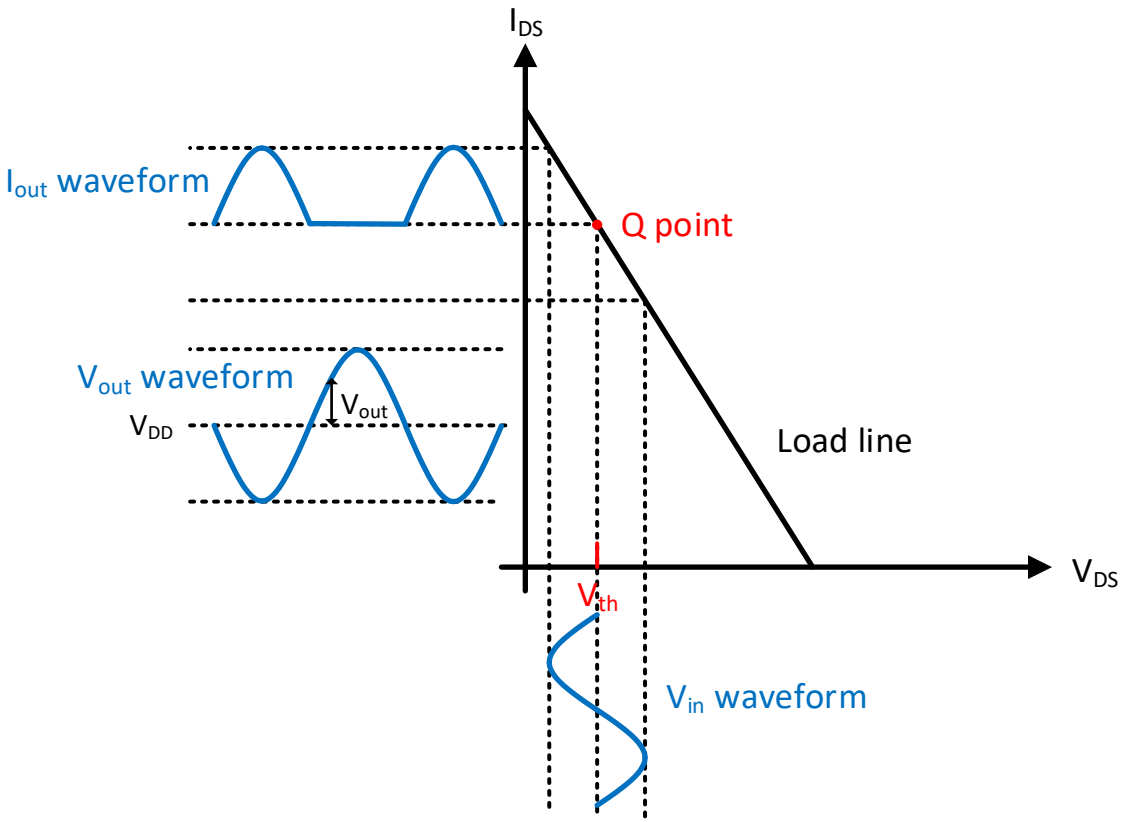

Figure 10. Class-B bias

2.2.3 Class-AB Amplifiers

The bias condition of Class-AB is between that of Class-A and Class-B. As a result, both linearity and power efficiency are between those of Class-A and Class-B. Figure 11 below shows its bias condition on the load line.

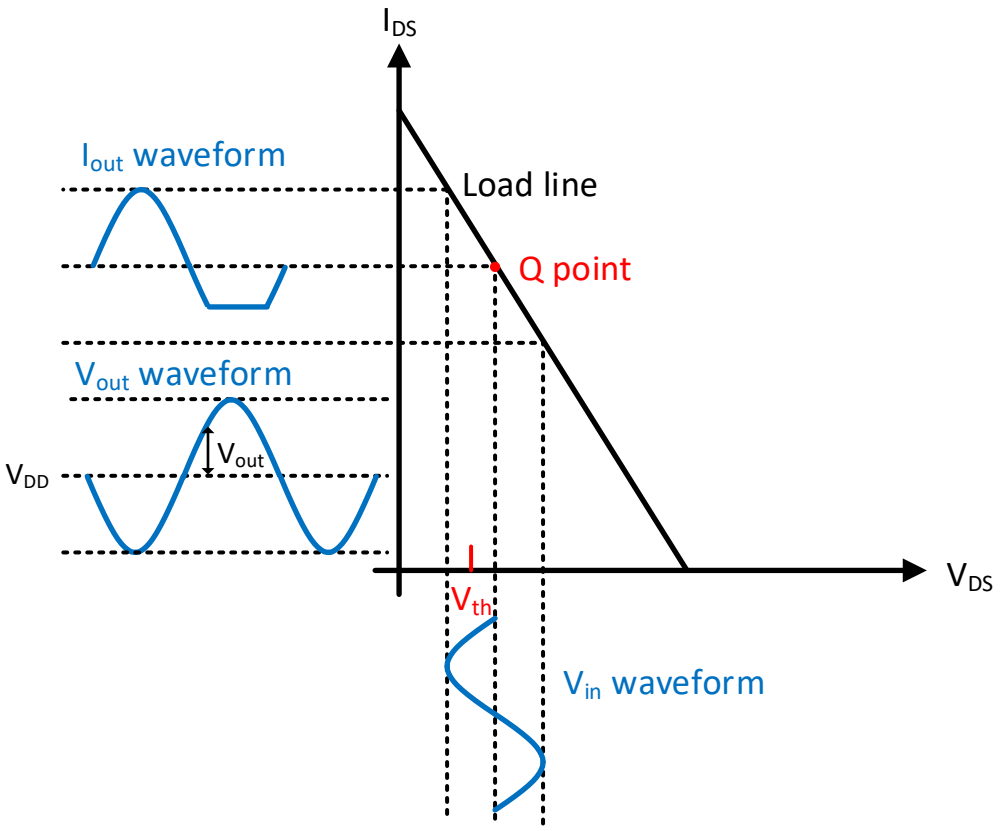

Figure 11. Class-AB bias

2.2.4 Class-C Amplifiers

The bias voltage of Class-C amplifiers is even lower than that of Class-B amplifiers. Class-C amplifiers have worse linearity, but better efficiency than Class-B amplifiers. Figure 12 below shows its bias condition on the load line.

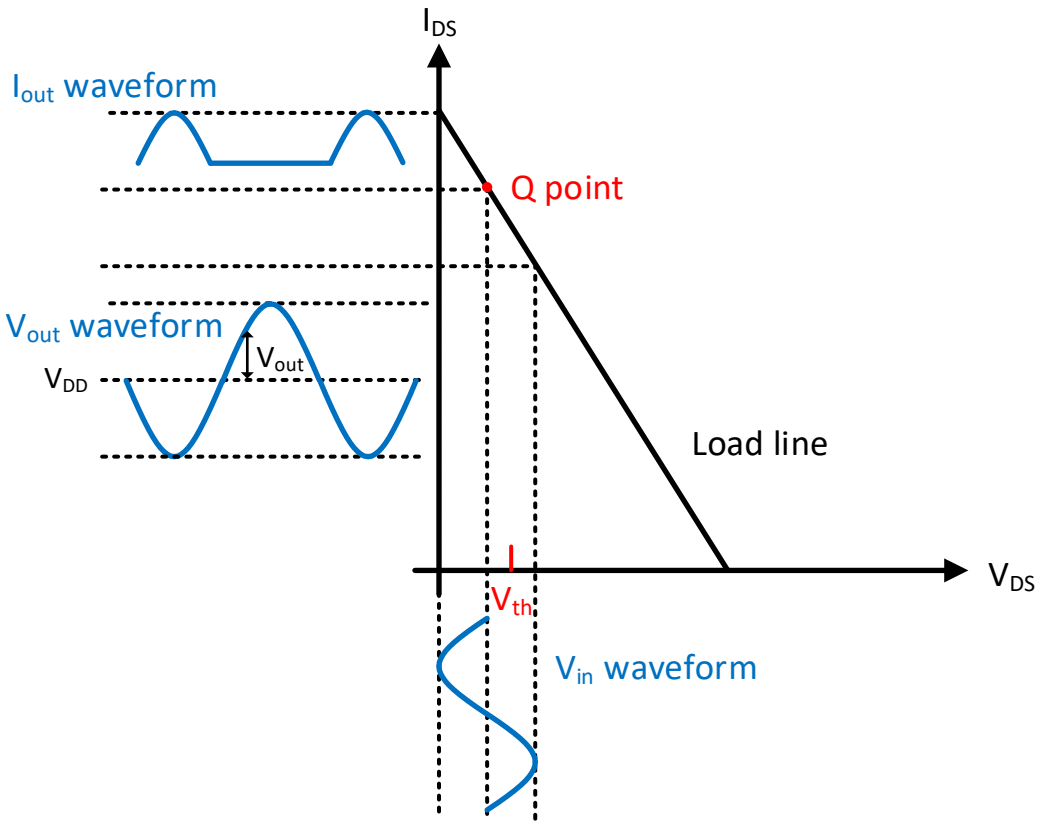

Figure 12. Class-C bias

2.2.5 Class-D Amplifiers

Class-D amplifiers are switching amplifiers. They are mainly used in audio applications to encode audio signals. The audio signal is converted to square wave and then fed to the amplifier. The amplifier is either on or off, and outputs a rail-to-rail pulse train, which is the encoded audio signal. Figure 13 is a block diagram of a typical Class-D power amplifier for audio applications.

When the amplifier is off, there is no output current. When it is on, the V_{DS} of the transistor is low. Theoretically, the efficiency of this type of amplifiers is 100%.

Class-D amplifiers are not used in mm-Wave frequencies because it is almost impossible to generate square wave in such high frequencies.

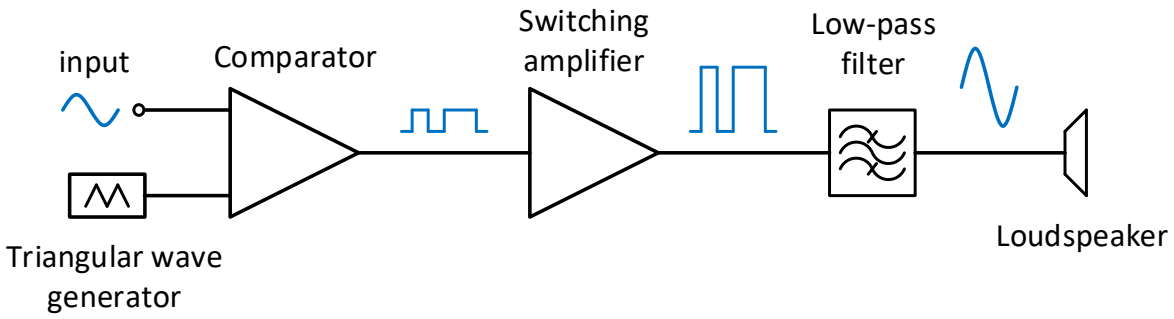

Figure 13. Block diagram of a Class-D audio amplifier

2.2.6 Class-E and E^{-1} Amplifiers

A Class-E amplifier also uses a transistor as a switch. Its loading is a passive network that tunes the output voltage into sinusoidal waveform. Figure 14 is the schematic of a typical Class-E amplifier. The ideal output voltage and current waveform is shown in Figure 15 [21].

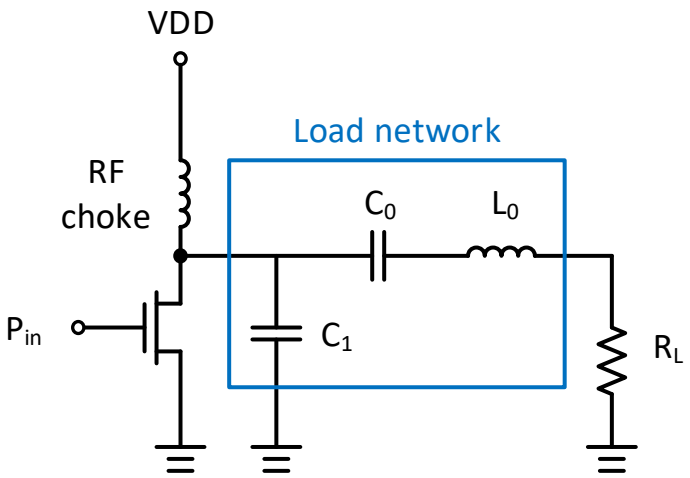

Figure 14. Class-E amplifier

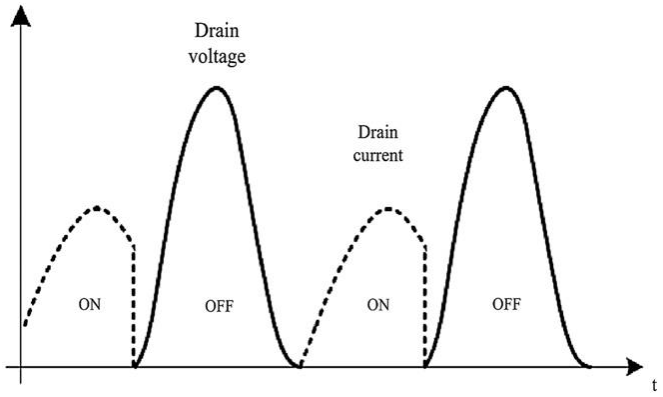

Figure 15. Ideal output waveform of a Class-E amplifier

The inverse Class-E amplifier, or Class-E^{-1} amplifier, is a dual of the Class-E amplifier. The voltage and current behavior are swapped in the Class-E^{-1} amplifier. The output current is tuned into sinusoidal waveform through the passive network at the output. An example of the output waveform of a Class-E-1 amplifier is shown in Figure 16 [22].

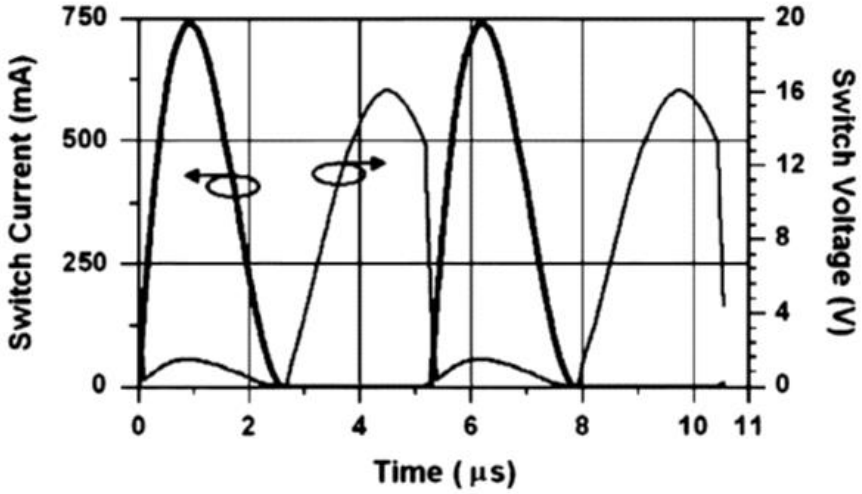

Figure 16. Output voltage (non-bold) and current (bold) waveform of a Class-E^{-1} amplifier

A typical schematic of a Class-E^{-1} amplifier [22] is shown in Figure 17.

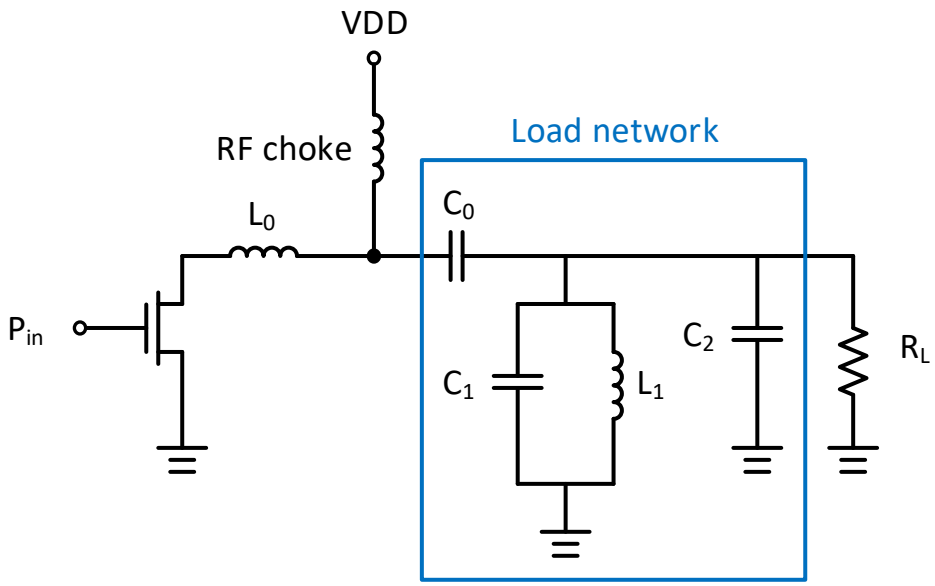

Figure 17. Class-E^{-1} amplifier

2.2.7 Class-F and F^{-1} Amplifiers

In a Class-F amplifier, the passive loading network resonates at one or more harmonic frequencies. The transistor acts as a current source. Figure 18 is the schematic of a typical Class-F amplifier.

Ideally, the output voltage waveform should be a perfect square wave, and the current waveform should be half sine wave that is 180° out of phase with the voltage waveform. Figure 19 plots the ideal voltage waveform (solid) and current waveform (dotted) at the output.

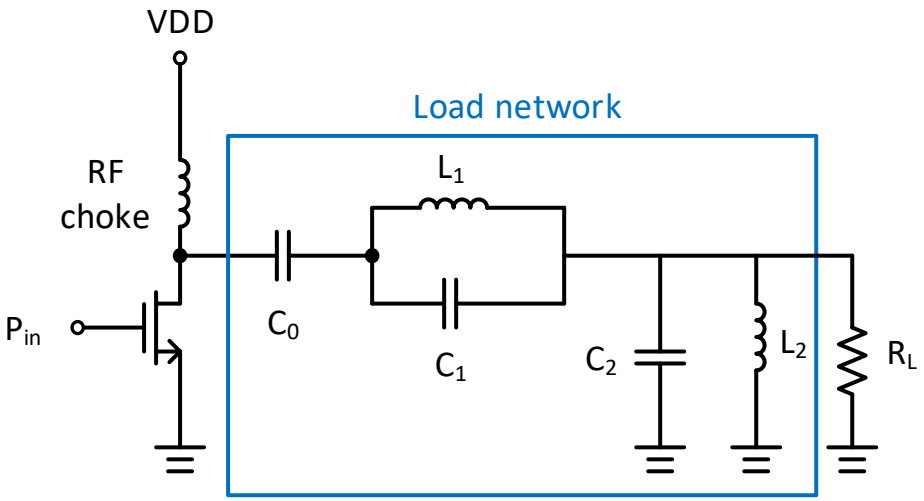

Figure 18. Schematic of a Class-F amplifier

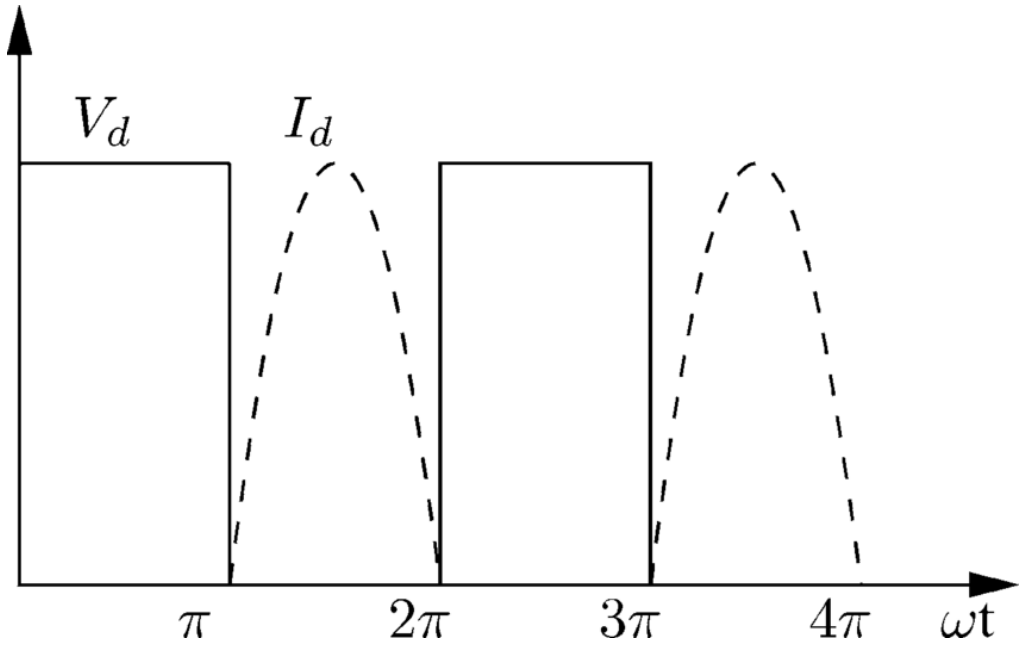

Figure 19. Ideal output waveform of a Class-F amplifier

Same as the Class-E amplifier, the Class-F amplifier also has a dual topology, which is the Class-F-1 amplifier. The voltage and current behavior are swapped in the Class-F^{-1} amplifier. The ideal output current waveform is a perfect square wave, and the ideal voltage waveform is half sine wave that is 180° out of phase with the current waveform.

Figure 20 is the schematic of a Class-F^{-1} amplifier [23], and the ideal output waveform of this type of amplifier is plotted in Figure 21 [24].

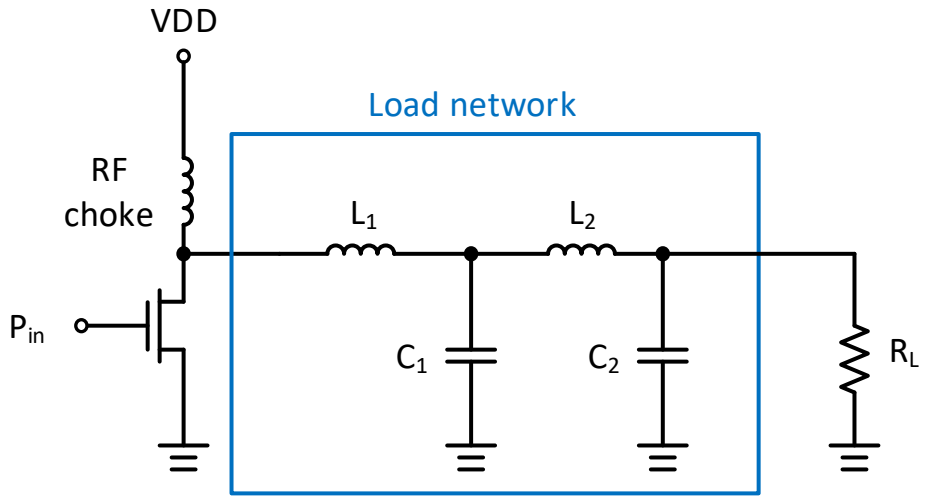

Figure 20. Class-F^{-1} amplifier

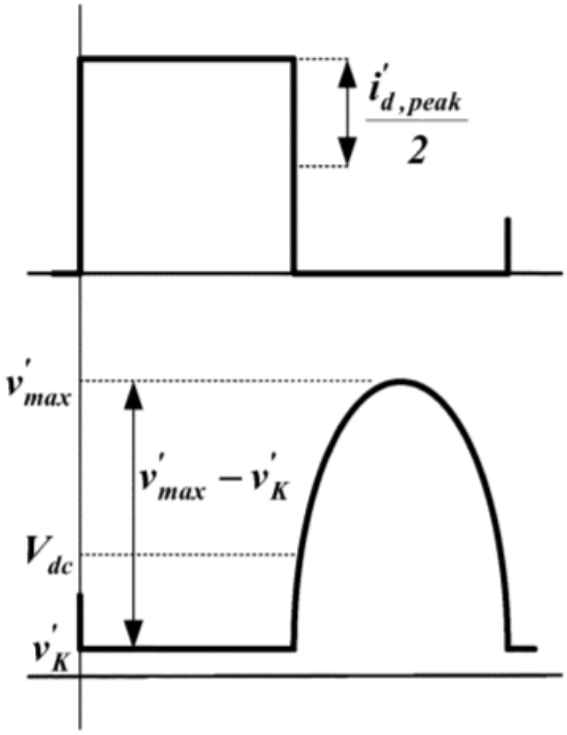

Figure 21. Ideal output current (top) and voltage (bottom) waveform of a Class-F^{-1} amplifier

2.2.8 Class-S Amplifiers

In a Class-S amplifier, the transistors and diodes form a switch. Similar to a Class-D amplifier, it converts analog signal to digital square wave pulses and then amplifies it. In addition to a Class-D amplifier, the amplified square wave pulses are fed into a low-pass filter that allows only the average voltage component to be delivered to the load. When the pulse width of the input varies, the average voltage in the output also varies. The low-pass filter acts as a demodulator to convert the square wave pulses back into sinusoidal wave.

This type of amplifiers is also mostly used in audio applications.

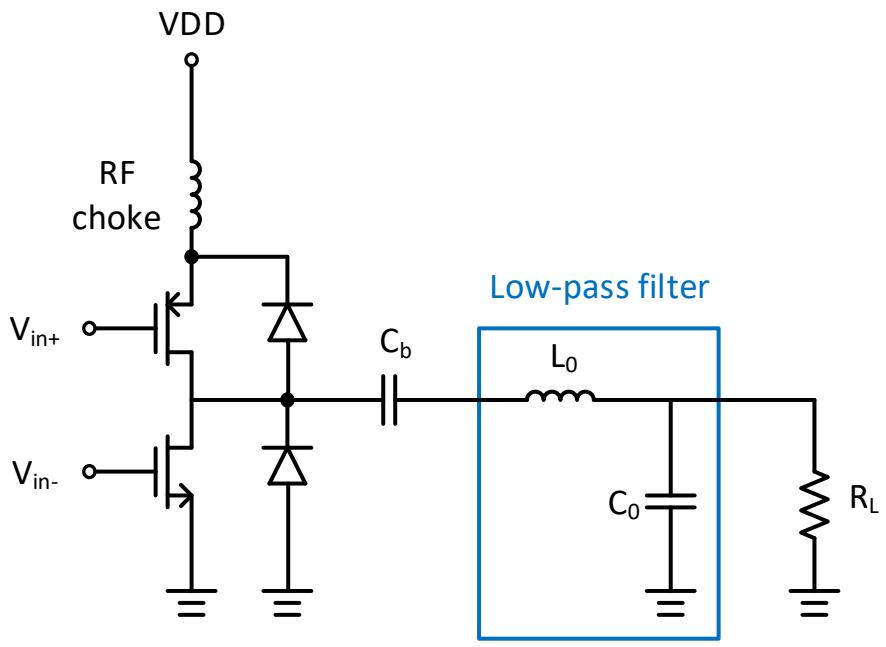

Figure 22. Schematic of a Class-S amplifier

2.3 Power Amplifier Design Requirement

2.3.1 Linearity Requirement in QAM

In wireless communication, the digital signal in the baseband is transmitted through one or more carriers, which are usually sinusoidal waves. In the transmitter, the carrier is modulated by the digital baseband signal, and then transmitted. In the receiver, the modulated carrier is received, and then de-modulated into baseband signal.

The methods to modulate and de-modulate baseband signal is called modulation schemes. Numerous modulation schemes include phase-shift keying (PSK), frequency-shift keying (FSK), amplitude-shift keying, on-off keying (OOK), quadrature phase-shift keying (QPSK), quadrature amplitude modulation (QAM), continuous phase modulation (CPM), etc. Among them, QAM is one of the most popular modulation schemes in modern wireless communication systems.

In QAM [5], the modulated signal is of the form:

$$x(t) = \alpha_1 A_C \cos \omega_C t - \alpha_2 A_C \sin \omega_C t \qquad (2.17)$$

Where A_C and ω_C are the amplitude and frequency of the carrier, respectively. α_1 and α_2 are positive and negative integers. There are two terms on the right-hand side of Equation (2.17); one is called the "I" component and the other is called the "Q" component.

For example, if $\alpha_1 = \pm 1, \pm 2$ and $\alpha_2 = \pm 1, \pm 2$, then there are 16 possible combinations of [α_1, α_2]. This type of QAM is thus called 16-QAM. If $\alpha_1 = \pm 1, \pm 2, \pm 3, \pm 4$ and $\alpha_2 = \pm 1, \pm 2, \pm 3, \pm 4$, then there are 64 possible combinations of [α_1, α_2]. This type of QAM is thus called 64-QAM. In modern wireless communication, 64-QAM or higher is becoming more and more popular.

These combinations of [α_1, α_2] are called **symbols**; the plot of the symbols is called the **constellation**. An ideal constellation of 64-QAM is plotted in Figure 23 below.

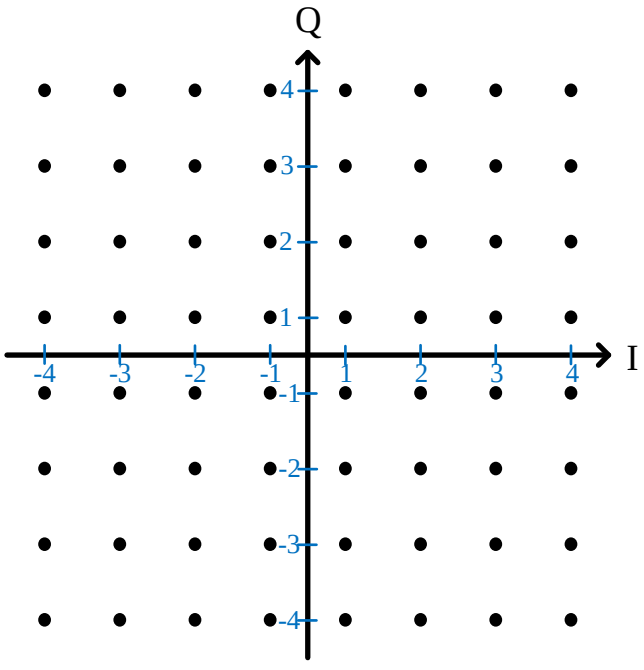

Figure 23. Ideal constellation of 64-QAM

If the PA in the transmitter does not have enough linearity, then it cannot sustain the gain for input of higher power levels. Consequently, the constellation will be distorted as shown in Figure 24 below.

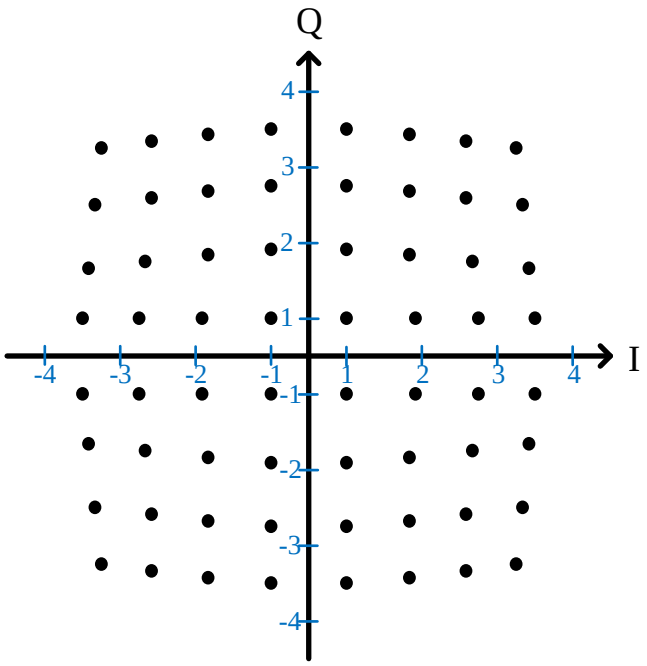

Figure 24. Distorted constellation of 64-QAM due to poor linearity

Furthermore, the AM-AM distortion and AM-PM distortion also show up in the constellation. Figure 25 plots the distorted constellation of 64-QAM due to AM-AM distortion. The undesired amplitude modulation causes an offset of each point. Figure 26 plots the distorted constellation of 64-QAM due to AM-PM distortion. Because of the undesired phase modulation, the entire constellation is rotated.

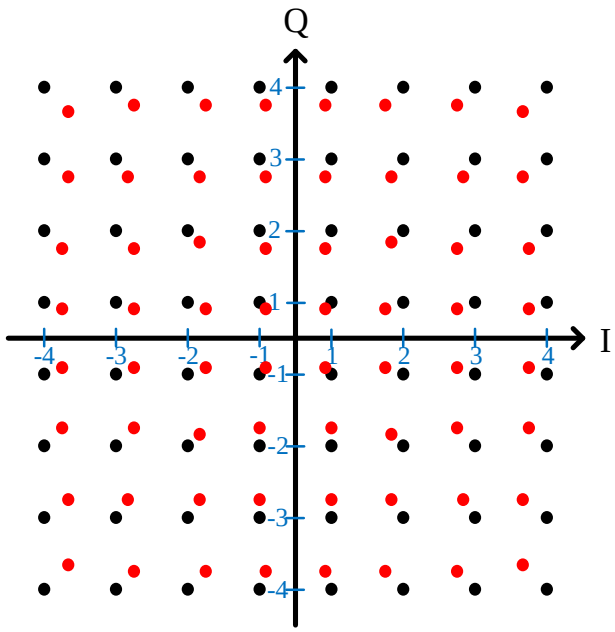

Figure 25. Ideal constellation (black) and constellation with AM-AM distortion (red) of 64-QAM

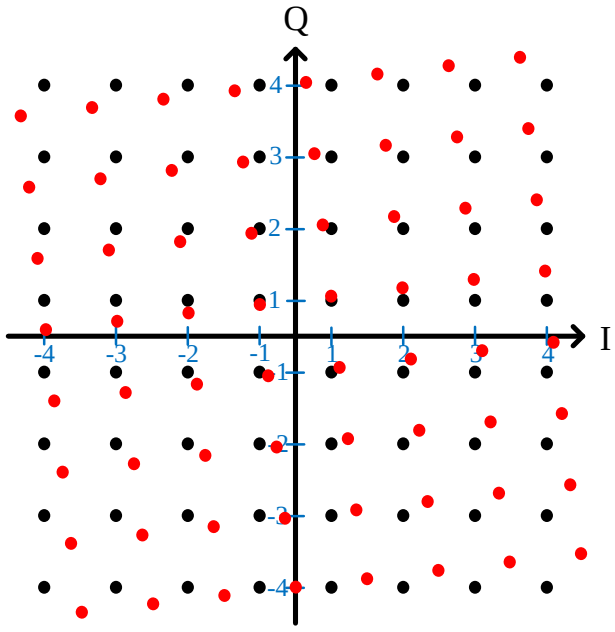

Figure 26. Ideal constellation (black) and constellation with AM-PM distortion (red) of 64-QAM

As can be seen, in QAM, the linearity of PAs is crucial.

In addition, other non-idealities will corrupt the signal and distort the constellation. These non-idealities include noise, interfering signals, PVT variations, etc.

In a distorted constellation, each symbol is deviated from its ideal position. The measurement of this deviation is called the **error vector magnitude (EVM)**. As shown in Figure 27, the error vector is a vector that starts from the distorted symbol (red dot) and ends at the symbol of ideal position (black dot). The EVM, usually measured in dB, is defined as follows:

$$EVM(dB) = 10log_{10}\left(\frac{P_{error}}{P_{ideal}}\right) \tag{2.18}$$

Where P_{error} is the power of the error vector and P_{ideal} is the power of the ideal vector in Figure 27.

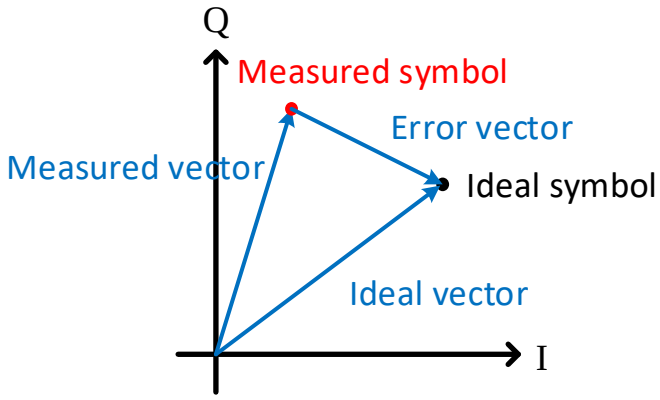

Figure 27. EVM

If the measured symbol is too far away from the ideal symbol, it will not be detected correctly. For example, if a measured symbol is much closer to its neighboring ideal symbol, it will be

detected as the neighboring symbol. As a result, there is a required EVM in each modulation schemes. If the EVM exceeds this requirement, the symbols will not be transmitted correctly. The more complex the modulation scheme, the more stringent the requirement of EVM. Table 2 below lists the EVM requirement of some of the modulation schemes [18].

Table 2. EVM Requirement

Modulation scheme	EVM requirement (dB)
QPSK	-7.57
16-QAM	-9.03
64-QAM	-10.97

2.3.2 PAE Requirement in OFDM

Orthogonal frequency-division multiplexing (OFDM) is a widely used coding scheme to transmit modulated signals. It is being used in many latest wireless and telecommunications standards, including Wi-Fi standards, such as 802.11a, 802.11n, 802.11ac, and cellular standards, such as LTE.

Rather than transmit a high-rate stream of data with a single subcarrier, OFDM uses many closely spaced orthogonal subcarriers that are transmitted in parallel, as shown in Figure 28 [25]. Each subcarrier is modulated with a conventional digital modulation scheme (such as QPSK, 16-QAM, 64-QAM, etc.) at low symbol rate.

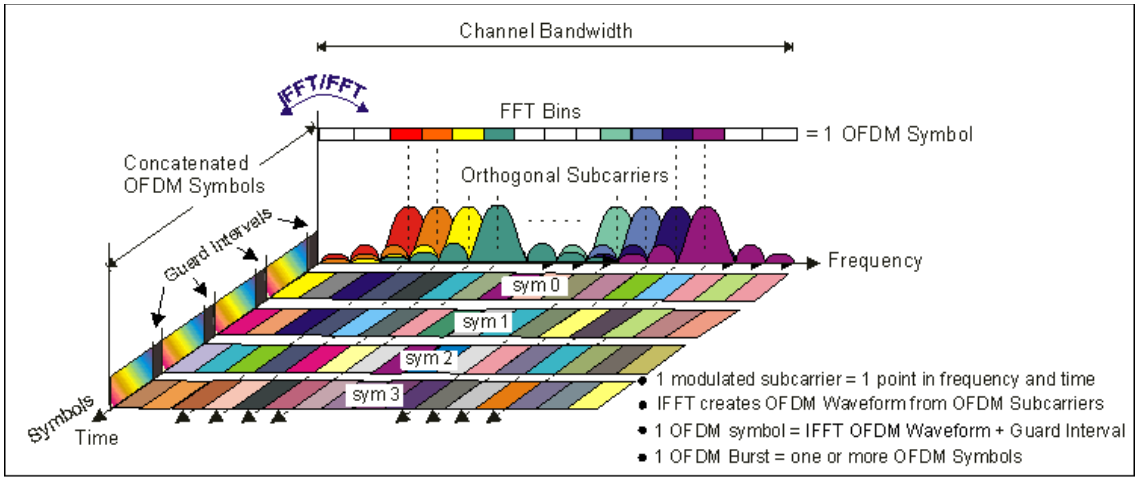

Figure 28. Frequency-time plot of an OFDM signal

As shown in the block diagram of Figure 29 [26], the input signal is first modulated by Inverse Discrete Fourier Transform (IDFT), and then is convolved with each subcarrier channel. To distinguish the subcarriers, a different cyclic prefix is added to the signal on different subcarriers. Thus, an OFDM symbol is created and is ready to be transmitted. Figure 30 [26] shows that this symbol is obtained by multiplying the corresponding values of x (representing the input signal) and h (representing the subcarriers) on the circle, and outputs at different times are obtained by rotating the x-values with respect to the h-values. Then the subcarriers transmit the symbols to the receiver. Finally, the prefixes are removed, and the received symbols are demodulated through the Discrete Fourier Transform (DFT) process.

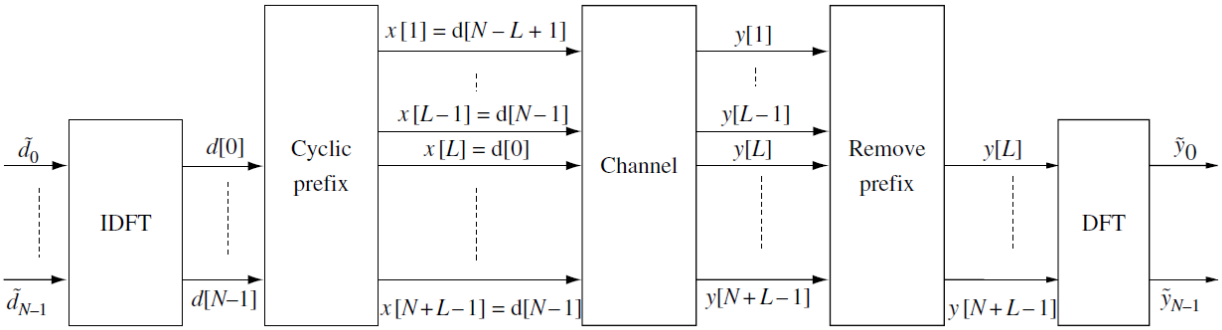

Figure 29. Block diagram of OFDM transmission and reception schemes

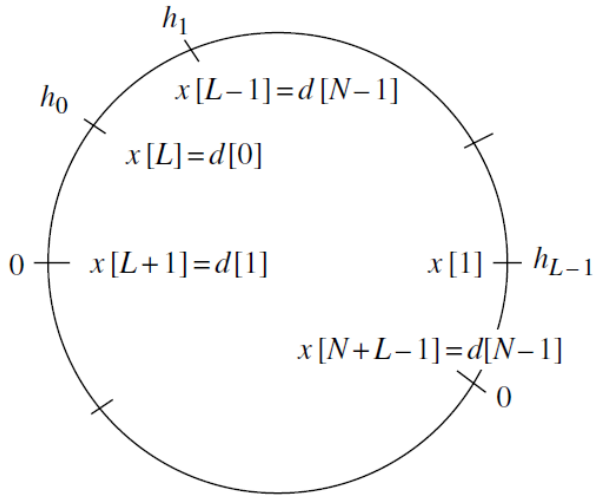

Figure 30. Convolution between each symbol and each subcarrier

The advantages of OFDM include:

i. Less selective fading: because instead of a carrier with a single frequency, multiple subcarriers of different carrier frequencies transmit signals.

ii. Spectrum efficiency: the subcarriers are close-spaced overlapping. Since the subcarriers are orthogonal to each other, they do not interfere with each other.

iii. Less inter-symbol interference (ISI): this is because the data rate on each of subcarrier is low.

iv. Simpler channel equalization: this is because the bandwidth of each subcarrier is narrow, which requires simpler channel equalization filters.

However, there are prices along with the above benefits. Besides high complexity, the most significant drawback is that the OFDM signal has high peak-to-average power ratio (PAPR). Typical signals transmitted using OFDM is plotted in Figure 31 [27] in frequency-domain.

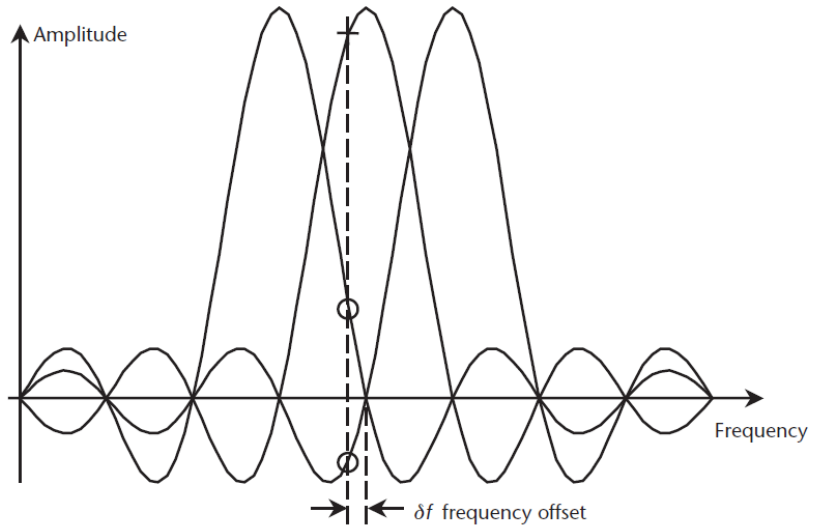

Figure 31. Typical signals in OFDM in frequency-domain

As can be seen, the peak power level is much higher than the average power level. Therefore, the PA in the transmitter needs to accommodate from average power to peak power, which is a

broad range of power levels. Most of the time, the PA operates at the average power level. Thus, the PAE at the average power level is especially important.

Most people use back-off point to define the average power level at the input. A **back-off point** of n dB means the input power level of subtracting n dB from the IP_{1dB} point. As plotted in Figure 32 below, a typical range between 6-dB and 10-dB backoff is considered the average power level at the input.

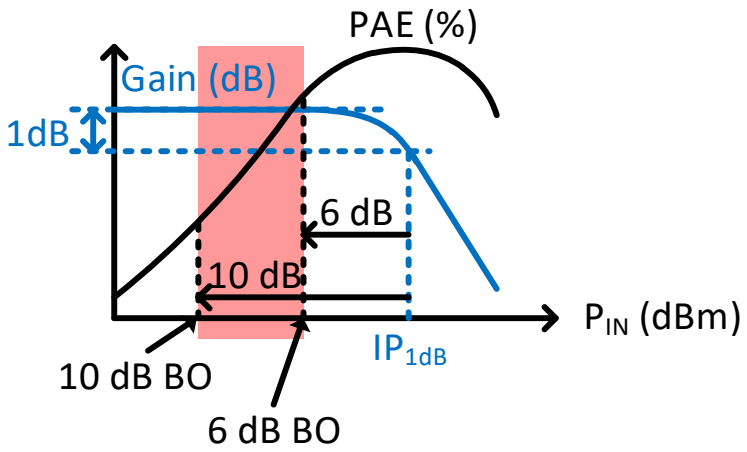

Figure 32. Plot of back-off points

Others [28] use the input power that produces an IMD_3 level of -30 dBc as the average power level at the input.

2.4 Previous Research on PA Designs

Numerous researches have been done to improve the PAE or the linearity of power amplifiers. This section explores some of the major methods.

2.4.1 Doherty Amplifiers

The most common structure to boost PAE is the Doherty configuration. The Doherty amplifier was first introduced in 1936 by W. H. Doherty [6]. As shown in Figure 33, it consists of two branches, one is the main amplifier that is usually biased in Class-A or Class-AB, and the other one is the peaking amplifier that is usually biased in Class-C [29].

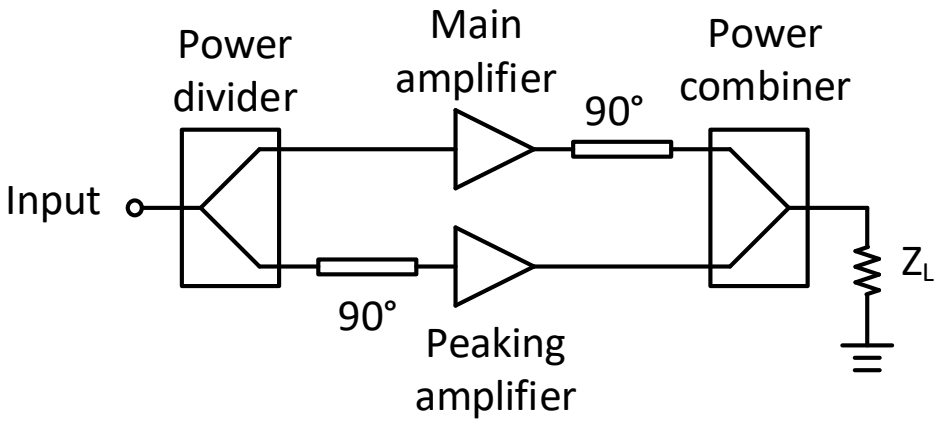

Figure 33. Structure of a Doherty amplifier

The operation of a Doherty amplifier is based on the active load concept, which modulates the load impedance of an active amplifying device and thus forces this device to operate at its maximum efficiency condition for a pre-determined range of input and/or output power levels [30]. When the input power is low, only the main amplifier is operating, which is terminated on an impedance load of twice the optimum output impedance (denoted as $2R_{opt}$). At the same time, the peaking amplifier is kept off. When the input power level increases, once the main amplifier saturates, the auxiliary amplifier switches on. The output current of the peaking amplifier starts modulating the load seen by the main amplifier by decreasing it from $2R_{opt}$ to R_{opt}. Thus, the main

amplifier's output current swing is increasing up to its maximum. To perform the load modulation, the two branches of amplifiers are connected at the output through an impedance inverter network, which is typically implemented with a lambda-quarter (λ/4) impedance transformer.

Figure 34 [30] is a typical plot of the efficiency (η) vs. back-off power of a Doherty amplifier. The kink in the plot represents when the peaking amplifier is turned on.

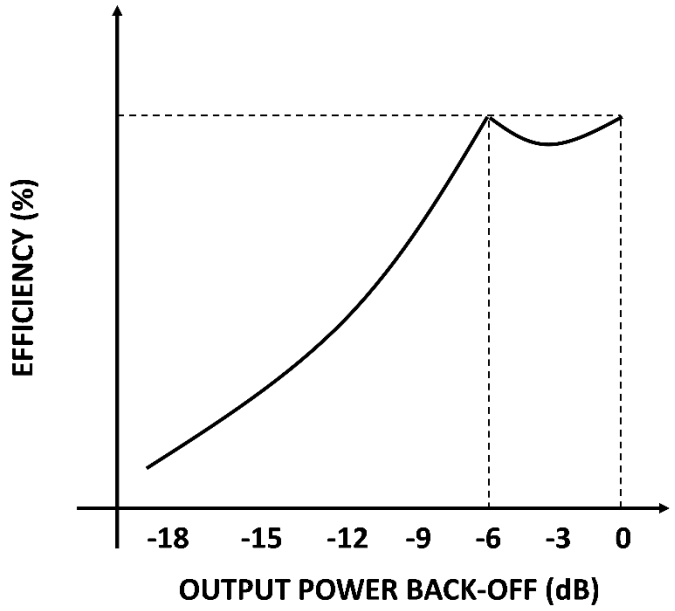

Figure 34. Typical plots of efficiency of a Doherty amplifier

One major draw-back of Doherty amplifiers is that they suffer from poor IIP_3 [7]. For the peaking amplifier to turn on, the main amplifier needs to be saturated, which leads to poor linearity.

2.4.2 Outphasing

Another method to improve PAE is outphasing [8]. As shown in Figure 35 [32], any modulated signal, S(t), can be decomposed into two signals with equal constant envelopes and opposite modulated phase variations. If the original signal is of the form:

$$S(t) = A(t)e^{j[\omega_C t+\theta(t)]} \tag{2.19}$$

Where A(t) and θ(t) is the envelope amplitude and phase of the signal at time t, respectively, and ω_C is the frequency of its carrier. Then the two decomposed signals, $S_1(t)$ and $S_2(t)$, can be calculated as follows:

$$\begin{aligned} S_1(t) &= \frac{A_M}{2} \cdot e^{j[\omega_C t+\theta(t)+\Phi(t)]} \\ S_2(t) &= \frac{A_M}{2} \cdot e^{j[\omega_C t+\theta(t)-\Phi(t)]} \end{aligned} \tag{2.20}$$

Where A_M is the amplitude of the constant envelope, and ϕ(t) is calculated as follows:

$$\Phi(t) = cos^{-1}[A(t)/A_M] \tag{2.21}$$

After decomposition, the two signals are amplified by two identical PAs. Since the envelope is fixed, the "peak power" is the "average power", thus reducing the PAPR, and the PA can be optimized to operate at this envelope [8]. The two signals are then combined at the output.

Outphasing eliminates the issues that come from high PAPR, but the phase tuning requirement is stringent. To use these two signals to represent the original signal, the phase tuning of them must be accurate. To tune the phase in mm-Wave frequencies, the bandwidth of the tuning loop needs to be large. Therefore, the drawback of this technique is that it requires wide band and accurate phase tuning circuits. Otherwise, the decomposed signal would not reconstruct to the original signal.

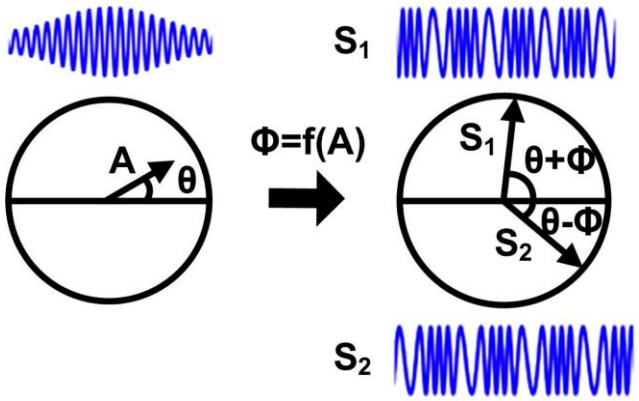

Figure 35. Decomposition of an arbitrary signal

2.4.3 Envelope Tracking

Envelope tracking is a method in which the supply voltage of a PA, rather than being a fixed value, closely tracks the envelope of the signal. When the signal amplitude is large, the supply voltage is large too; when the signal amplitude is small, the supply voltage is small too. In this way, the amount of DC supply drawn changes according to the amplitude of the signal. Thus, the PAE of the PA is improved.

Figure 36 [32] plots the block diagrams of a conventional PA (top) and a PA with envelope tracking technique (bottom). For conventional PAs, the supply voltage is maintained at a fixed value. When the amplitude of the signal is low, only a low supply power is needed to amplify such signal, and therefore, the extra supply power is mainly dissipated as heat. This problem of wasting of energy is mitigated by using a variable supply voltage that tracks the changing amplitude of the signal. To achieve this, a sensing circuitry is needed to sense the envelope of the signal and to feed the result to a DC-DC converter, which adjusts the DC supply voltage of the PA.

This technique is popular in RF frequencies, but not widely used in mm-Wave frequencies. The main reason is that it takes time to sense the signal envelope and to adjust the supply voltage accordingly, but in mm-Wave frequencies, signal envelope changes fast, making it difficult to track.

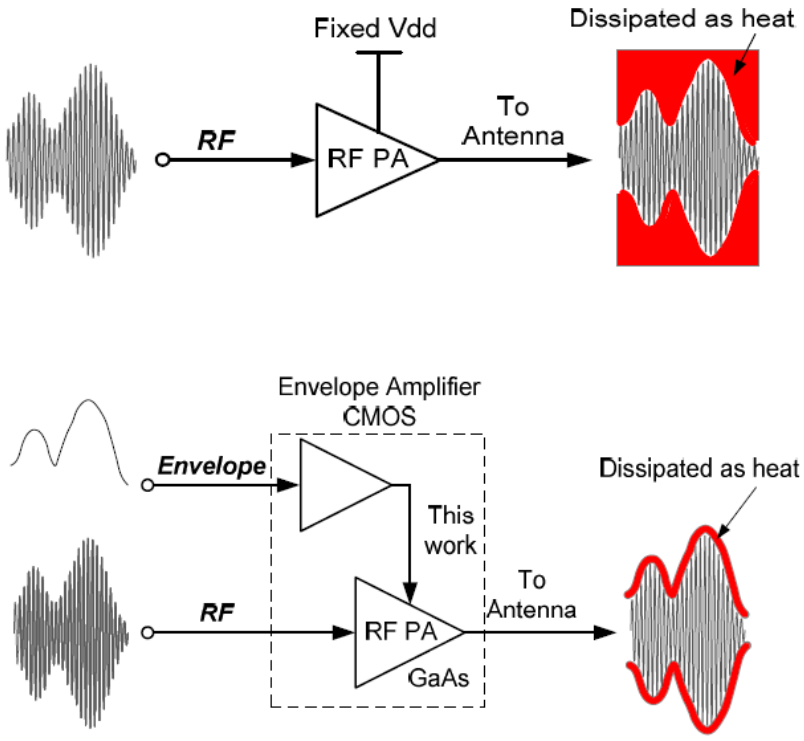

Figure 36. conventional PA and envelope tracking PA

2.4.4 Body-bias Adjustment

Adjusting body bias can improve the linearity. In [10], a Class-AB cell and a Class-C cell are connected in parallel. By adjusting the body bias, the threshold voltage of transistors can be

lowered, thus increasing the signal headroom and improving linearity. The threshold voltage of an NMOS transistor is calculated as follows [34]:

$$V_{TN} = V_{TNO} + \gamma \left(\sqrt{|V_{SB} + 2\phi_F|} - \sqrt{|2\phi_F|} \right) \quad (2.22)$$

Where V_{SB} is body bias voltage, which is the voltage difference between source and bulk, V_{TNO} is the threshold voltage when $V_{SB} = 0$, φ_F is the Fermi potential, and γ is the body effect coefficient. Adjusting V_{SB} such that the second term of the right-hand side of Equation (2.22) becomes negative can lower the threshold voltage.

However, since the supply voltage of modern CMOS technology is low, the improvement of voltage headroom is limited. Also, this tuning method requires triple-well devices, which are not standard devices in bulk CMOS technology.

2.4.5 Other Methods

To improve PAE with negligible sacrifice on linearity, parallelly combined PA cells can be used. In [35], as shown in Figure 37, two Class-AB cells are in parallel. when input is low, only one cell is turned on, and when input power is high, both cells are turned on. This operation improves PAE without compromising the linearity.

However, these types of structures require power combiners at the output. This increases the complexity. Moreover, at mm-Wave frequencies, the parasitics of these power combiners, which are usually designed using transmission lines, can cause considerable amounts of loss.

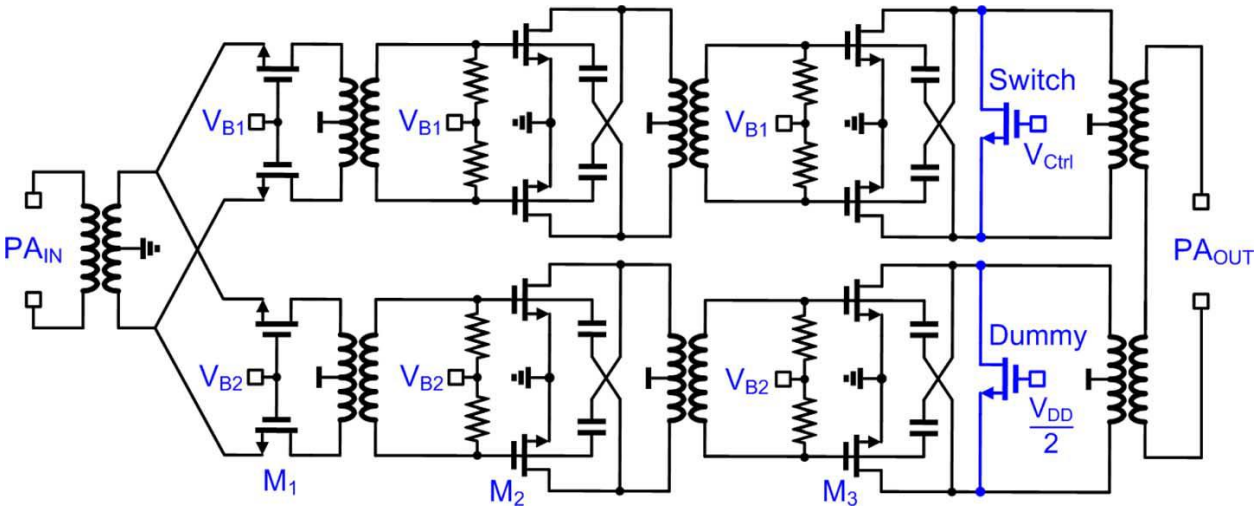

Figure 37. PA with parallel cells

2.4.6 Limitations of Existing Methods

The existing methods are to improve either linearity or PAE. However, as explained in Section 2.3, both linearity and PAE are important. The purpose of this work is to improve both linearity and PAE at the same time.

CHAPTER 3: PARAMETRIC AMPLIFICATION

3.1 Objective

As explained in previous chapters, designing a PA with high linearity and high PAE is crucial in wireless communication applications. In most of cases, these two objectives are conflicted, requiring different design optimizations and trade-offs. For example, in Class-A power amplifier designs, the transistor is biased such that it is turned on for the entire cycle of each cycle of the input voltage. The entire input voltage swing is above the threshold voltage of the transistor. The DC value of the output voltage is positioned at around half of the rail voltage to ensure the output voltage can have a maximum swing without distortion. This high bias point provides high linearity for the PA. However, it also causes high DC current even at small input power level. As a result, the PAE of Class-A power amplifiers are low. This is especially true in a high PAPR modulation system, such as the most popular OFDM system. Therefore, a PA design methodology improving both linearity and PAE is highly desirable.

Different from the methods described in Chapter 2, Section 2.4, this chapter introduces the application of the theory of parametric amplification to improve PAE and linearity of PAs at the same time.

3.2 Theory

Parametric amplifiers are a class of amplifiers that use non-linear devices to transfer energy from “pump” circuits to “signal” circuits. If the phases of the pump and signal match well, then when the signal is at its peak value, the pump signal pumps this peak value even more. This concept is analogous to the person on swing, as depicted in Figure 38 below [36]. When the swing travels from left to right, which is a half cycle, the person’s position changes from standing up to crouching down and back to standing up, which is a full cycle. Through these movements, the

person can make the swing higher. Here, the swing represents the signal, and the person represents the pump. The frequency of the pump signal is twice the frequency of the swing.

Also, the movement of the person needs to be aligned with the movement of the swing, such that when the swing is at its highest position, the person stands up, and when the swing is at its lowest position, the person crouches down. If not, for example, the person stands up when the swing is at its lowest position, then the movement of this person will counteract the swing, making the swing lower.

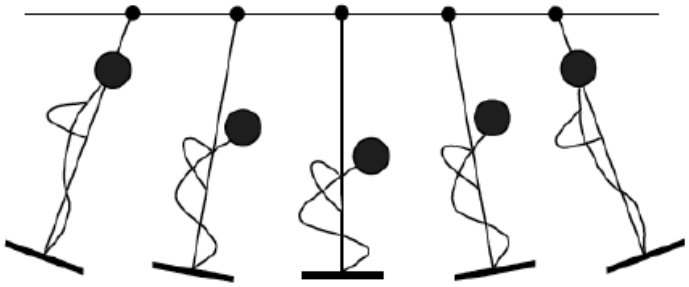

Figure 38. The concept of parametric amplifiers

An equivalent circuit model of a parametric amplifier is shown in Figure 39 [36].

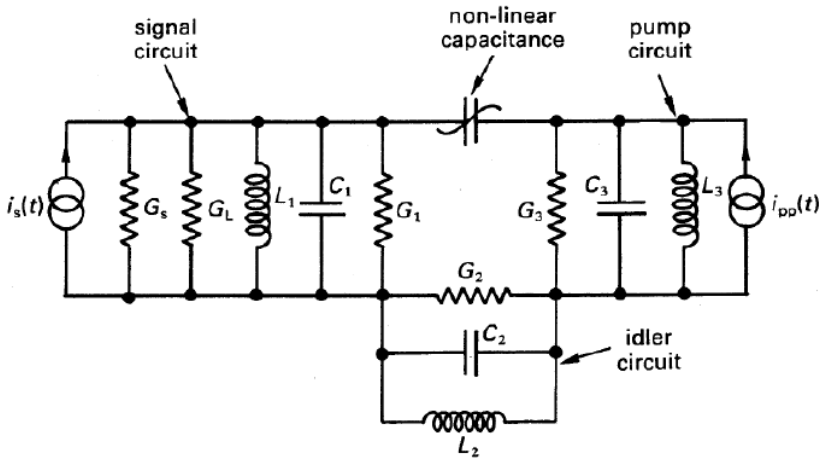

Figure 39. Simplified equivalent circuit of the parametric amplifier

The charge, *q*, on the non-linear capacitance is a function of the voltage across its terminals, *v(t)*. The charge can be expressed using the Taylor series expansion as follows:

$$q(t) = a_1 v(t) + a_2 v^2(t) + a_3 v^3(t) + \cdots \tag{3.1}$$

Eliminating higher-order terms and replacing a_1 with the capacitance, *C*, Equation (3.1) becomes:

$$q(t) = Cv(t) + a_2 v^2(t) \tag{3.2}$$

The AC current that flows in the non-linear capacitance can be expressed as:

$$i(t) = \frac{dq(t)}{dt} = C\frac{dv(t)}{dt} + 2a_2 v(t)\frac{dv(t)}{dt} \tag{3.3}$$

The voltage across the nonlinear capacitance, *v(t)*, consists of the signal, idler and pump waves of frequencies ω_1, ω_2, and ω_3, respectively. Therefore, *v(t)* can be expressed as:

$$v(t) = v_1(t) + v_2(t) + v_3(t)$$
$$= V_1 \cos(\omega_1 t + \phi_1) + V_2 \cos(\omega_2 t + \phi_2) \quad (3.4)$$
$$+ V_3 \cos(\omega_3 t + \phi_3)$$

For parametric amplification to occur, the frequencies of ω_1, ω_2, and ω_3 satisfy the relation below:

$$\omega_3 = \omega_1 + \omega_2 \quad (3.5)$$

From Equations (3.3) and (3.4), the AC current *i(t)* can be expressed as:

$$i(t) = i_1(t) + i_2(t) + i_3(t) \quad (3.6)$$

Where

$$i_1(t) = C\frac{dv_1(t)}{dt} + \frac{a_2 V_2 V_3}{V_1}\left[\cos(\phi_3 - \phi_2 - \phi_1)\frac{dv_1(t)}{dt} - \omega_1 v_1(t)\sin(\phi_3 - \phi_2 - \phi_1)\right] \quad (3.7)$$

$$i_2(t) = C\frac{dv_2(t)}{dt} + \frac{a_2 V_1 V_3}{V_2}\left[\cos(\phi_3 - \phi_2 - \phi_1)\frac{dv_2(t)}{dt} - \omega_2 v_2(t)\sin(\phi_3 - \phi_2 - \phi_1)\right] \quad (3.8)$$

$$i_3(t) = -C\frac{dv_3(t)}{dt} + \frac{a_2 V_1 V_2}{V_3}\left[\cos(\phi_3 - \phi_2 - \phi_1)\frac{dv_3(t)}{dt} + \omega_3 v_3(t)\sin(\phi_3 - \phi_2 - \phi_1)\right] \quad (3.9)$$

The admittance Y_1, Y_2, and Y_3, seen by the signal, idler, and pump circuits, respectively, can be calculated by taking the Fourier transform of Equations (3.7), (3.8), and (3.9):

$$Y_1(t) = \frac{I_1(j\omega)}{V_1(j\omega)} = j\omega_1 C + j\omega_1 a_2 \frac{V_2 V_3}{V_1} e^{j(\phi_3 - \phi_2 - \phi_1)} \quad (3.10)$$

$$Y_2(t) = \frac{I_2(j\omega)}{V_2(j\omega)} = j\omega_2 C + j\omega_2 a_2 \frac{V_1 V_3}{V_2} e^{j(\phi_3 - \phi_2 - \phi_1)} \quad (3.11)$$

$$Y_3(t) = \frac{I_3(j\omega)}{V_3(j\omega)} = j\omega_3 C + j\omega_3 a_2 \frac{V_1 V_2}{V_3} e^{-j(\phi_3 - \phi_2 - \phi_1)} \quad (3.12)$$

In the three circuits (signal, idler, and pump), the relations between current and voltage can be expressed as:

$$I_S(j\omega) = \left[G_T + j\omega_1 a_2 \frac{V_2 V_3}{V_1} e^{j(\phi_3 - \phi_2 - \phi_1)}\right] V_1(j\omega) \quad (3.13)$$

$$0 = \left[G_2 + j\omega_2 a_2 \frac{V_1 V_3}{V_2} e^{j(\phi_3 - \phi_2 - \phi_1)}\right] V_2(j\omega) \quad (3.14)$$

$$I_P(j\omega) = \left[G_3 + j\omega_3 a_2 \frac{V_1 V_2}{V_3} e^{-j(\phi_3 - \phi_2 - \phi_1)}\right] V_3(j\omega) \quad (3.15)$$

Where $I_S(j\omega)$ and $I_P(j\omega)$ are the Fourier transforms of the input signal and pump currents, respectively, and $G_T = G_S + G_L + G_1$.

From Equations (3.13), (3.14), and (3.15), the admittance of the signal circuit, Y_S, is calculated as follows:

$$Y_S = G_T - \frac{\omega_1 \omega_2 {a_2}^2}{G_2 {G_3}^2} \cdot \frac{|I_P(j\omega)|^2}{\left[1 + \frac{\omega_2 \omega_3}{G_2 G_3} {a_2}^2 {V_1}^2\right]^2} \tag{3.16}$$

The second term on the right-hand side of Equation (3.16) is a negative conductance due to the non-linear capacitance driven by the pump wave of frequency ω_3.

If V_1 satisfy the condition that

$$\frac{\omega_2 \omega_3}{G_2 G_3} {a_2}^2 {V_1}^2 \ll 1 \tag{3.17}$$

Then Equation (3.16) can be approximated as:

$$Y_S \approx G_T - \frac{\omega_1 \omega_2 {a_2}^2}{G_2 {G_3}^2} \cdot \frac{|I_P(j\omega)|^2}{1} = G_T - \frac{\omega_1 \omega_2 {a_2}^2}{G_2 {G_3}^2} |I_P(j\omega)|^2 \tag{3.18}$$

The negative conductance, $-\frac{\omega_1 \omega_2 {a_2}^2}{G_2 {G_3}^2} |I_P(j\omega)|^2$, is independent of the signal input, and is dependent of the pump current. This indicates a linear parametric amplification.

The power gain, G, is ratio of the power delivered to the load (G_L) to the input power to the source (G_S).

$$G = \frac{G_L {V_1}^2}{|I_S|^2/(4G_S)} = \frac{4 G_S G_L}{|Y_S|^2} \tag{3.19}$$

Figure 40 (a) is an example of implementing parametric amplification in CMOS. The varactor is formed from an NMOS device. Its source and drain nodes are tied together, forming one terminal of the varactor. The other node of the varactor is the gate node of the NMOS. The bulk of this device is connected to ground.

V_P is the pump. It is supplied to the varactor at its gate. V_{IN} is the signal to be amplified. It is the voltage difference between the two terminals. V_P modifies C at twice the frequency of V_{IN}. Since the charge in the varactor, Q, is calculated as $Q = C \cdot V_{IN}$, reducing C will increase V_{IN}.

As shown in Figure 40 (b), when V_{IN} reaches its peak, C is decreased, causing V_{IN} to increase. When V_{IN} is at its zero-crossing point, the capacitance returns to its original value. At the zero-crossing point, where V_{IN} returns to its DC bias value, the AC charge in the varactor is zero, and changing its capacitance does not affect V_{IN}. Then when V_{IN} reaches its valley, C can be decreased again to amplify V_{IN}. Thus, when V_{IN} runs one cycle, V_P runs two cycles.

This operation continues for cycles and V_{IN} is amplified until it saturates.

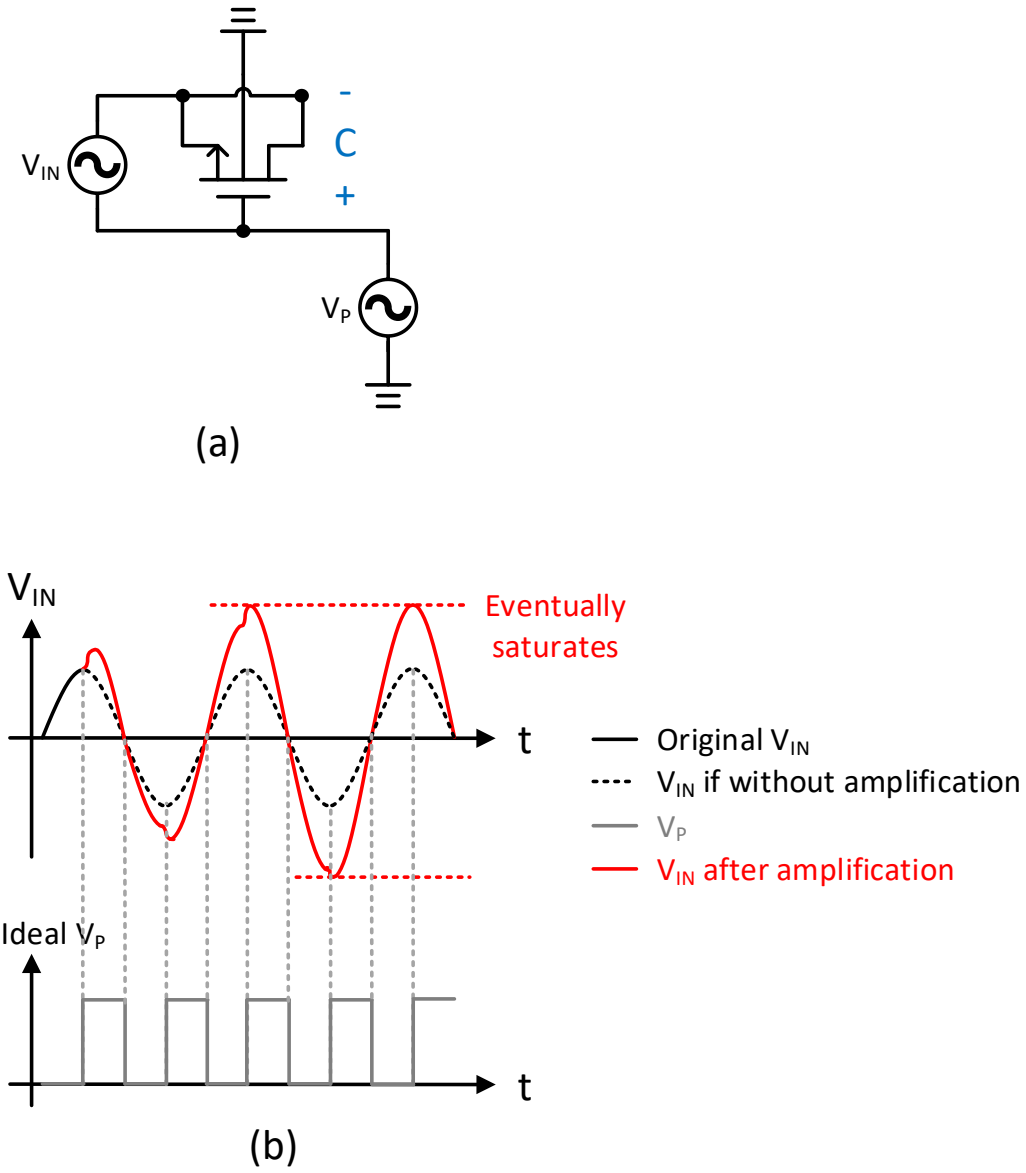

Figure 40. Implementation of parametric amplification

3.3 Improving Parametric Amplification in mm-Wave

As explained previously, a parametric amplifier needs a pump signal of twice the operating frequency. To implement a complete parametric amplifier, an oscillator is needed to produce such pump signal. This will lead to additional complexity and DC power supply. More importantly, in

mm-Wave range, with the operating frequency being already high, it is difficult to generate another waveform with twice the operating frequency.

To solve this problem, this work introduces a novel parametric amplifier design without using an external 2x-frequency pump signal. It utilizes the nonlinearity of the PA itself. For a differential circuitry, the second-harmonic tone appears at the virtual ground points (the power supply or the common current tail). For large signal circuities like power amplifiers, these 2x-frequency tones are very strong. A high impedance filter circuit is design at this virtual ground to boost the second-harmonic tone as the parameter amplification pump signal. In addition, an LC phase shifter is used to align this 2x-pump signal with the PA fundament signal to meet the parameter amplification criteria. Details will be explained in the next chapter.

CHAPTER 4: PARAMETRIC AMPLIFICATION-BASED PA DESIGNS

4.1 Background

The PA in this work is designed to be used in beamforming applications in the 57-to-64-GHz band. To begin the design, the range of the PA's output power needs to be calculated.

First, the output power range of the beamforming system is to be calculated. According to the FCC rules [37], the maximum effective isotropic radiated power (EIRP) of the transmitter cannot exceed 43 dBm. EIRP measures the output power of an antenna in a single direction. In a transmitter, the EIRP is the power that the transmitter finally outputs. Thus, the upper bound is 43 dBm.

The lower bound is $P_{sen} + FSPL$, where P_{sen} is the sensitivity of the receiver and FSPL is the free-space propagation loss of the signal path. The sensitivity is the minimum signal level that a receiver can detect with acceptable quality. It is calculated by the formula below:

$$P_{sen} = -kT(dBm/Hz) + NF + 10logB + SNR_{min} \quad (4.1)$$

Where -kT is the thermal noise and -kT = -174 dBm/Hz if at 300 K, NF is the noise figure of the receiver, B is the bandwidth of the receiver, and SNR is the signal-to-noise ratio.

To find out some examples of the sensitivity of 60-GHz wireless systems, various research works in this area are studied [38][39][40][41]. In general, the sensitivity of such systems is in the range of -95 ~ -55 dBm.

The free-space propagation loss (FSPL) depends on the propagation distance. It is calculated by the formula below:

$$FSPL(dB) = 20log\left(\frac{4\pi df}{c}\right) \quad (4.2)$$

Where f is the frequency of signal, and c is the speed of light. For a 60-GHz signal, the calculated FSPL of various distances are shown in the table below:

Table 3. FSPL of various distances at 60 GHz

Propagation distance (m)	FSPL (dB)
1	68
5	82
10	88
20	94

Therefore, the allowed range of the total EIRP of the transmitter ($EIRP_{TX}$) is:

$$P_{sen} + FSPL < EIRP_{TX} < 43\ dBi \tag{4.3}$$

Since the transmitter is to be designed in beamforming arrays, in which each element consists of a PA and an antenna, the allowed range of the P_{SAT} of each PA is determined in the following.

Consider the P_{SAT} of each PA is P dBm. If the array has N elements, the total EIRP of this array is the sum of the total P_{SAT} of N PAs and the total gain of N antennas. The total P_{SAT} of N PAs is calculated as the P_{SAT} of each PA plus the array gain. In dB scale, when power is doubled, it is equivalent to adding 3 dB. Therefore, for an array with N elements, the array gain is $3 \cdot \log_2 N$. Thus, the total P_{SAT} of N PAs is:

$$P_{SAT\_total} = P(dBm) + 3 \cdot \log_2 N\ (dB) \tag{4.4}$$

The total gain of N antennas is calculated in the same way.

$$G_{ant\_gain\_total} = G_i(dBi) + 3 \cdot \log_2 N\ (dB) \quad (4.5)$$

Where G_i is the gain of each antenna. Various research works [42][43][44][45][46] are studied and the typical range of G_i at 60 GHz is found out to be at least 5 dBi.

Adding Equations (4.4) and (4.5), the total EIRP of this *N*-element array is:

$$EIRP_{TX} = (P + G_i + 6 \cdot \log_2 N)\ dBi \quad (4.6)$$

Substitute Equation (4.6) into (4.3):

$$P_{sen} + FSPL < (P + G_i + 6 \cdot \log_2 N)\ dBi < 43 \quad (4.7)$$

Solve for P:

$$P_{sen} + FSPL - G_i - 6 \cdot \log_2 N < P < 43 - G_i - 6 \cdot \log_2 N \quad (4.8)$$

The range of *P* depends on the size of the array, the propagation distance, and the sensitivity of the receiver, which depends on modulation schemes, coding schemes, bandwidth, and temperature.

Based on the findings from [38][39][40][41], a reasonable value of the sensitivity of the receiver would be -60 dBm. Based on the findings from [42][43][44][45][46], a reasonable value of the antenna gain of each antenna would be 5 dBi. If the propagation distance is 10 meters, then the FSPL is 88 dB according to Equation (4.2). If the beamforming array is 4x4, then N = 16. Then, based on Equation (4.8), the P_{SAT} of each PA is in the range of:

$$-60 + 88 - 5 - 6 \cdot \log_2 16 < P < 43 - 5 - 6 \cdot \log_2 16 \quad (4.9)$$

Or:

$$-1 < P < 14 \quad (4.10)$$

This is a practical situation that this work targets at. The P_{SAT} of the PA to be designed falls in the range specified in Equation (4.10), and the PA can be used in beamforming systems to produce a much larger total power.

4.2 Reference Conventional PA Design

In order to demonstrate the parameter amplification PA design theory, a conventional PA operates at 60 GHz is designed at first as a base-line design. As shown in Figure 41, it has two common-source stages. Both stages are biased at Class-AB to accommodate both gain and linearity. In each stage, source-degenerating inductors (L_s) are employed to improve linearity, and neutralizing capacitors (C_n) are employed to improve stability. The matching networks are realized by transistors, which are also used to supply bias voltages.

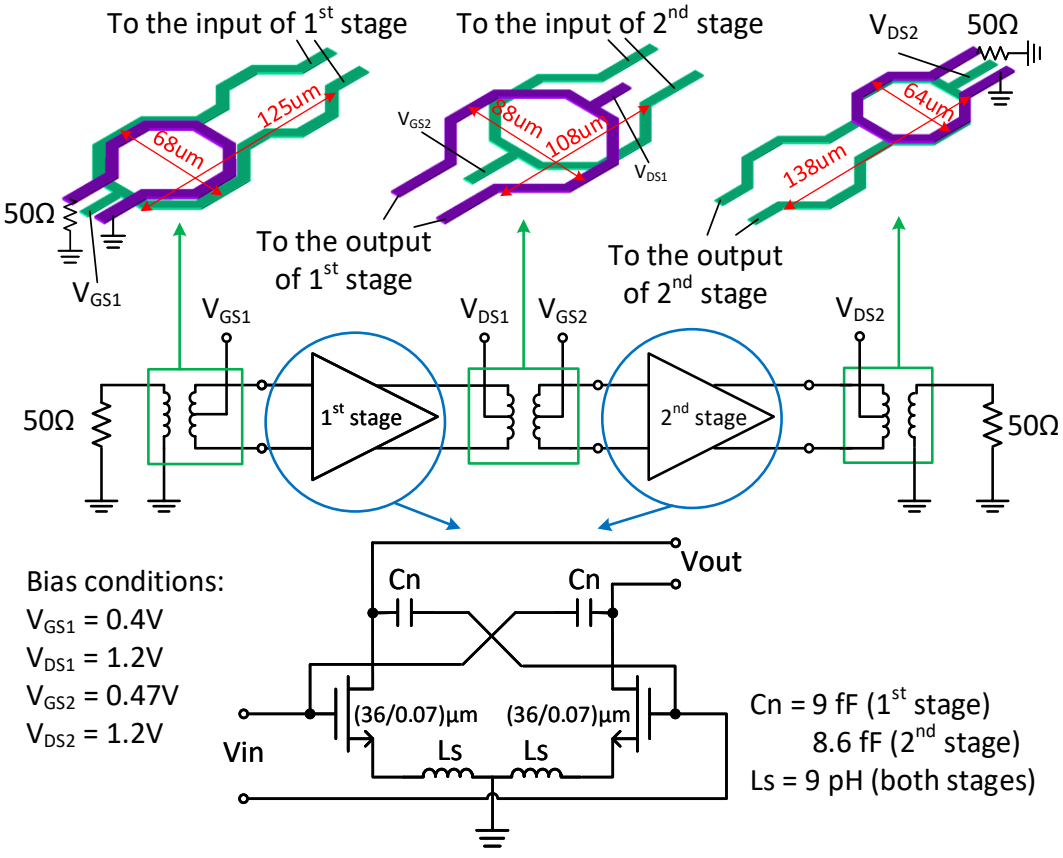

Figure 41. Schematic of the conventional 60-GHz PA

To improve stability, neutralization using MOM capacitors (C_n in Figure 41) has been used. To ensure that the stability factor (k) is greater than 1 from DC to 80 GHz, Cn was found to be between 8.8 and 14.6 fF for the first stage, and between 8.2 and 14.7 fF for the second stage. Values of 9 and 8.6 fF have been used respectively for the first and second stages to cover process variation and parasitic capacitances.

The simulated k factors of with and without C_n versus frequency are shown in Figure 42. Without C_n, k < 1 from 50 to 63 GHz.

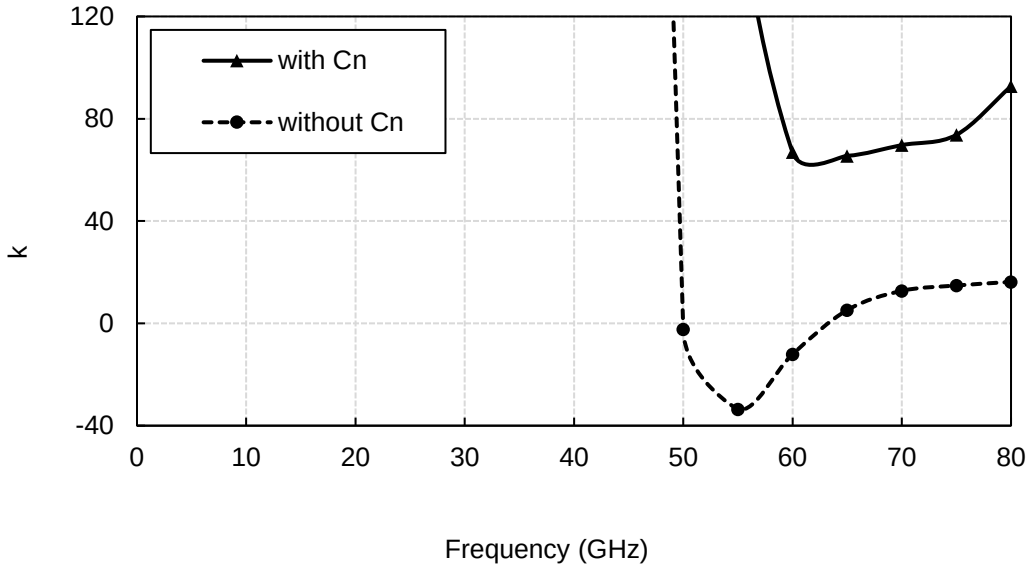

Figure 42. Effect of the neutralizing capacitors

The transformers serve as both matching networks and bias supplying networks. They are implemented using top level copper and the ALCAP redistribution layer to maximize self-resonance frequency and quality factor over wide frequency range, resulting to a 6 μm width to support the current consumption.

Each matching network is designed in a T-configuration of three inductors at the beginning, and then converted into a transformer. Figure 43 shows how it is converted.

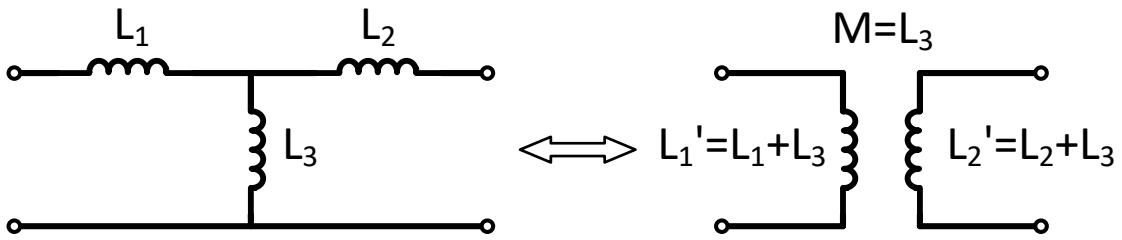

Figure 43. T-network and transformer

To find the values of L_1, L_2, and L_3 for each matching network, the Smith Chart is used. The effects on the impedance of changing inductance are capacitance values are depicted in Figure 44 [47].

i. Consider a network with a series inductor, if its inductance increases, then, on the Smith Chart, the impedance looking into the network will travel clockwise on the constant-resistance circles, as shown in the top left graph of Figure 44.

ii. Consider a network with a shunt inductor, if its inductance decreases, then, on the Smith Chart, the impedance looking into the network will travel counterclockwise on the constant-conductance circles, as shown in the bottom left graph of Figure 44.

iii. Consider a network with a series capacitor, if its capacitance decreases, then, on the Smith Chart, the impedance looking into the network will travel counterclockwise on the constant-resistance circles, as shown in the top right graph of Figure 44.

iv. Consider a network with a shunt capacitor, if its capacitance increases, then, on the Smith Chart, the impedance looking into the network will travel clockwise on the constant-conductance circles, as shown in the top left graph of Figure 44.

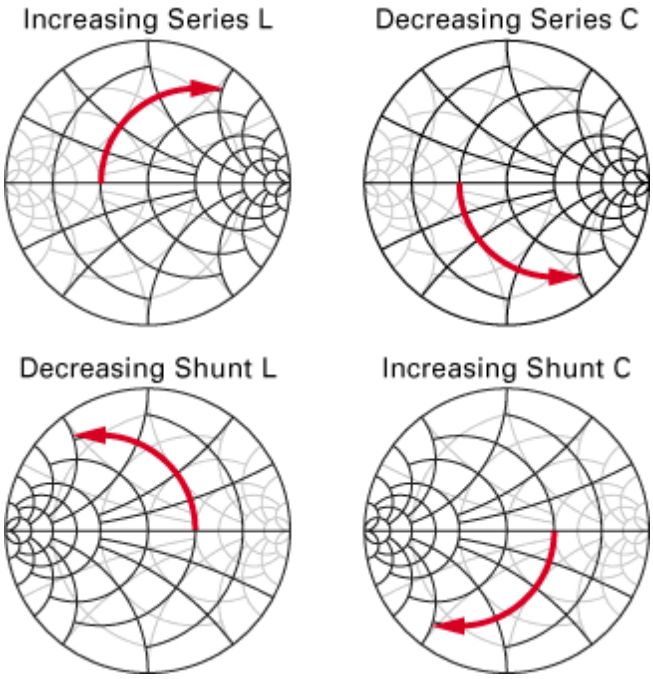

Figure 44. L and C on the Smith Chart

Figure 45 shows how the Smith Chart is used to determine the values of L_1, L_2, and L_3 of each matching network. To ensure that the maximum power is transferred, conjugate matching is performed. The steps are as follows:

i. Plot the source impedance (Z_{source}) and load impedance (Z_{load}) on the Smith Chart. One of them needs to be a conjugate value. In this case, the conjugate of Z_{source}, Z_{source}*, is plotted.

ii. Starting from Z_{load}, the series L_2 is added to convert the impedance from Z_{load} to Point A.

iii. The shunt L_3 is added to convert the impedance from Point A to Point B.

iv. The series L_1 is added to convert the impedance from Point B to Z_{source}*.

v. Adjusting the values of L_1, L_2, and L_3 to make sure that the impedance finally reaches Z_{source}*.

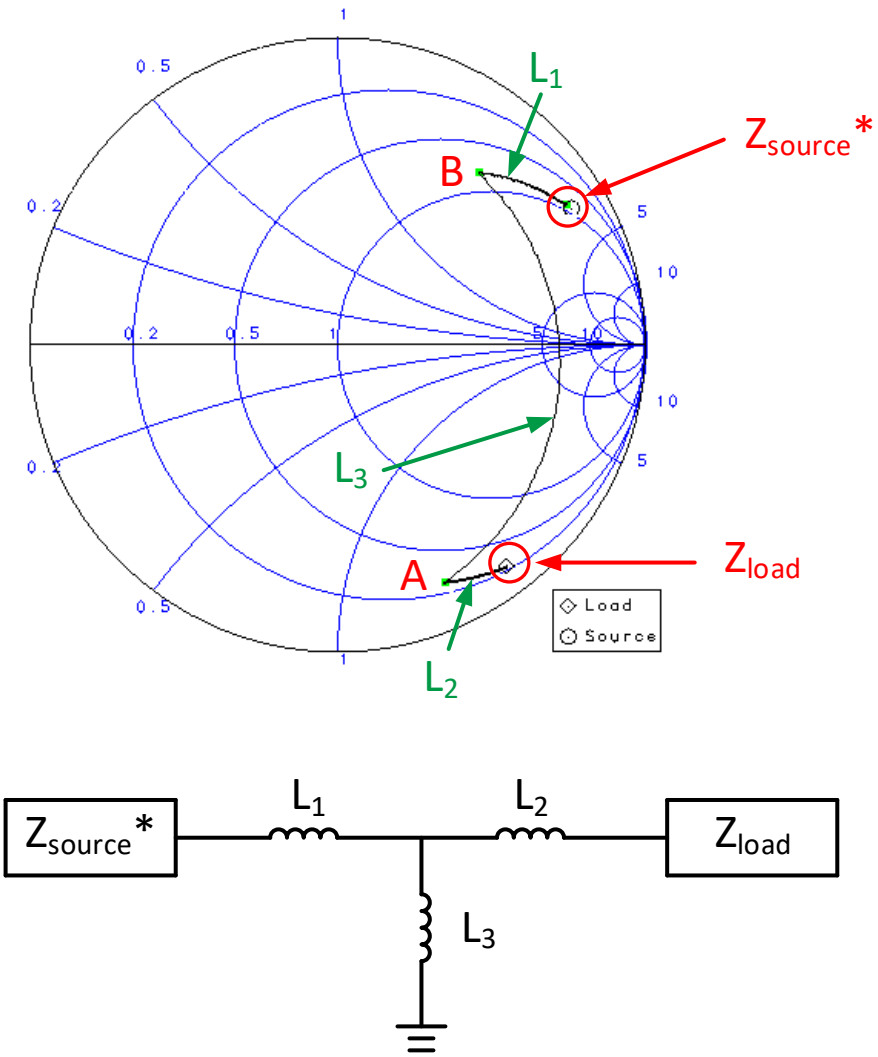

Figure 45. Matching using the Smith Chart

Once the values of L_1, L_2, and L_3 are found, the matching network can be converted to a transformer. The transformer is laid out in ADS Momentum. To simulate if the transformer has required values of L_1', L_2', and M, the electromagnetic (EM) simulation is conducted. The EM simulation can simulate the S-parameters of the layout of a passive structure. The setup of EM simulation of the transformer is shown in Figure 46.

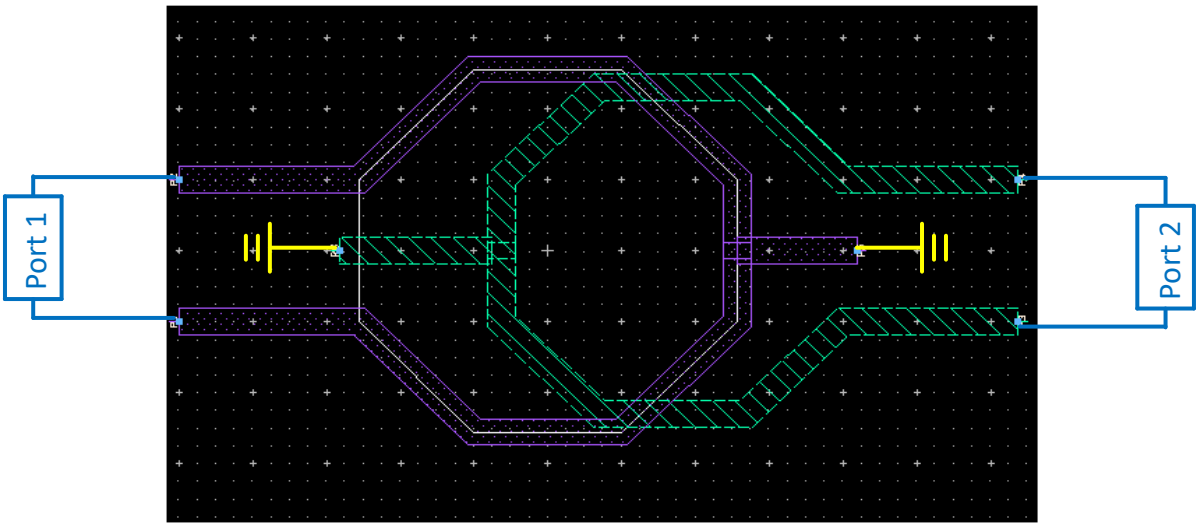

Figure 46. Setup of EM simulation

The transformer is simulated as a two-port network. For inductors with center-taps, the center-taps are grounded. Once the S-parameters are simulated, they can be converted to Z-parameters and Y-parameters through simulation.

For two-port networks, conversion from S-parameters to Z-parameters is as follows:

$$Z_{11} = \frac{(1 + S_{11})(1 - S_{22}) + S_{12}S_{21}}{\Delta S} \cdot Z_0 \qquad (4.11)$$

$$Z_{12} = \frac{2S_{12}}{\Delta S} \cdot Z_0 \tag{4.12}$$

$$Z_{21} = \frac{2S_{21}}{\Delta S} \cdot Z_0 \tag{4.13}$$

$$Z_{22} = \frac{(1 - S_{11})(1 + S_{22}) + S_{12}S_{21}}{\Delta S} \cdot Z_0 \tag{4.14}$$

Where Z_0 is the characteristic impedance of the system, and

$$\Delta S = (1 - S_{11})(1 - S_{22}) - S_{12}S_{21} \tag{4.15}$$

And the Y-parameters matrix is simply the inverse of the Z-parameters matrix:

$$\begin{bmatrix} Y_{11} & Y_{12} \\ Y_{21} & Y_{22} \end{bmatrix} = \frac{\begin{bmatrix} Z_{22} & -Z_{12} \\ -Z_{21} & Z_{11} \end{bmatrix}}{\Delta \mathrm{Z}} \tag{4.16}$$

Where

$$\Delta \mathrm{Z} = Z_{11}Z_{22} - Z_{12}Z_{21} \tag{4.17}$$

The values of L_1', L_2', M, k (coupling factor) and the Q (quality factor) of L_1' and L_2' can be calculated from the Z-parameters and Y-parameters as follows:

$$L_1{}' = \frac{Im\{Z_{11}\}}{2\pi f} \tag{4.18}$$

$$Q_1 = \frac{Im\{Y_{11}\}}{Re\{Y_{11}\}} \tag{4.19}$$

$$L_2{}' = \frac{Im\{Z_{22}\}}{2\pi f} \tag{4.20}$$

$$Q_2 = \frac{Im\{Y_{22}\}}{Re\{Y_{22}\}} \tag{4.21}$$

$$M = \frac{Im\{Z_{21}\}}{2\pi f} \tag{4.22}$$

$$k = \frac{M}{\sqrt{L_1{}' L_2{}'}} \tag{4.23}$$

After these values are calculated, they are compared to the required values. If they do not match the required values, the layout of the transformer needs to be modified and simulated again until the required values are obtained.

Table 4 lists the final simulated parameters of all three transformers at 60 GHz.

Table 4. Parameters of the matching networks

	Input transformer	Inter-stage transformer	Output transformer
Inductance of L_1 (pH)	175	220	320
Q of L_1	17.4	18.7	14.4
Inductance of L_2 (pH)	282	200	242
Q of L_2	15.0	19.3	15.8
Mutual inductance (pH)	100	60	145
Coupling factor	0.45	0.29	0.52

In the transistor layout, the spacing between each finger exceeds the minimum spacing required by the DRC rules, leading to a 1 – 2 fF reduction of parasitic capacitance of the gate,

source, and drain nodes. With smaller parasitic capacitance, the transistors have better stability and smaller coupling to ground, which leads to higher f_{max}.

The supply voltage of the process is 1.2 V. The nominal threshold voltage (V_{th}) of this transistor is 0.37 V from simulation. To bias the PA at Class-AB, the first stage is biased at 0.4 V, and the second stage at 0.47 V. The first stage is biased lower than the second stage to save DC power consumption because it works with lower power levels than the second stage.

4.3 Measurement Results

The PA was fabricated in a 65 nm 8-metal CMOS process. Figure 47 shows the die photo of the PA. The area of the PA is 100 × 550 μm^2, excluding the pads. The measurement is carried out on-wafer probing.

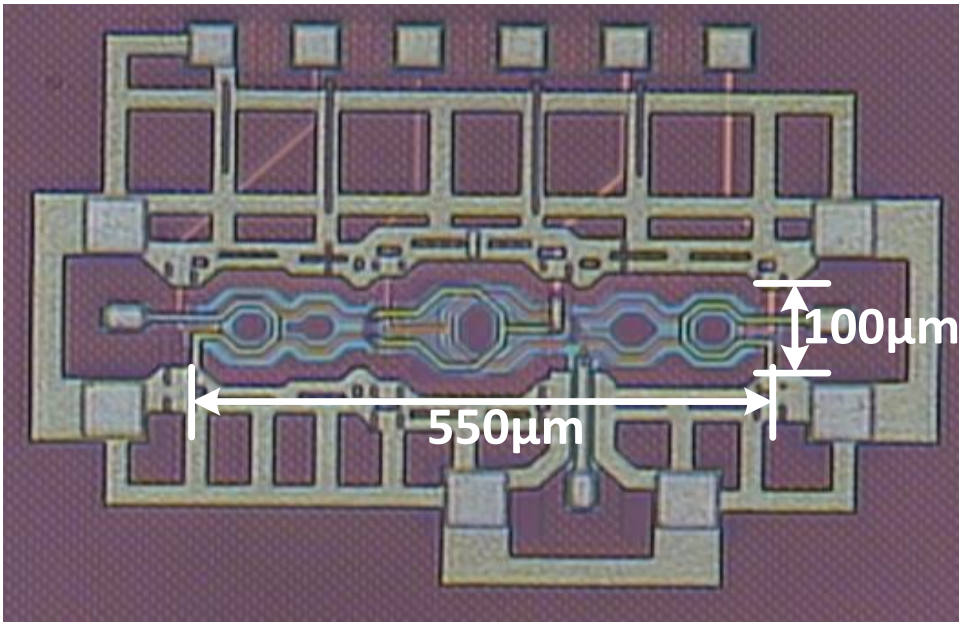

Figure 47. Die photo of the conventional PA

Figure 48 illustrates the measured and simulated S-parameters. The measured peak of S_{21} is 12 dB at 61 GHz, the small-signal gain is rather flat over more than 10 GHz. The 3-dB bandwidth is 14 GHz, ranging from 58 to 72 GHz. Measured return loss is below -10 dB from 65 to 75 GHz, and from 57 to 71 GHz at the input and the output ends, respectively. S_{12} is below -34 dB across the entire band. Simulation results agrees well with measured data.

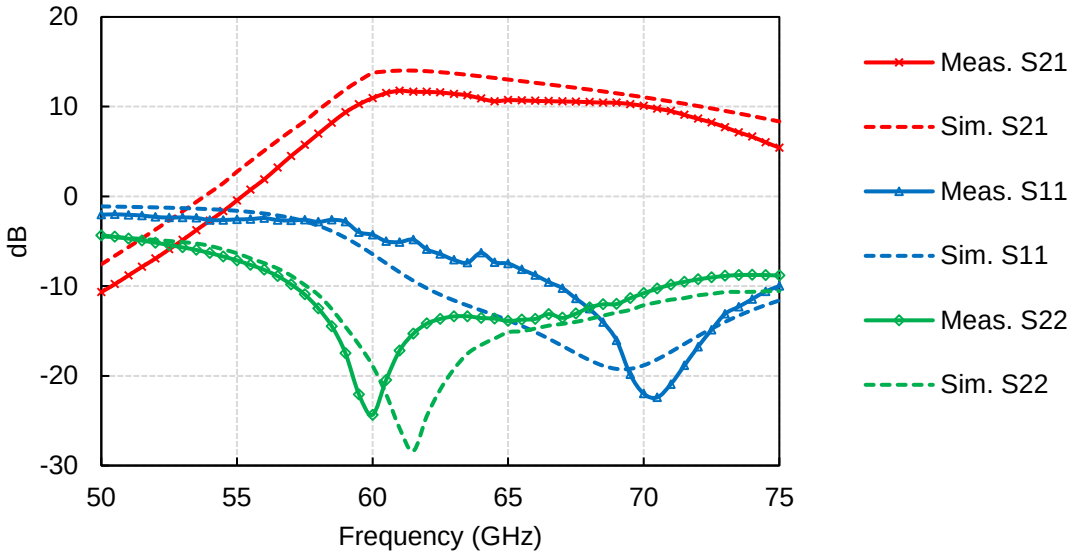

Figure 48. Small-signal measurement and simulation results

The large-signal measurement is conducted from 58 to 67 GHz due to the signal source limitation. The measured peak PAE, power gain, and P_{SAT} across this band are shown in Figure 49. Across this band, the peak PAE varies from 19.7% to 28.9%, P_{SAT} varies from 8.5 dBm to 9.2 dBm, and power gain varies from 11.8 dB to 13.9 dB.

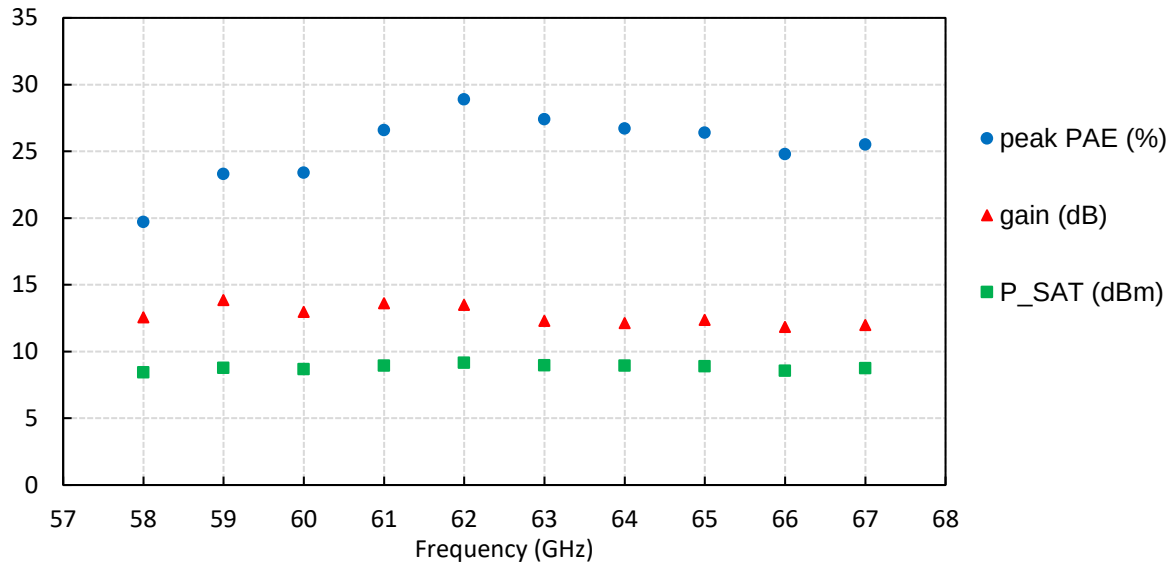

Figure 49. Large-signal performance from 58 to 67 GHz

Figure 50 shows the large-signal measurement and simulation results at 62 GHz. At -16 dBm input power level, the measured power gain is 13.5 dB. The measured P_{SAT} and peak PAE are 9.1 dBm and 27.9% at input power of 4 dBm and -0.3 dBm, respectively. Simulation results are in good agreement with the measurement data. The DC power consumptions are 11.6 and 24 mW at input power of -16 dBm and 4 dBm, respectively.

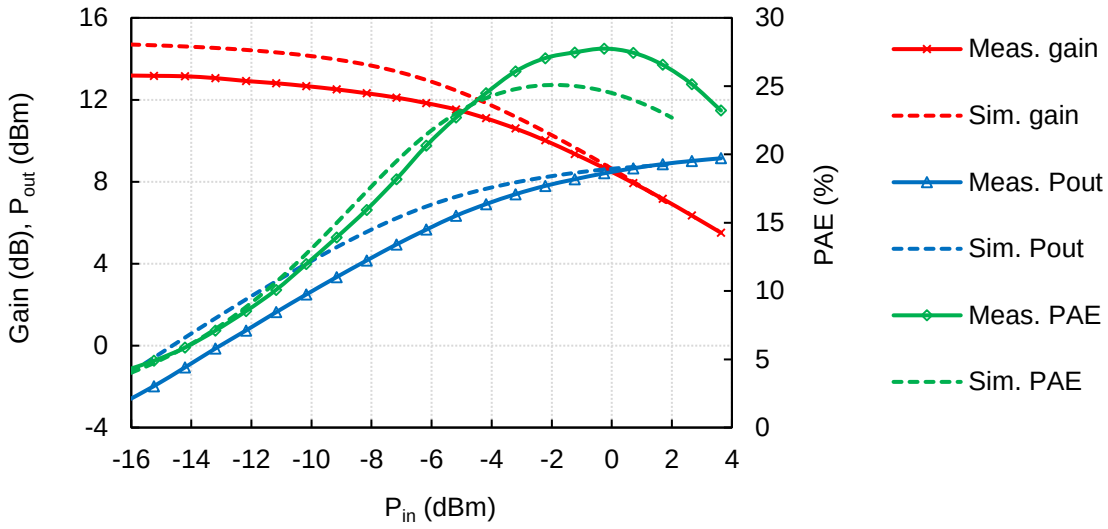

Figure 50. Large-signal measurement and simulation results at 62 GHz

The linear PAE of the PA is measured using the two-tone method. Two signal sources with equal power level and 1 MHz of frequency apart from each other are fed into the PA. The output of the PA is connected to an Agilent E4407B spectrum analyzer.

Figure 51 is a screenshot of the measured spectrum. The input power is -11 dBm each and the output power shown here is before de-embed. The center frequency is 62 GHz, and the resolution bandwidth is 1 kHz. IMD_3 increases as the input power level increases.

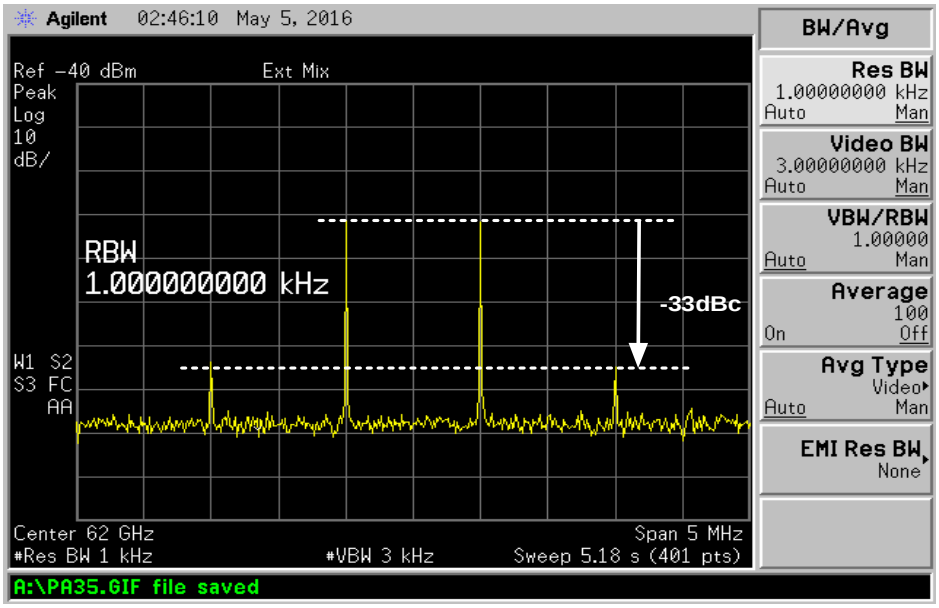

Figure 51. Two-tone measurement

Figure 52 plots the PAE versus IMD_3 at four different frequencies. At IMD_3 = -33 dBc, the PAE is 6.5%, 8%, 10%, and 6.5% at 60 GHz, 61 GHz, 62 GHz, and 63 GHz, respectively.

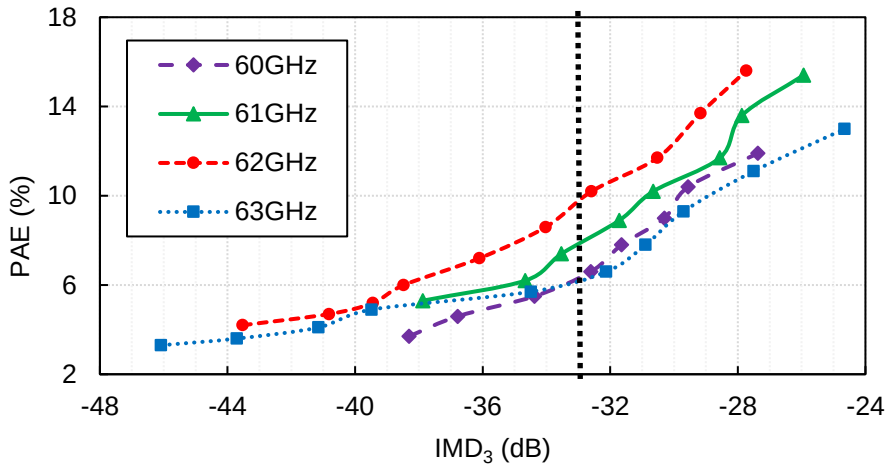

Figure 52. PAE vs. IMD_3

4.4 Parametric PA Design

Figure 53 shows the improved PA with parametric matching networks. As can be seen in Figure 55, the PA output capacitance increases with input power level, resulting in reduced linearity of the power amplifier. To overcome this nonlinearity, the varactors are added at the output of the second stage. The varactors are realized with NMOS devices with source and drain tied together.

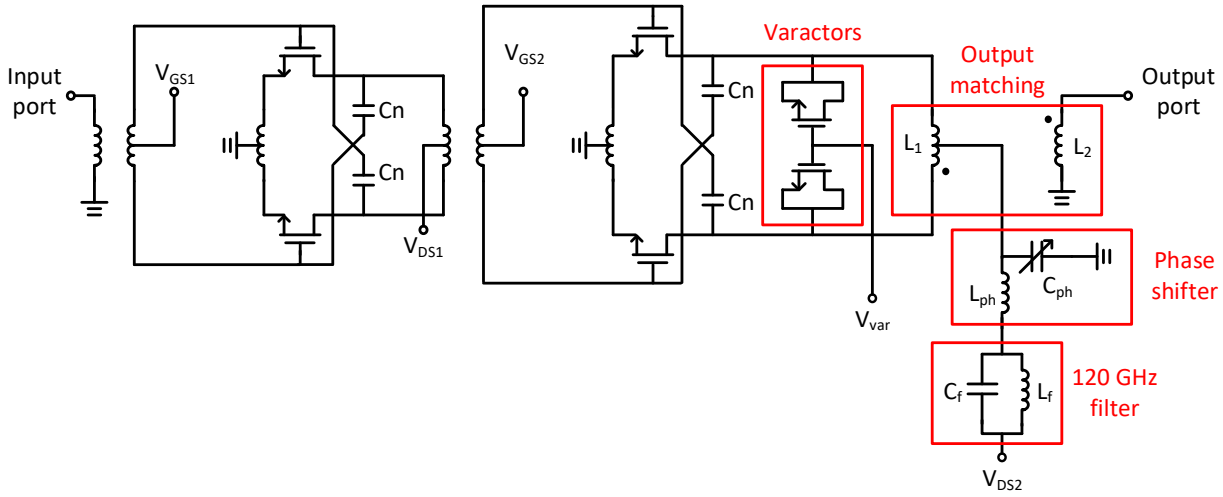

Figure 53. Schematic of the improved 60-GHz PA

As input power increases, the capacitance seen at the output of the PA also increases. The varactor acts in the opposite way. That is, when the input power increases, its capacitance decreases. Figure 54 shows the capacitance simulation setup of the PA output without the pair of varactors (C_{OUT}), the pair of varactors (C_{VAR}), and the PA output with the pair of varactors (C_{OUT}').

Figure 55 plots the simulation results of these three capacitances. Without varactors, the output capacitance of the PA is simulated to be 12.5 fF when input power is -16 dBm and 20.1 fF

when input power is 2 dBm, which shows a 60.8% increase. On the other hand, the varactor decreases from 7.2 fF when input power is -16 dBm to 4.5 fF when input power is 2 dBm, indicating a 37.5% decrease. When combining the two capacitances, the final equivalent capacitance has a smaller variance. It varies between 21.4 fF and 25 fF, which shows a variance of 16.8%.

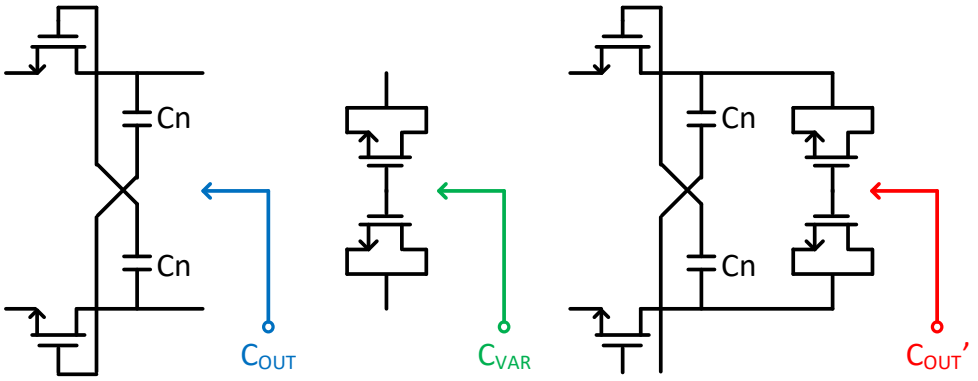

Figure 54. Simulation setup of output capacitance

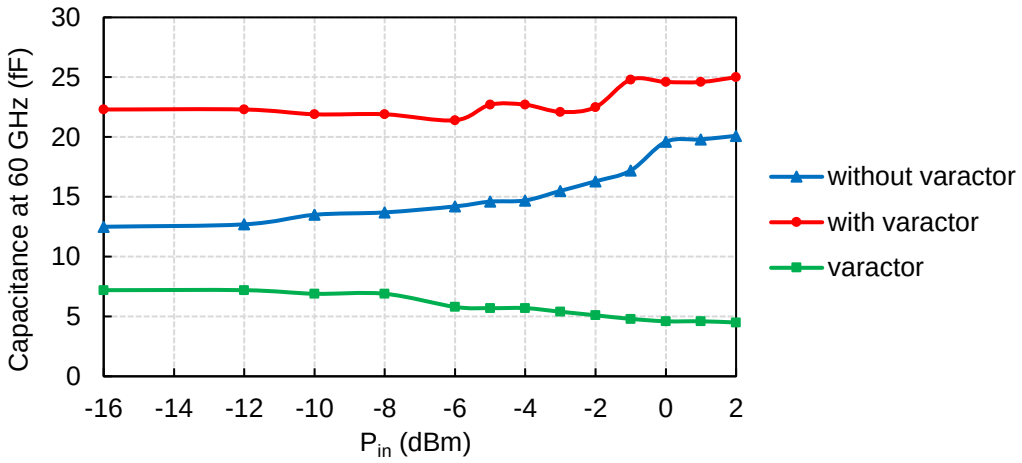

Figure 55. Simulated capacitance

However, the varactors introduce loss to the output load, and thus deteriorates the power gain. To maintain a high enough gain, the varactor cannot be too large. The size of this pair of varactors is 2μm / 1μm. To further study the effects of the size of the varactors, various sizes of varactors are simulated and compared.

Figure 56 plots the C_{OUT}' (as shown in Figure 54) for four different sizes of varactors compared to when there is no varactor.

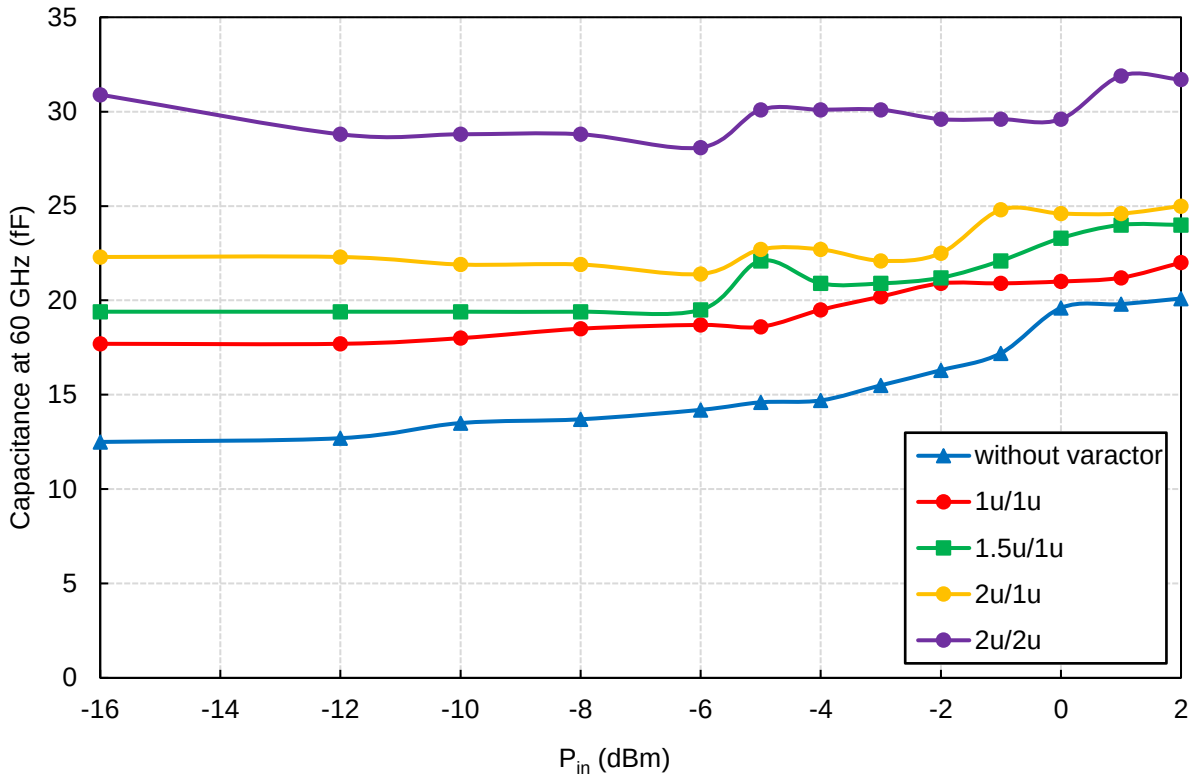

Figure 56. Output capacitance with various sizes of varactors

Table 5. Output capacitance with various sizes of varactors

C_{OUT}'	Smallest value (fF)	Largest value (fF)	Variance
Without varactor	12.5	20.1	60.8%
1μm / 1μm	17.7	22	24.3%
1.5μm / 1μm	19.4	24	23.7%
2μm / 1μm	21.4	25	16.8%
2μm / 2μm	28.1	31.9	11.9%

Table 5 lists the variance of C_{OUT}' of these five cases. Larger varactors reduce the variance drastically, but at a price of increasing the total output capacitance. The varactors of 2μm / 2μm reduces the variance from 60.8% to only 11.9%, but the overall output capacitance is increased from [12.5 fF, 20.1 fF] to around 30 fF. This results in the drop of power gain of the PA.

For each of the four varactors (1μm / 1μm, 1.5μm / 1μm, 2μm / 1μm, 2μm / 2μm), a PA is designed and simulated. With different sizes of varactors, the overall output capacitances are different, which require different sets of matching networks. To design the matching networks, the load-pull process is performed on these four PAs. The power gain of the four PAs with different phases (of the phase shifter as shown in Figure 53) is simulated and plotted in Figure 57, Figure 58, Figure 59, and Figure 60.

For each PA, the best result when the phase of the pump is aligned well with the phase of the output signal is plotted in solid lines. If the phase is not aligned well, two results happen: 1, the

power gain is boosted when P_{in} is low, but drops much faster; 2, the power gain is suppressed. These two types of results are plotted in dotted lines for each PA.

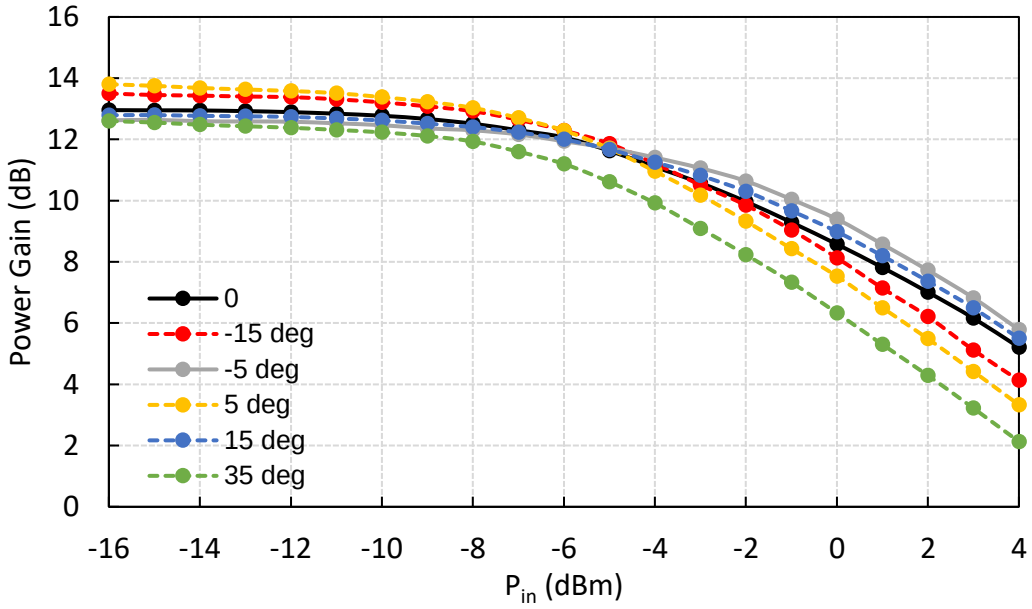

Figure 57. Power gain vs. Pin, varactors size = 1 µm /1 µm

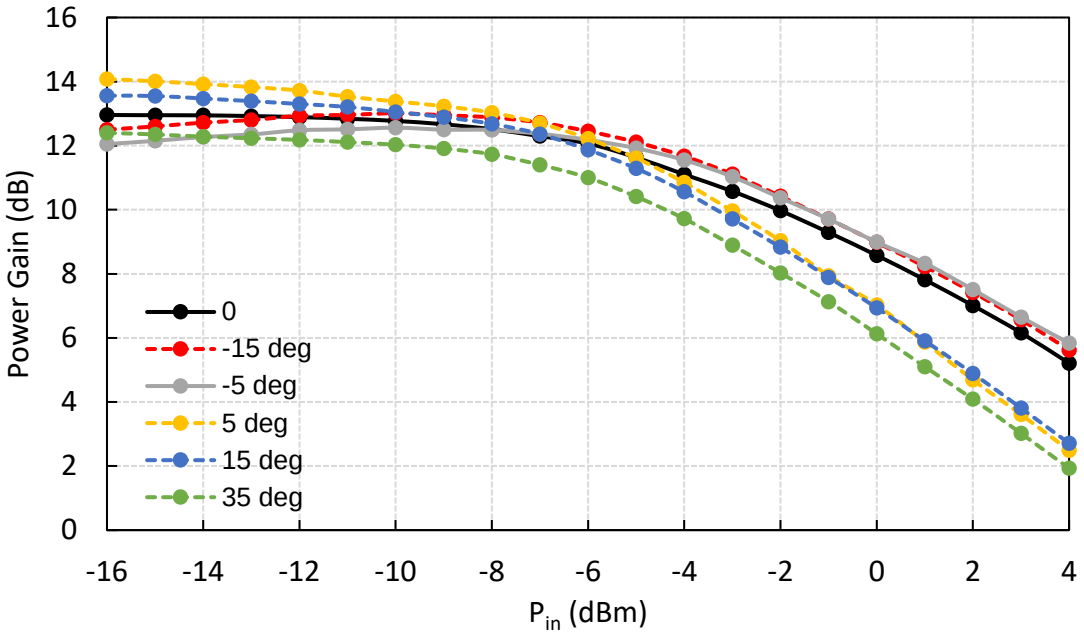

Figure 58. Power gain vs. Pin, varactors size = 1.5 µm /1 µm

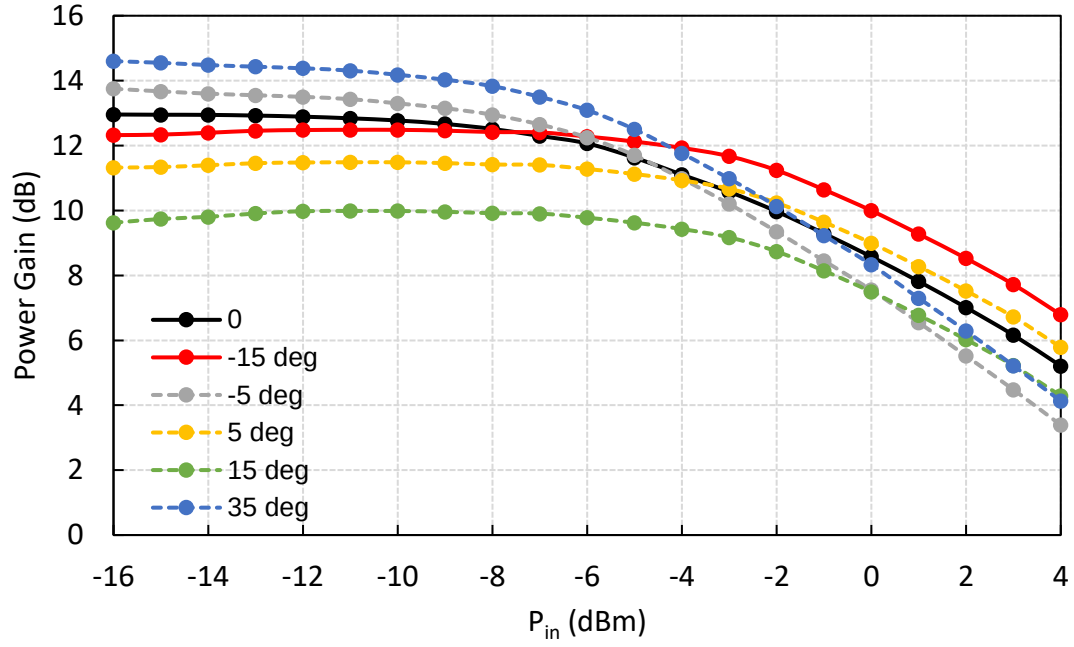

Figure 59. Power gain vs. Pin, varactors size = 2 µm /1 µm

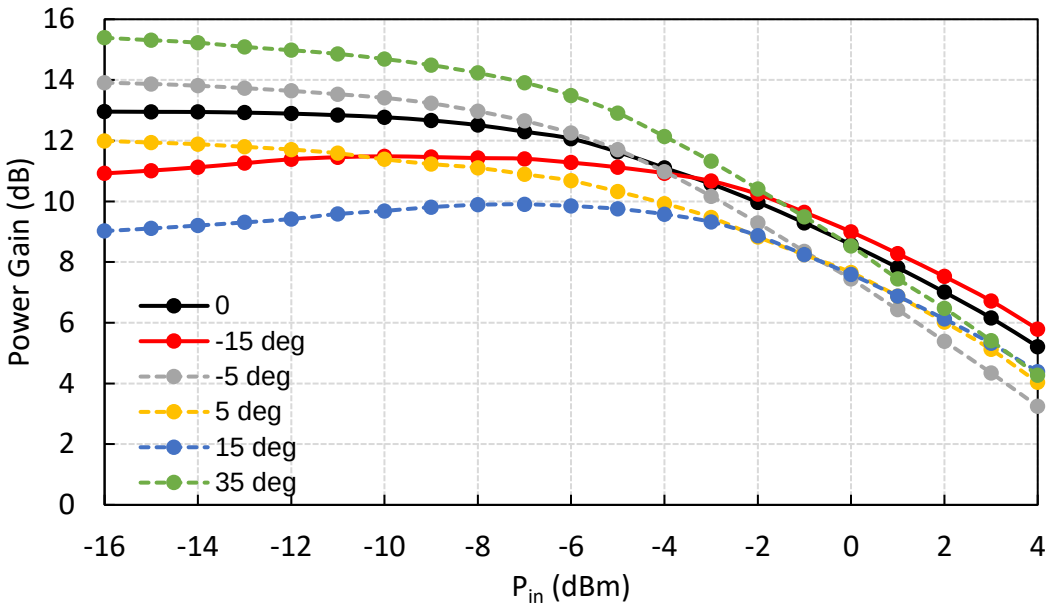

Figure 60. Power gain vs. Pin, varactors size = 2 μm /2 μm

Figure 61 plots the best result of power gain improvement for each varactor size. As predicted, smaller varactors have less impact on the power gain. The largest varactors (2μm / 2μm) lead to the highest P_{1dB} among the four cases, but also cause the largest amount of gain drop.

Table 6 summarizes the gain drop and P_{1dB} improvement for each varactor size. The P_{1dB} needs to be improved but the power gain cannot be sacrificed too much. As a result, the size of 2μm / 1μm is chosen. With this size of varactors, the P_{1dB} is improved by 4 dB while the gain drop is only 0.64 dB.

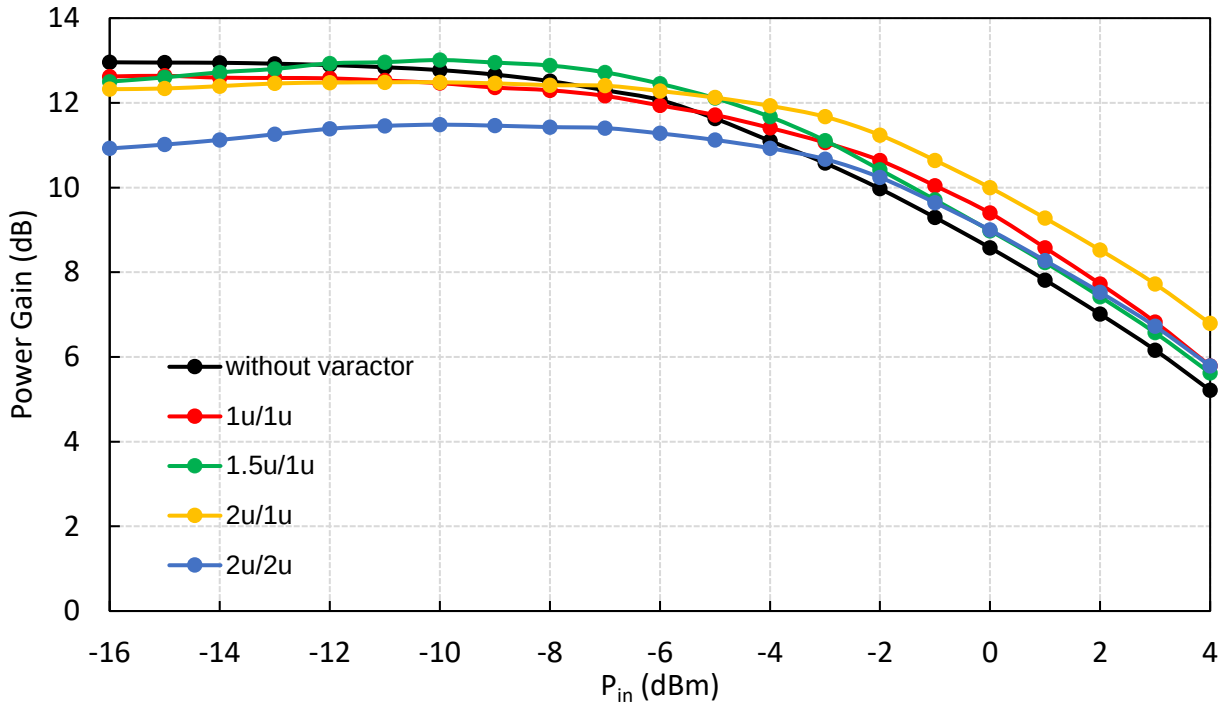

Figure 61. Improvement of power gain for different sizes of varactors

Table 6. Gain drop and P_{1dB} improvement for different sizes of varactors

Varactor size	Gain drop (dB)	IP_{1dB} (dBm)
No varactor	N/A	-6
1µm / 1µm	0.34	-5
1.5µm / 1µm	0.46	-4
2µm / 1µm	**0.64**	**-2**
2µm / 2µm	2.04	-1

C_f and L_f form an LC filter, which resonates at 120 GHz, to boost the second-harmonic tone at the virtual ground. With this filter, the second harmonic tone sees a high impedance, and is kept at this node from leaking into the ground. As shown in Figure 62, different sets of values of C_f and L_f is simulated, and 200 pH and 8.83 fF are used to construct this filter, whose Q is 50.

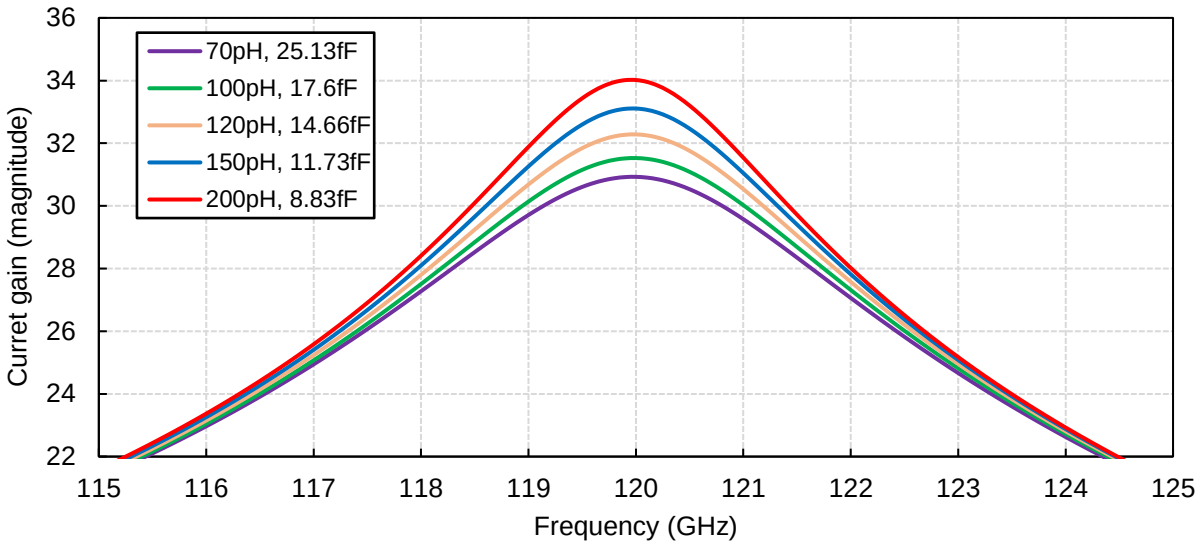

Figure 62. Q-factor of the LC filter

4.5 Performance Improvement

Simulation shows that linearity is significantly improved with the parametric matching network. Figure 63 below plots the power gain, output power, and PAE vs. input power of powers amplifiers with conventional matching network and parametric matching network. For the conventional PA, the power gain starts to drop at an input power level of as low as -11 dBm, and the input P_{1dB} is -6 dBm. With parametric matching network, the input P_{1dB} is -2 dBm. Although at low input power level, the power gain is lower than that of the conventional PA, it increases as

input power becomes larger before dropping. As the input power increases from -16 to -8 dBm, the power gain increases. It then starts to drop after 8 dBm.

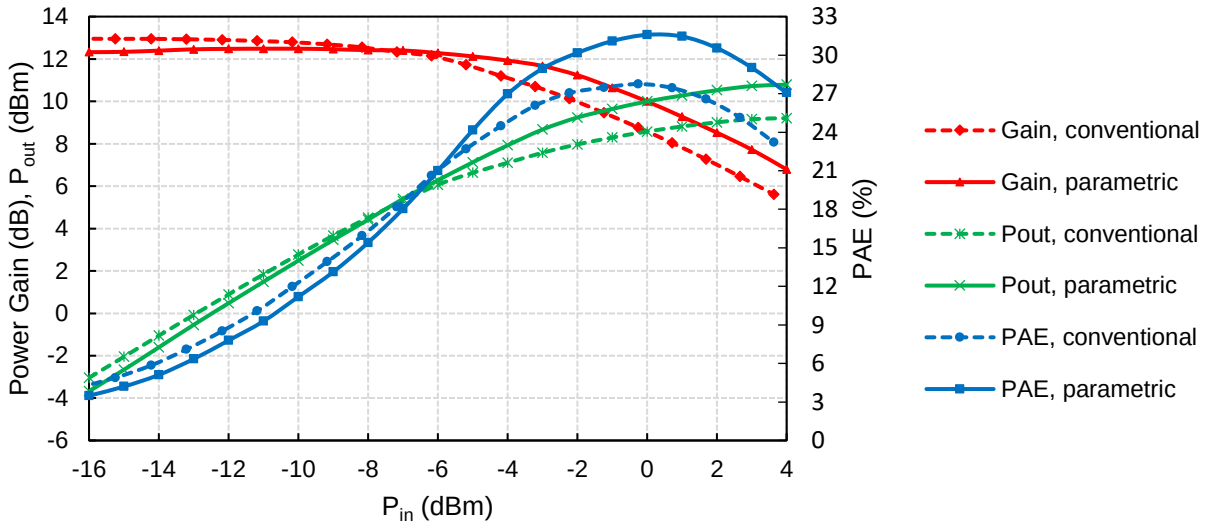

Figure 63. Improvement on large-signal performance

Figure 64 plots PAE and output power versus the back-off points from P_{1dB}. The plots of two cases are normalized to their back-off points from P_{1dB}, i.e., "0" in the x-axis represents IP_{1dB}, "-6" represents -6 dB back-off from IP_{1dB}, etc. Since the IP_{1dB} of PA with parametric matching network is 4 dB higher than that of the other PA, the PAE at each back-off point is consequently higher. At -6 dB back-off, the PAE of the conventional PA is only 8.8%, whereas the PAE of the PA with parametric matching network is 15.4%, which is significantly improved.

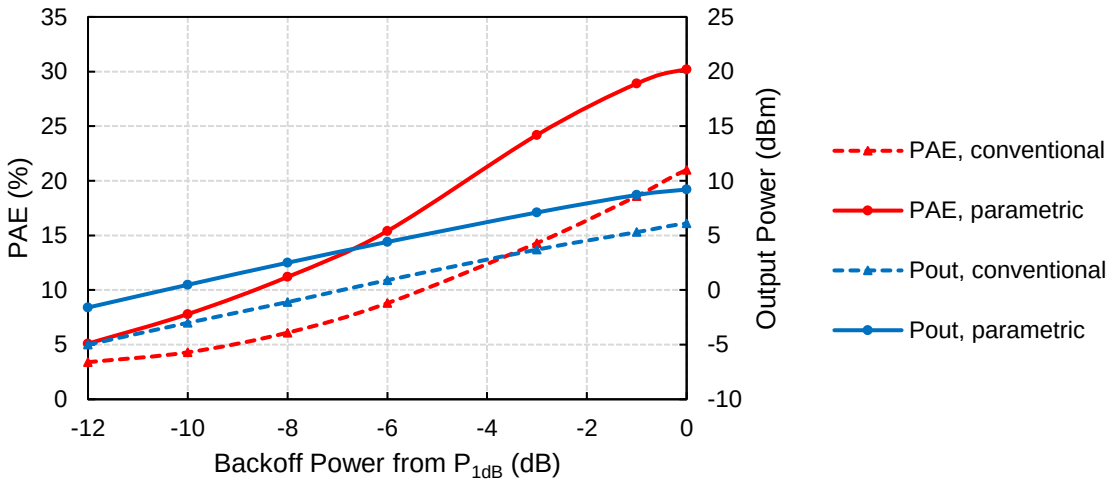

Figure 64. PAE and Pout vs. power back-off

Figure 65 plots the simulated AM-AM distortion vs. input power of the parametric PA and the conventional PA.

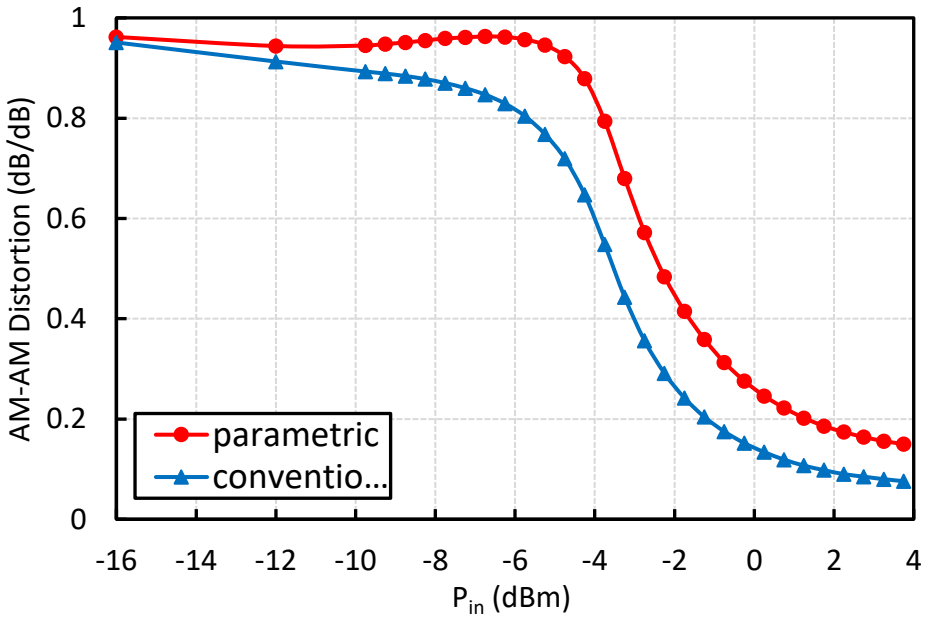

Figure 65. AM-AM distortion vs. P_{in}

Figure 66 plots the simulated AM-AM distortion vs. input power of the parametric PA and the conventional PA.

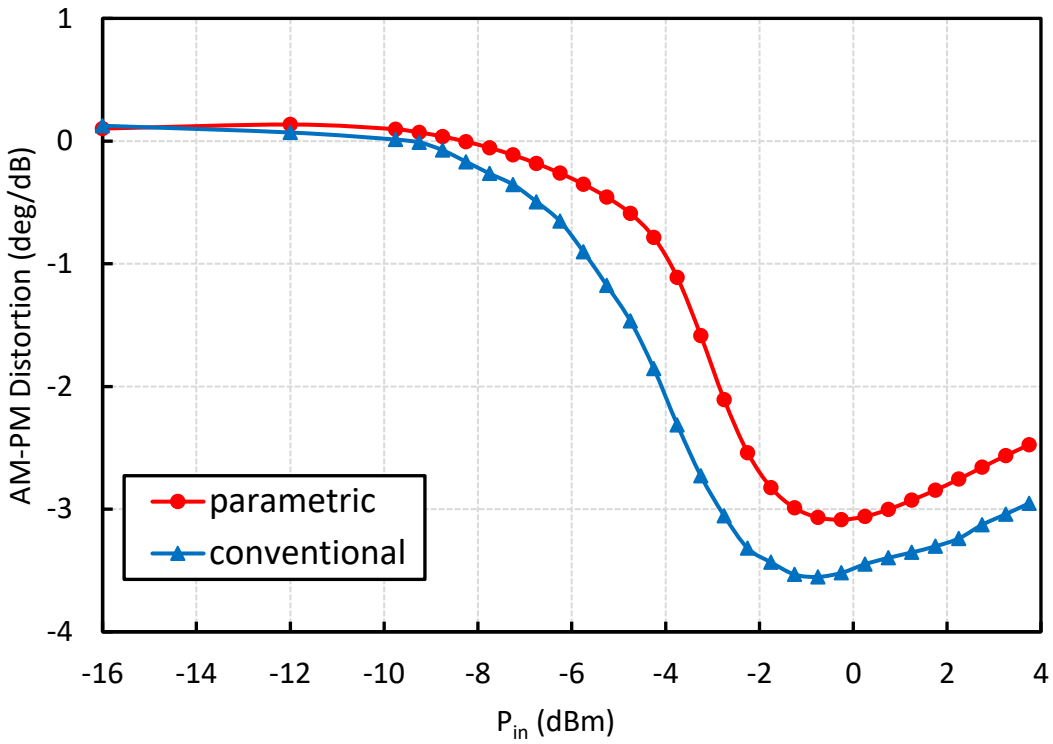

Figure 66. AM-PM distortion vs. P_{in}

4.6 Results Summary

In this parametric PA design, PAE and linearity are both improved. For PAs, high linearity is demanded in QAM, which is one of the most popular modulation schemes in modern wireless communication systems. And high PAE at back-off power is demanded in OFDM, which is one of the most popular coding schemes in modern wireless communication systems.

In existing parametric amplifiers, an external pump is needed. In this work, the pump is generated from the PA itself, eliminating the need of an extra circuitry to produce the pump. This reduces the overall complexity, saves circuit area, as well as DC power supply.

Table 7 summarizes the performance parameters of the conventional PA and the parametric PA.

Table 7. Performance Comparison between Conventional and Parametric PAs

	Conventional PA	Parametric PA	Improvement
P_{SAT} (dBm)	9.1	10.8	1.7 dB
IP_{1dB} (dBm)	-6	-2	4 dB
OP_{1dB} (dBm)	6	9	3 dB
Peak PAE (%)	28	32	12.5%
PAE @ 6-dB back-off (%)	8.8	15.4	75%
PAE @ 8-dB back-off (%)	6.1	11.2	84%

Table 8 below compares the results of this work and some of the previous works. Although the P_{SAT} is not high in work, but the linear PAE is improved significantly. In real applications, several of these PAs can be combined to achieve high total P_{SAT}.

Table 8. Results comparison of 60-GHz PAs

	Freq. (GHz)	**CMOS Process**	**Peak PAE (%)**	**PAE @ 6dB Back-off (%)**	**PAE @ 8dB Back-off (%)**	**P_{SAT} (dBm)**
[48]	57 – 65	28nm SOI	21	~10	8	18.8
[49]	40 – 67	28nm bulk	16	~5	~3	13.3
[50]	50 – 67	28nm bulk	20.5	~5	N/A	17.9
[51]	59 – 67	40nm bulk	23	<8	N/A	16.4
This Work	**58 – 72**	**65nm bulk**	**31**	**15**	**11**	**9.1**

This work focuses on optimizing PAE and linearity, rather than optimizing the P_{SAT}. As analyzed in section 5.1, for 60 GHz applications, the allowed range of the total EIRP for a 4x4 transmitter array ($EIRP_{TX}$) is limited between -1 to 14 dBm. Thus, in this parametric amplification PA design, a P_{SAT} of 9 dBm is set as the design goal. In real-world applications, PAs with this range of P_{SAT} can be used to construct a beamforming system, in which many PAs with smaller P_{SAT} are formed into an array to produce a larger P_{SAT} [52].

It is worth to note that this parameter amplification PA design methodology and techniques can be applied to a PA design where the linearity and output power enhancement is required. As analyzed in Chapter 3, parametric amplification depends on the frequency and phase of the pump

and does not depends on the power level of the signal. Therefore, it can be applied to PAs with any power level.

CHAPTER 5: NON-LINEAR VARACTOR-BASED MIXER DESIGNS

5.1 Background

The non-linearity of the varactors can also be applied to mixers to improve their performances. In this section, the basic concepts of mixers [53] are explained.

A mixer is a three-port circuit that performs frequency translation. A mixer in a transmitter is called an **up-conversion mixer**. It inputs baseband or IF frequencies and outputs RF frequency. A mixer in a receiver is called a **down-conversion mixer**. It inputs RF frequency and outputs baseband or IF frequencies.

The three ports are: the **RF port**, the **LO port**, and the **IF por**t or the **baseband port**. The frequencies at the RF port and the LO port is usually high, and the frequency at the IF port is usually low.

The relationship of the three frequencies is as follows:

$$\omega_{IF} = |\omega_{RF} - \omega_{LO}| \tag{5.1}$$

Or:

$$A\cos\omega_{IF}t = A\cos(\omega_{RF} - \omega_{LO})t \tag{5.2}$$

To perform frequency conversion, two types of architectures can be used. In **heterodyne** architecture, several mixers are cascaded, and the frequency is converted in several stages. Figure 67 is a block diagram of a typical heterodyne receiver. In this system, two mixers are cascaded. The RF frequency is firstly converted to IF, the intermediate frequency, and then converted to baseband.

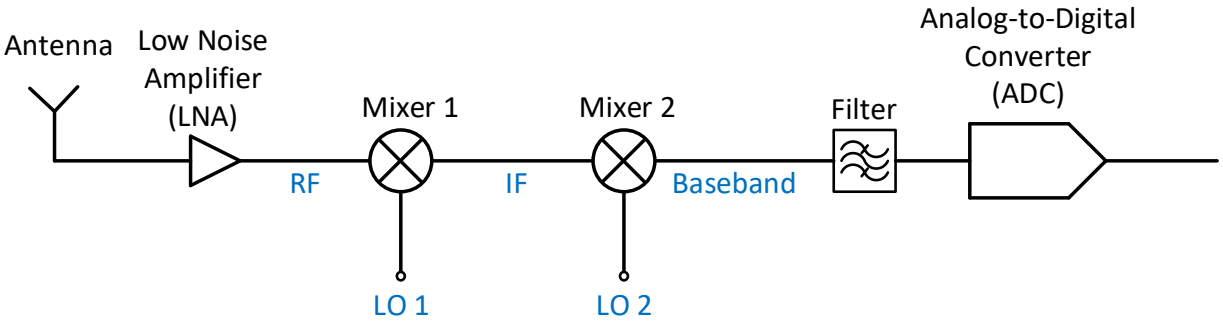

Figure 67. Heterodyne receiver

The other type of architecture is called **direct-conversion**, or **homodyne**. In this architecture, only one mixer is used to convert the RF frequency to baseband, or vice versa. Figure 68 is a block diagram of a typical direct conversion receiver. The RF frequency is directly converted to baseband by a single mixer.

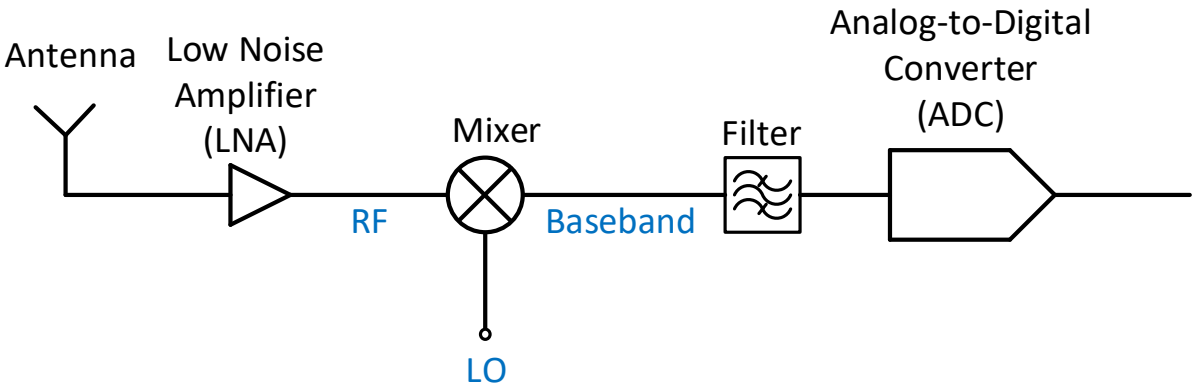

Figure 68. Direct-conversion receiver

For an up-conversion mixer, the **conversion gain** is the power of RF frequency minus the power of IF frequency. For a down-conversion mixer, the **conversion gain** is the power of IF frequency minus the power of RF frequency.

Besides power conversion gain, **voltage conversion gain** is also a design parameter to be considered. For down-conversion mixers, the voltage conversion gain is the ratio of the rms voltage of the IF signal to the rms voltage of the RF signal. And for up-conversion mixers, the voltage conversion gain is the ratio of the rms voltage of the RF signal to the rms voltage of the IF signal.

Image: Consider a heterodyne down-conversion mixer. From Equation (5.2), because of the nature of the cosine function that $\cos(\theta) = \cos(-\theta)$, whether $\omega_{in} - \omega_{LO}$ is positive or negative, it yields the same IF, as shown in Equation (7.3):

$$A\cos\omega_{IF}t = A\cos(\omega_{in} - \omega_{LO})t = A\cos(\omega_{LO} - \omega_{in})t \qquad (5.3)$$

This leads to the fact that both the frequencies above LO and below LO are converted to the same IF. As shown in Figure 69, the desired signal is below LO, the image is above LO, and their distance to LO is the same. As a result, both the desired signal and the image are down-converted to IF.

In direct-conversion mixers, there is no image problem. The RF is directly converted to baseband, whose center frequency is DC. This means that the RF and LO are the same frequency.

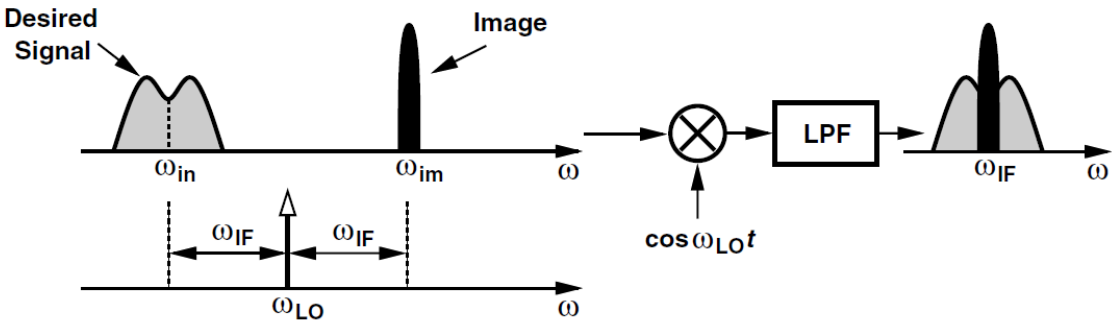

Figure 69. Signal and image

There are two types of noise figures for mixers: **single sideband (SSB) noise figure** and **double sideband (DSB) noise figure**.

SSB noise figure is the noise figure of the mixer that converts both signal band and image band to the output, as shown in Figure 70. This type of mixer is usually used in a heterodyne system.

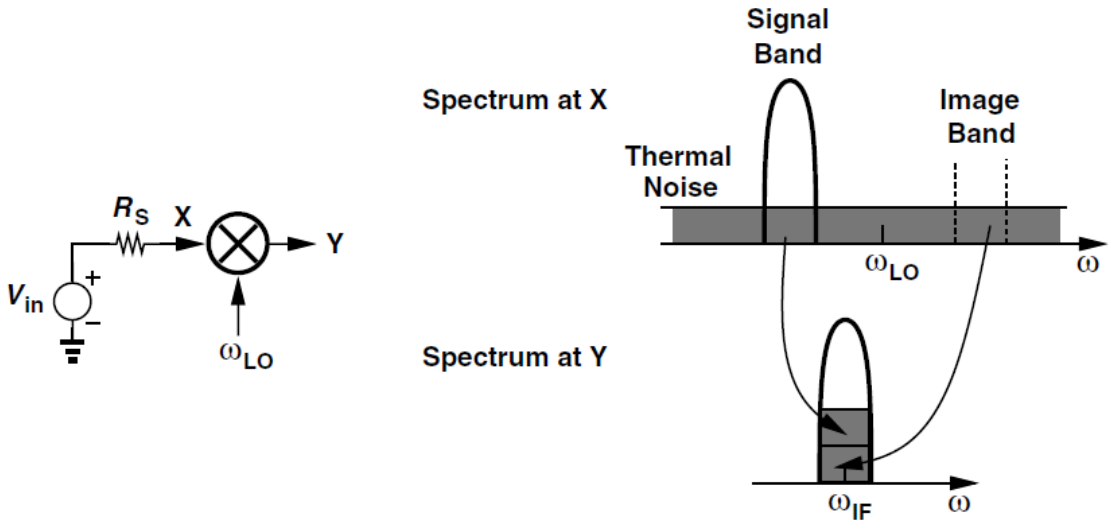

Figure 70. SSB noise figure

DSB noise figure is the noise figure of the mixer that converts only signal band to the output, as shown in Figure 71. This type of mixer is usually used in a direct-conversion system.

For a same mixer, its SSB noise figure is 3 dB higher DSB noise figure.

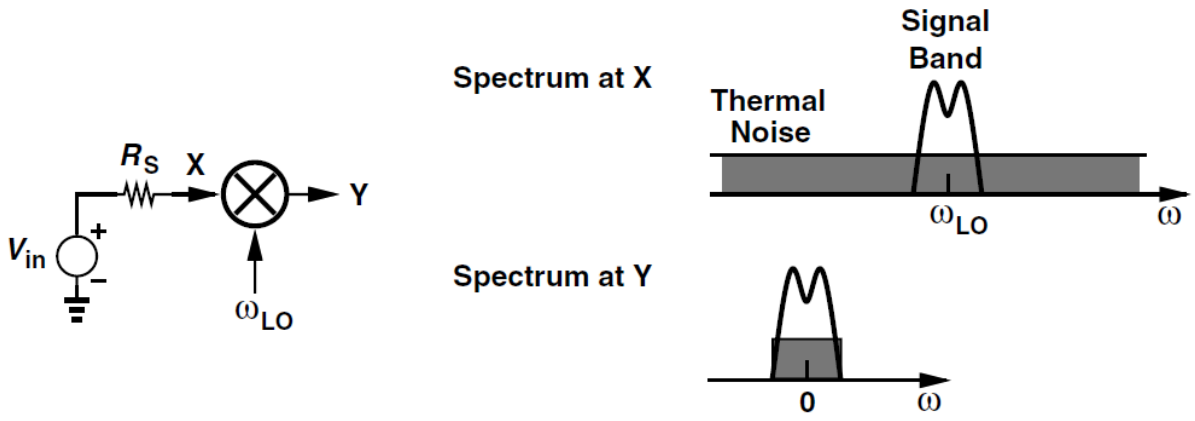

Figure 71. DSB noise figure

5.2 Types of Mixers

Mixers are generally categorized into passive mixers and active mixers. Passive mixers consume no DC power. They usually provide higher linearity but suffer from conversion loss. On the other hand, active mixers need constant DC current, and thus consume DC power. They provide higher conversion gain but suffer from limited linearity.

6.2.1 Passive mixers

In a passive mixer, the transistors operate as switches, and the mixer does not have gain. The most significant advantage of a passive mixer is that its noise figure is low. Figure 72 and Figure

73 are the schematic of a typical single-balanced passive down-conversion mixer and a double-balanced passive down-conversion mixer, respectively. A single-balanced mixer employs a simple gilbert cell as switching transistors, whereas in the double-balanced structure, two gilbert cells are cross-couple to prevent LO feedthrough.

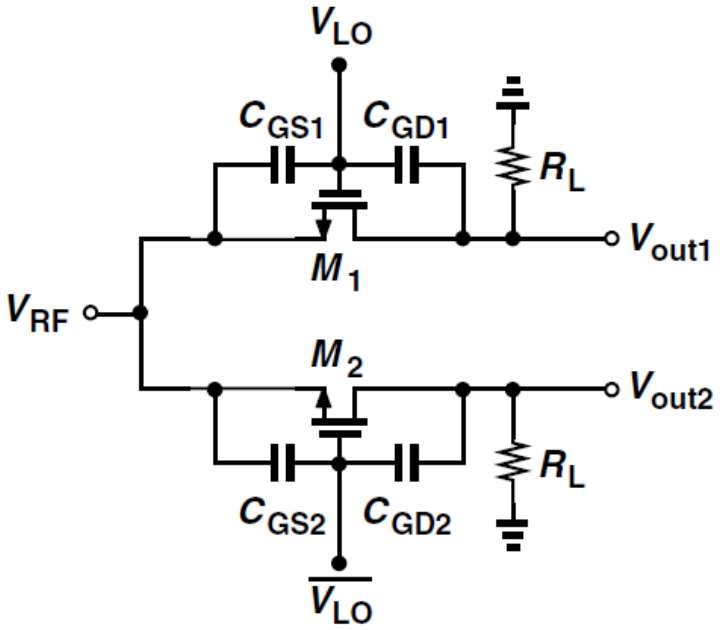

Figure 72. Passive single-balanced down-conversion mixer

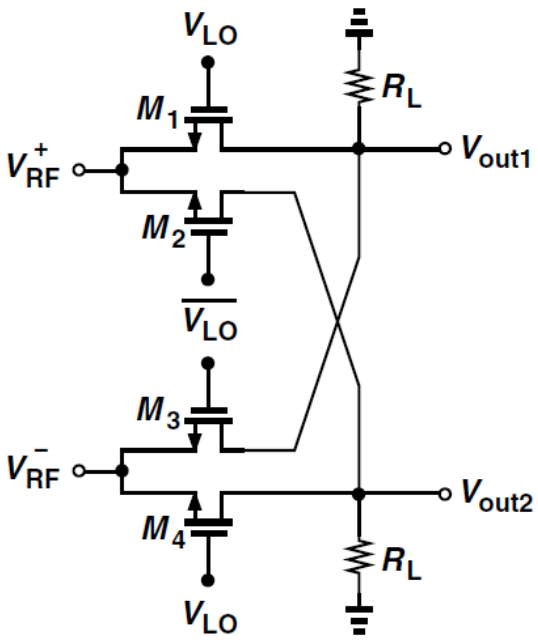

Figure 73. Passive double-balanced down-conversion mixer

6.2.2 Active mixers

An active mixer has a gain stage besides the pair of switching transistors. The gain stage amplifies the output signal, and thus the mixer can have gain. However, because of its gain, the noise figure is higher than that of a passive mixer. Figure 74 and Figure 75 are the schematic of a typical single-balanced active down-conversion mixer and a double-balanced active down-conversion mixer, respectively. In both topologies, there are transistors acting as amplifying devices at the bottom of the switching pairs.

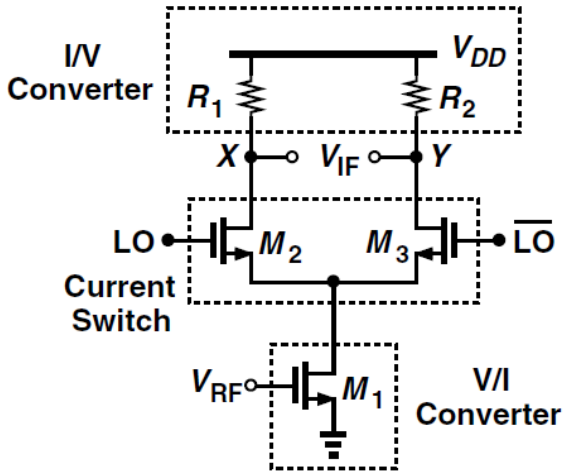

Figure 74. Active single-balanced down-conversion mixer

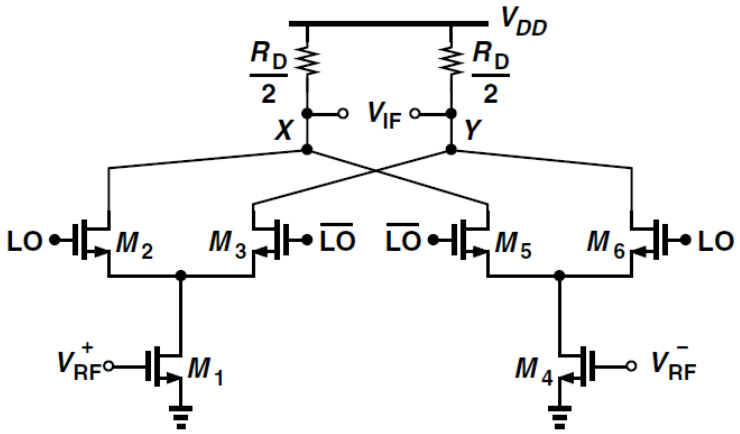

Figure 75. Active double-balanced down-conversion mixer

5.3 Non-Linear Transmission Line

The non-linear transmission line (NLTL) is a type of transmission line that is constructed of series inductors and shunt varactors [57], as shown in Figure 76. The difference between this transmission line and the conventional transmission line is that NLTL has varactors, instead of fix-valued capacitors.

Conventional transmission lines have dispersion effect, which causes the pulses to become wider, and causes the amplitude to become smaller. With the non-linear varactors, the non-linear transmission lines can compensate this effect. And when there is over-compensation, the pulses become sharper and taller.

When the voltage across the varactor increases, its capacitance decreases, and then the decreased capacitance leads to larger propagation velocity. As a result, for a pulse traveling along the NLTL, the portion with higher voltage propagates faster, and the portion with lower voltage propagates slower.

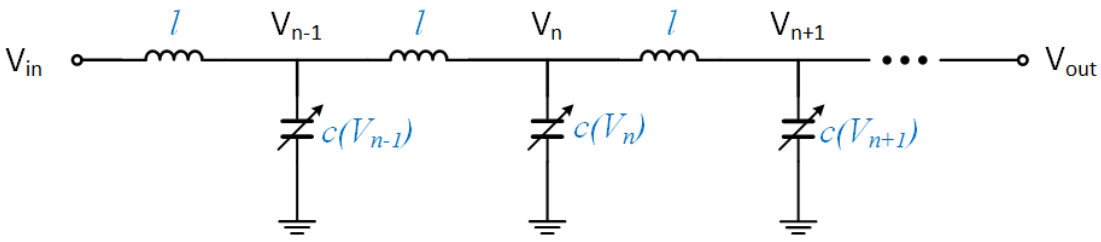

Figure 76. Structure of NLTL

Applying KVL, the relations of voltages of adjacent nodes can be shown in:

$$l\frac{d}{dt}\left[c(V_n)\frac{dV_n}{dt}\right] = V_{n+1} + V_{n-1} - 2V_n \tag{5.4}$$

The right-hand side of Equation (5.4) can be approximated with partial derivatives with respect to *x*, which is the distance from the beginning of the line. The spacing between two adjacent sections is δ, such that $x_n = n\delta$. Using Taylor expansions and ignoring the high order terms, Equation (5.4) can be derived into:

$$L\frac{\partial}{\partial t}\left[C(V)\frac{\partial V}{\partial t}\right] = \frac{\partial^2 V}{\partial x^2} + \frac{\delta^2}{12}\frac{\partial^4 V}{\partial x^4} \tag{5.5}$$

Where C and L are the capacitance and inductance per unit length, respectively.

If the capacitance of the varactor, C(V), is in the form of:

$$C(V) = C_0(1 - bV) \tag{5.6}$$

Where C_0 and b are constants. Then, Equation (5.5) becomes:

$$\frac{\partial^2 V}{\partial t^2} - LC_0\frac{\partial^2 V}{\partial x^2} = \frac{\partial^2}{12}\frac{1}{LC_0}\frac{\partial^4 V}{\partial x^4} + \frac{b}{2}\frac{\partial^2 (V^2)}{\partial t^4} \tag{5.7}$$

The solution to the above wave equation is as follows:

$$V(x,t) = \frac{3(v^2 - {v_0}^2)}{bv^2}\operatorname{sech}^2\left[\frac{\sqrt{3(v^2 - {v_0}^2)}}{v_0}\cdot\frac{x - vt}{\delta}\right] \tag{5.8}$$

Where *v* is the propagation velocity of the pulse and $v_0 = 1/\sqrt{LC_0}$.

Figure 77 **Error! Reference source not found.**plots three pulses for different L and C values. For pulse (a), L = 1 nH and C = 1 nF; for pulse (b), L = 2 nH and C = 2 nF; For pulse (c), L = 4 nH and C = 4 nF.

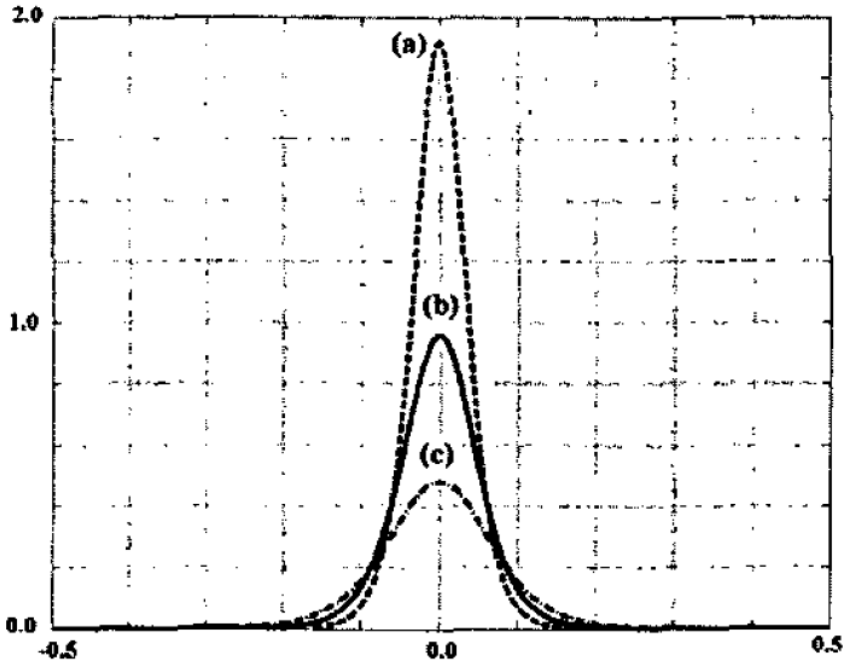

Figure 77. Three normalized pulses for different L and C values

This solution of V(x,t) is a function a propagation velocity, location of the pulse on the transmission line, and time, and is not a function of the input waveform.

If *v* is express in the form:

$$v = 1/\sqrt{LC_{eff}} \tag{5.9}$$

where C_{eff} is the effective capacitance of the transmission line section where the pulse is located, the height of the pulse, V_{max}, can be expressed as:

$$V_{max} = \frac{3}{b} \cdot \frac{v^2 - {v_0}^2}{v^2} = \frac{3}{b}\left(1 - \frac{C_{eff}}{C_0}\right) \tag{5.10}$$

Substitute Equation (5.6) into Equation (5.10), it can be shown that the effective voltage, V_{eff}, associated with C_{eff} is:

$$V_{eff} = \frac{V_{max}}{3} \tag{5.11}$$

This shows that the effective propagation velocity is determined by the capacitance at 1/3 of the peak voltage.

From Equations (5.8), (5.10), and (5.11), the half-height width of the pulse, *W*, is calculated to be:

$$W = \frac{\delta}{v} \cdot \frac{v_0}{\sqrt{v^2 - {v_0}^2}} \tag{5.12}$$

Equation (5.12) shows that in a weakly dispersive and non-linear transmission line, the effect of non-linearity counteracts the effect of dispersion. For an arbitrary pulse, the NLTL makes the pulse sharper and taller as it travels along it. The resulting sharper and taller pulse is called a **soliton** pulse. This effect of NLTL is depicted in Figure 78.

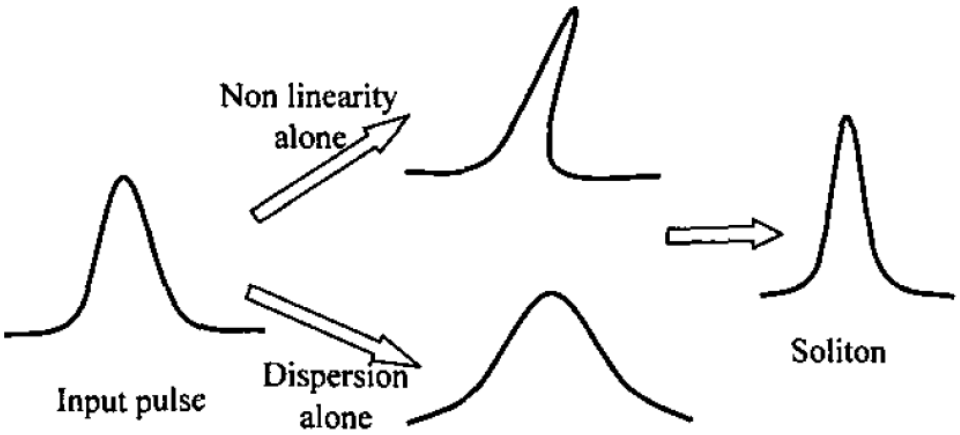

Figure 78. Soliton on a NLTL

5.4 LO-Reshaping

The NLTL can also be applied to mixers to re-shape the LO signal [58].

In the ideal situation, the LO should be square wave, and LO and $\overline{LO}$ should not overlap with each other, as shown in Figure 79. As a result, the switching transistors (M_1 and M_2) turn on and off instantly. When M_1 is turned on fully, M_2 is completely turned off, and vice versa.

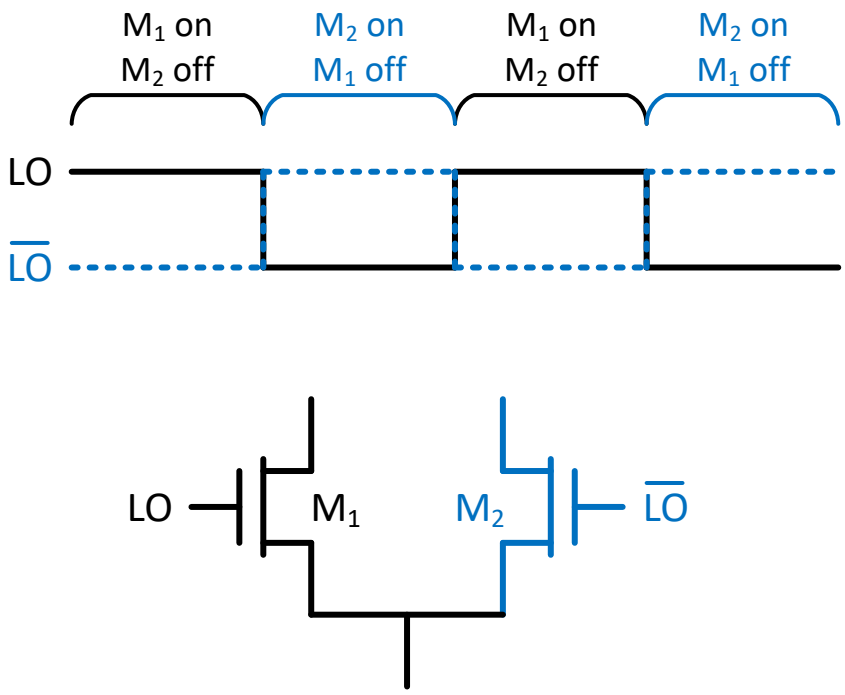

Figure 79. Ideal LO waveform

However, in mm-Wave frequencies, square wave is not practical. Instead, the LO is sinusoidal. As shown in Figure 80, the sinusoidal LO waveform leads to the short time period in which both M_1 and M_2 are turned on. For MOS transistors, the transition between on and off is not abrupt. They are not fully off just below the threshold voltage (V_{th}) or fully on just above V_{th}. When V_{GS} is slightly below or slightly above V_{th}, the transistors are in the stage between fully on

and fully off. In this stage, the drain current is small, and g_m is small. And the small current leads to noise. For the mixer shown in Figure 80, the final output is the difference between the IF+ terminal and the IF- terminal. If both transistors are turned on, there will be output in both IF+ and IF- terminals, thus the final output is degraded.

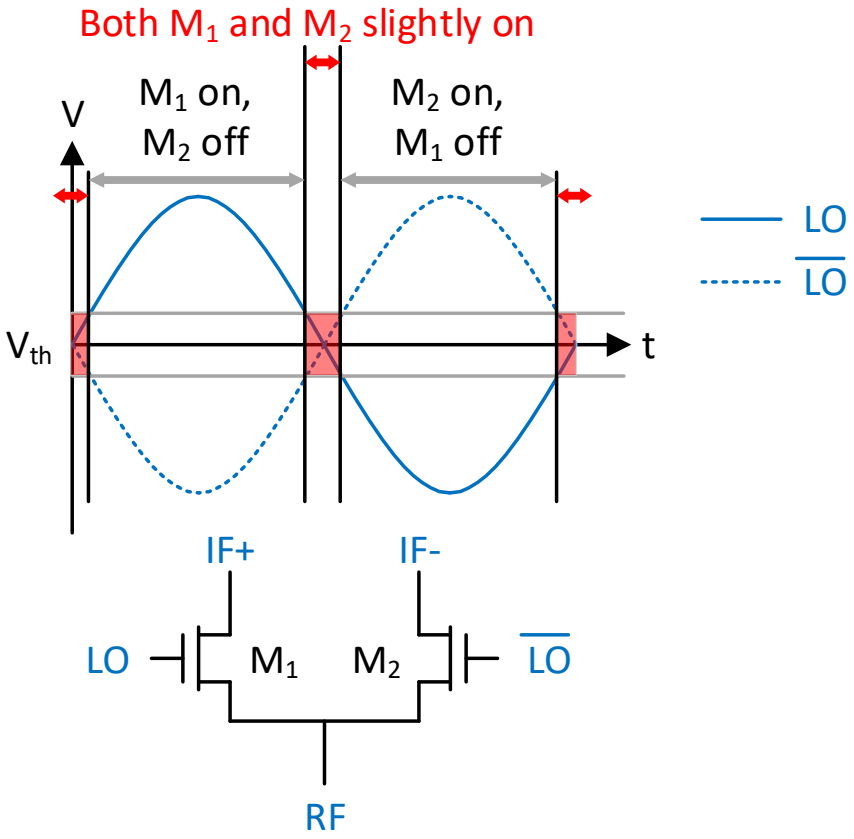

Figure 80. Sinusoidal LO waveform

The situation is even worse for passive I-Q mixers. As shown in Figure 81 (a), the ideal LO waveform should be square wave with 25% duty-cycle [54], thus LO_I, $\overline{LO_I}$, LO_Q, and $\overline{LO_Q}$ do not overlap with each other. Each switching transistor should turn on one at a time. From Figure 81

(b), if the LO waveform is sinusoidal, when one transistor in the I (or Q) channel turns on, the other two transistors in the Q (or I) channel turn on slightly. In principle, when the I channel turns on, the Q channel should be completely turned off, and vice versa. When both I and Q channels are turned on, the gain of the mixer will degrade, and the NF of the mixer will increase. To avoid this situation, the duty-cycle of the LO waveform should be 25% instead of the conventional 50%, which is the duty-cycle of sinusoidal waveform.

From [55], the mixer conversion loss for different duty-cycle can be derived through the Fourier series expansion of the LO waveform. A passive mixer can be illustrated as an idealized circuit consisting of a switch in series with the RF signal. The switch opens and closes at the LO rate of F(t). The RF signal can be written in the form of:

$$v_{RF}(t) = \sin(\omega_{RF} t) \tag{5.13}$$

A value of 0 or 1 can be assigned to F(t) to represent the action of the switch, with 0 representing the switch is turned off and 1 representing the switch is turned on. The output of the mixer is the convolution of the input signal (which is the RF signal) with the Fourier series of the LO waveform.

For a differential LO waveform with 50% duty-cycle, the Fourier series representation is as follows:

$$F_{50\%}(t) = \frac{4}{\pi}\left[\cos(\omega_{LO} t) - \frac{1}{3}\cos(3\omega_{LO} t) + \frac{1}{5}\cos(5\omega_{LO} t) - \cdots\right] \tag{5.14}$$

For an LO waveform with 50% duty-cycle, the Fourier series representation is as follows:

$$F_{25\%}(t) = \frac{2\sqrt{2}}{\pi}\left[\cos(\omega_{LO} t) + \frac{1}{3}\cos(3\omega_{LO} t) - \frac{1}{5}\cos(5\omega_{LO} t) + \cdots\right] \tag{5.15}$$

The current of the RF signal can be written as:

$$i_{RF}(t) = G_M v_{RF} \sin(\omega_{RF} t) \tag{5.16}$$

When multiplying either Equation (5.14) or (5.15) with Equation (5.16), the output current $i_{RF}(t)$ at the frequency of $(f_{RF} - f_{LO})$ can be represented as follows:

$$i_{IF}(t) = \left[\frac{2}{\pi}\sin(\pi t)\right]\frac{1}{2d} G_M v_{RF} \sin(\omega_{IF} t) \tag{5.17}$$

Where *d* is the duty-cycle of the LO waveform.

The voltage conversion gain, *G*, of this mixer is

$$G = v_{IF}/v_{RF} \tag{5.18}$$

The difference of *G* between a mixer driven with 25% duty-cycle to that of 50% duty-cycle, *ΔG*, is calculated as follows:

$$\begin{aligned} \Delta G &= 20log\left[\frac{2\sqrt{2}}{\pi} G_M v_{RF} \sin(\omega_{IF} t)\right] - 20log\left[\frac{2}{\pi} G_M v_{RF} \sin(\omega_{IF} t)\right] \\ &= 3.0\ dB \end{aligned} \tag{5.19}$$

This shows that when the duty-cycle of the LO waveform is reduced from 50% to 25%, the voltage conversion gain of this mixer is improved by 3 dB.

Since the mixer is passive, the voltage conversion gain is usually negative, which means that it is indeed the voltage conversion "loss". In this situation, the NF (in dB) equals to the loss (in dB). For example, if the gain is -5 dB, that means the loss is 5 dB and NF is 5 dB. Thus, the improvement of 3 dB of the voltage conversion "loss" of the passive mixer also means that the NF of this mixer is improved by 3 dB.

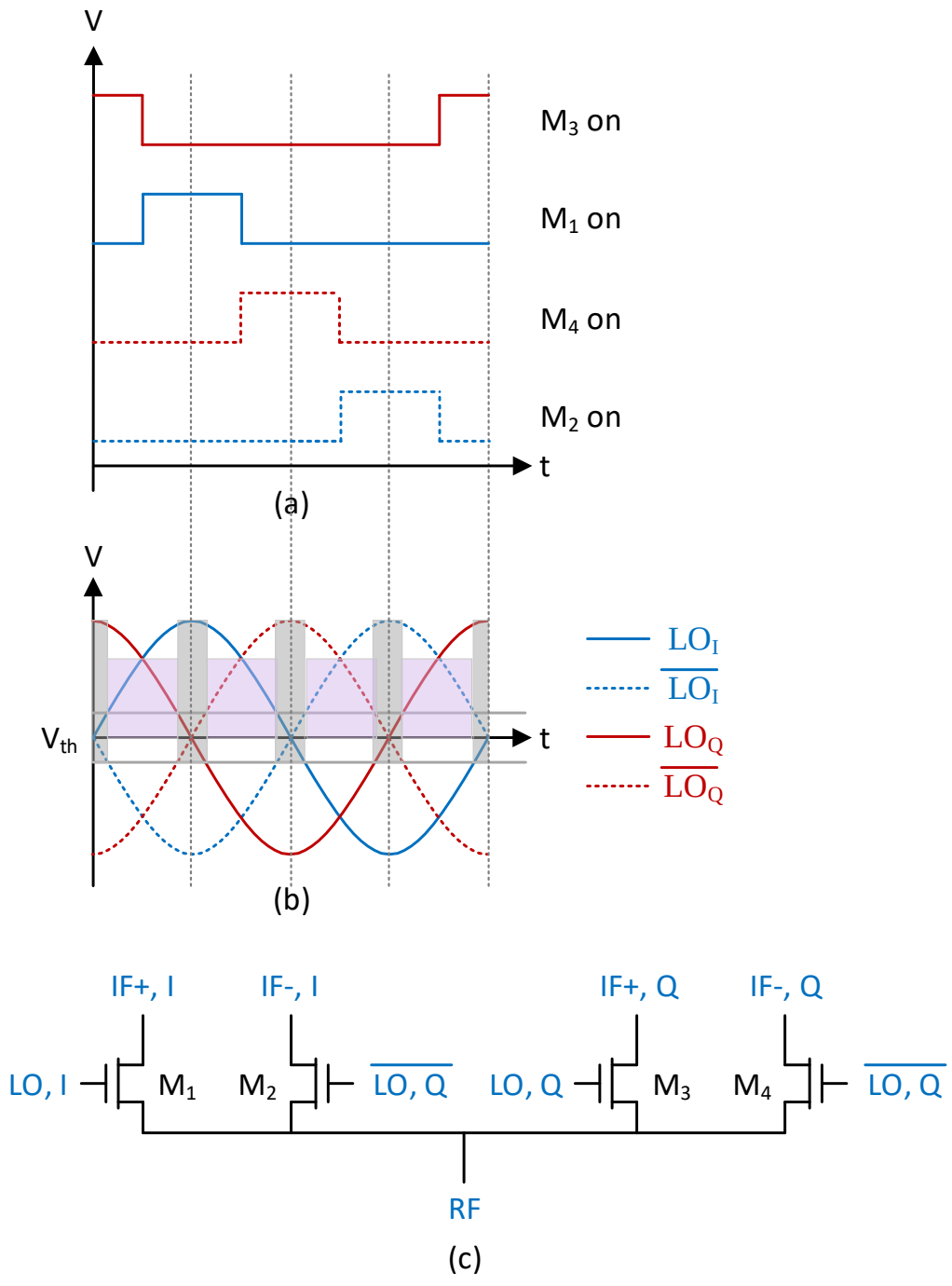

Figure 81. LO waveform in I-Q mixers

Thus, when designing passive mixers, to achieve better conversion gain and better NF, the LO waveform should have duty-cycle of as close to 25% as possible, instead of the sinusoidal waveform with duty-cycle of 50%.

In addition, the LO waveform with duty-cycle of 25% can reduce the effect on the mixer noise caused by 1/f noise. For passive mixers, although the output current has a mean value of zero, the output current is still time-varying, which causes the 1/f noise to appear around zero frequency and harmonics of excitation [56].

In a single mixer, when both transistors are turned on, the input impedance is different from the situation where only one transistor is turned on. This decrease of input impedance causes the total noise referred to the output of the baseband amplifier (which is the stage after the mixer) to increase. Also, in this situation, there is no mixing activity because of both sides of the mixer is turned on. As a result, the signal is shorted between the input and output of the mixer. This degrades the signal-to-noise ratio at the output, leading to larger contribution of 1/f noise to the total noise.

These effects also apply to I-Q mixers. When both I and Q channels are turned on, the output noise of the mixers are increased.

Furthermore, the linearity of the mixer is also improved with a LO waveform of 25% duty-cycle.

5.5 Mixer Design with Non-Linear Transmission Line

A 60-GHz down-conversion mixer has been designed in TSMC 65nm bulk CMOS to verify the proposed mixer concept. As shown in Figure 82, the RF signal is fed into a single-balanced

switching pair comprising NMOS transistors M_1 and M_2, sized at 0.9 μm / 0.06 μm for low power operation.

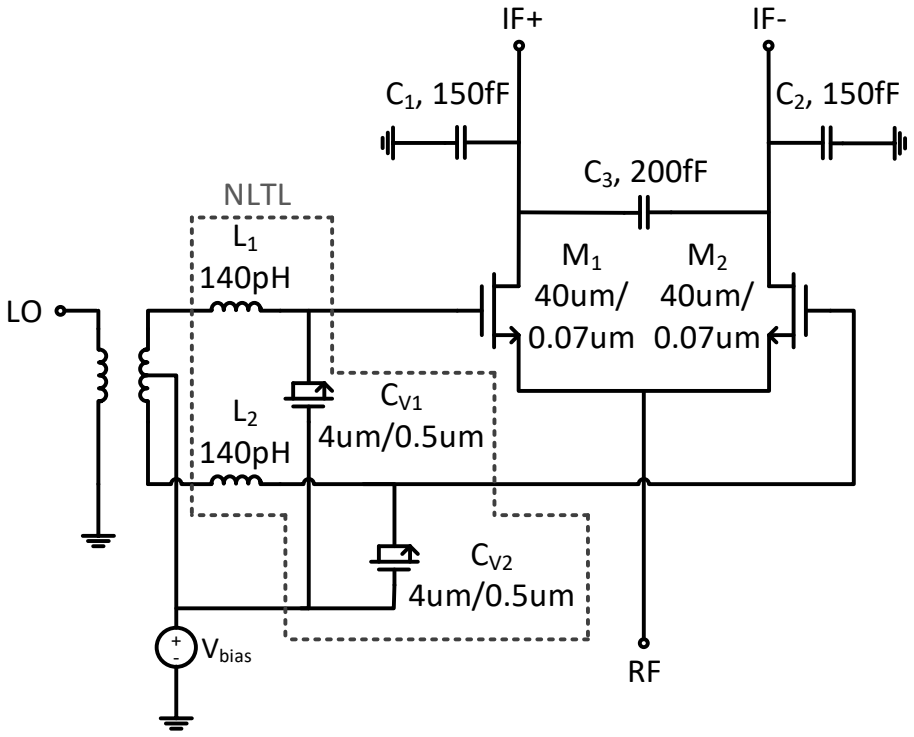

Figure 82. Mixer with NLTL

The LO signal is fed into a differential non-linear transmission line consisting of on-chip inductors L_1 and L_2 along with varactors C_{V1} and C_{V2}. Each varactor is of the reverse biased accumulation mode. It is constructed by tying an NMOS device's source and drain together to form one node, and its gate forms the other node. Its capacitance is inversely proportional to the voltage difference across it.

Figure 83 is the simulated capacitance of the varactor, where V_{bias} is 0.5V.

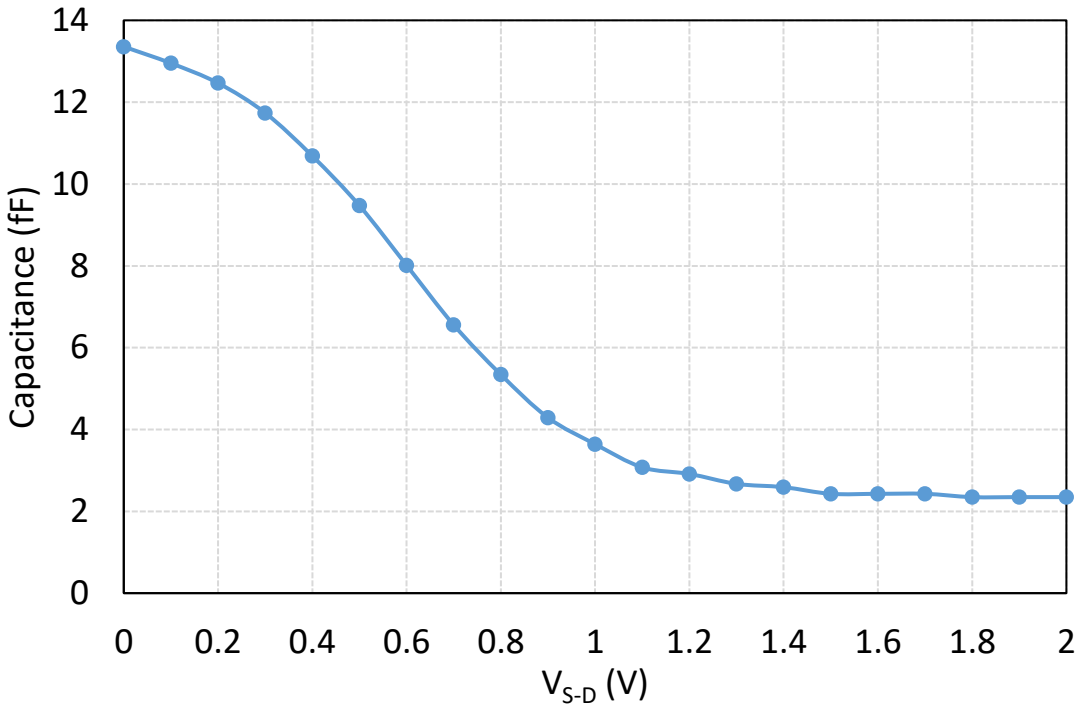

Figure 83. Simulated capacitance of the varactor

Through this NLTL structure, the LO signal is re-shaped to have sharper edges, narrower pulses, and a higher amplitude compared to the sinusoidal signal at the input of the NLTL, which further improves the mixer's conversion gain, port isolation, linearity, and noise performance.

The single-balanced structure has limited suppression on the second order harmonic (HD_2) of the LO leakage at the RF port. Therefore, a shunt LC notch filter is used to short the HD_2 of the LO leakage at the RF port to the ground. The output IF signal is loaded with a sampling capacitor C_3 of 200 fF. C_1 and C_2 represent the gate and parasitic capacitance of the following stage with a total capacitance of 300 fF. In the simulation, both the RF and the LO signals come from 50-Ω ports and the differential LO signal is generated through an ideal balun.

This topology allows simultaneous optimization of the gain and linearity for the mixer in such a way that the mixing devices operate at high-gain mode with low loss while the nonlinearity of the mixing devices is canceled by the nonlinear amplification resulting in a highly linear output. When the LO swing is made high by the NLTL, the varactor's capacitance is reduced, increasing the gate voltage furthermore to allow sufficient gain for high input, thus compensating the mixer's nonlinearity. Because of the gain and nonlinearity separation, this mixer topology does not require the RF-to-IF-ratio to be small [59]. Therefore, it can be used in the direct conversion system.

To see the improvement of adding the NLTL structure to the mixer, a conventional mixer without this NLTL structure is also designed. As shown in Figure 84, the conventional mixer has the same loading capacitance and the same size of transistors.

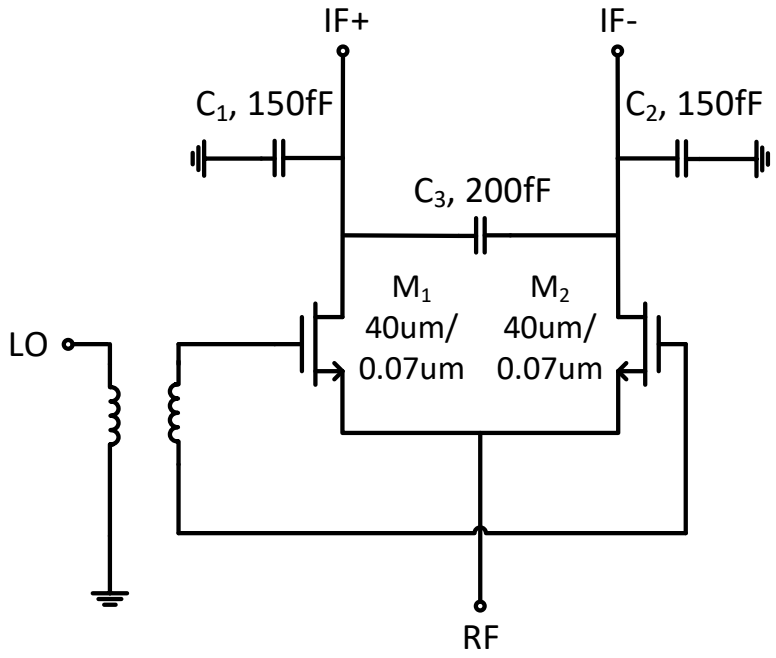

Figure 84. Conventional mixer

5.6 Performance Improvement

Figure 85 shows the transient simulation results of the NLTL-boosted 60 GHz LO signal (red). The LO input signal (blue) is a single-tone sinusoidal wave with an amplitude of 250 mV. The NLTL boosts it to a narrower pulse with a swing of around 470 mV, corresponding to a 5.5 dB voltage boosting gain.

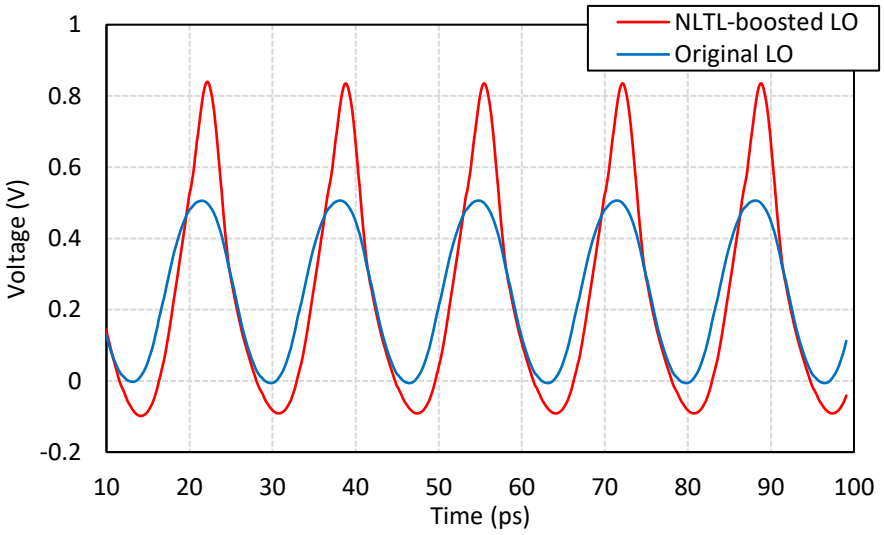

Figure 85. LO waveform before and after NLTL structure

Figure 86 and Figure 87 show the time-domain and the frequency-domain response of a 60 GHz mixer, respectively. The RF input signal is at 59 GHz and the LO signal is at 60 GHz. With the input signal's amplitude of -31.5 dB_V, the 1 GHz output IF signal's amplitude is -27.2 dB_V, representing a 4-dB conversion voltage gain from the passive mixer. Compared to the 1.48-dB gain from the regular non-return-to-zero sampling mixers in the ideal case, this 4-dB gain clearly shows the gain advantage provided by the mixer.

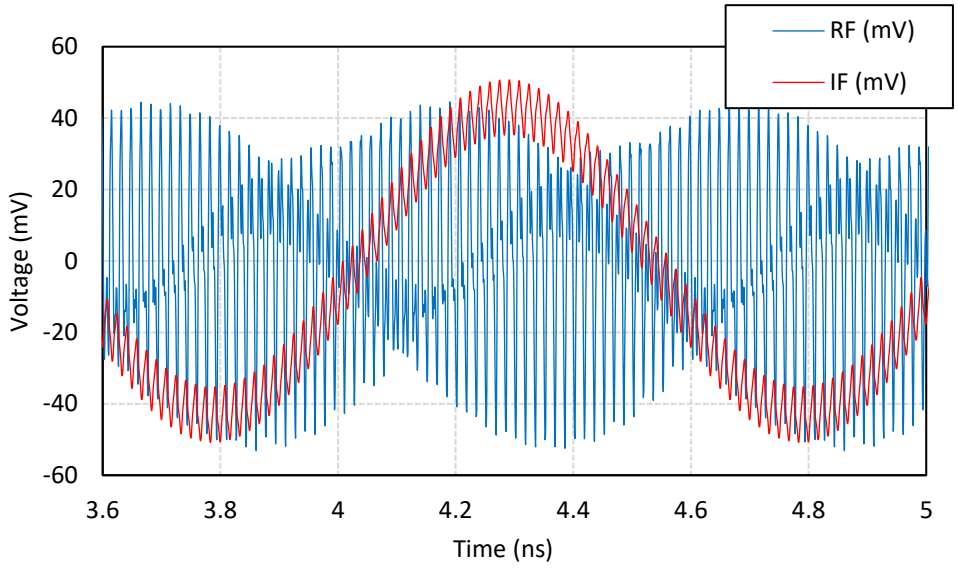

Figure 86. RF and IF waveform in time-domain

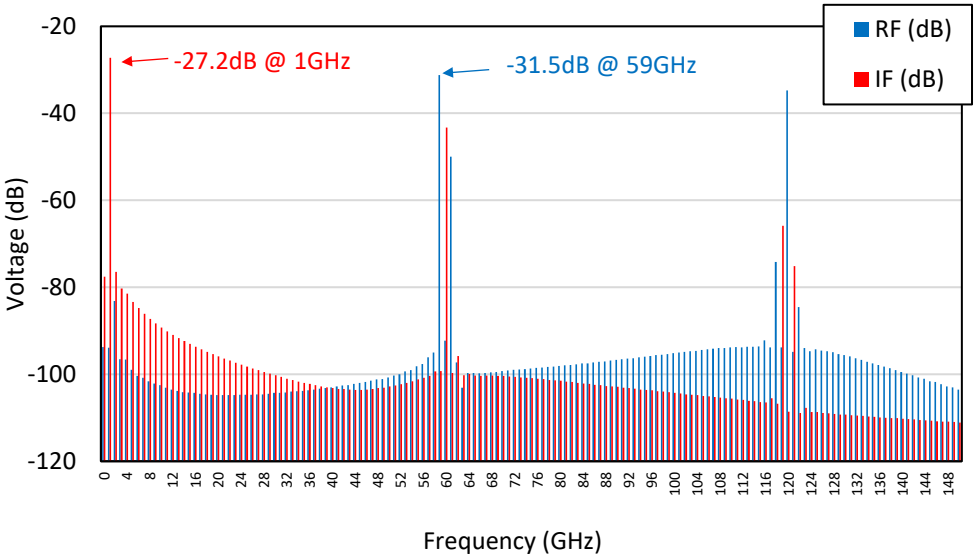

Figure 87. RF and IF specta

The conversion gain of the mixers is simulated for different RF power levels. The LO power is 0 dBm and the RF power varies from -30 dBm to 5 dBm. Figure 88 plots the simulated voltage conversion gain. The proposed passive mixer with NLTL boosts the voltage conversion gain by 2.2 dB, from -1 dB to 1.2 dB. The linearity is also improved. The IP_{1dB} is improved by 3 dB, from -3 dBm to 0 dBm.

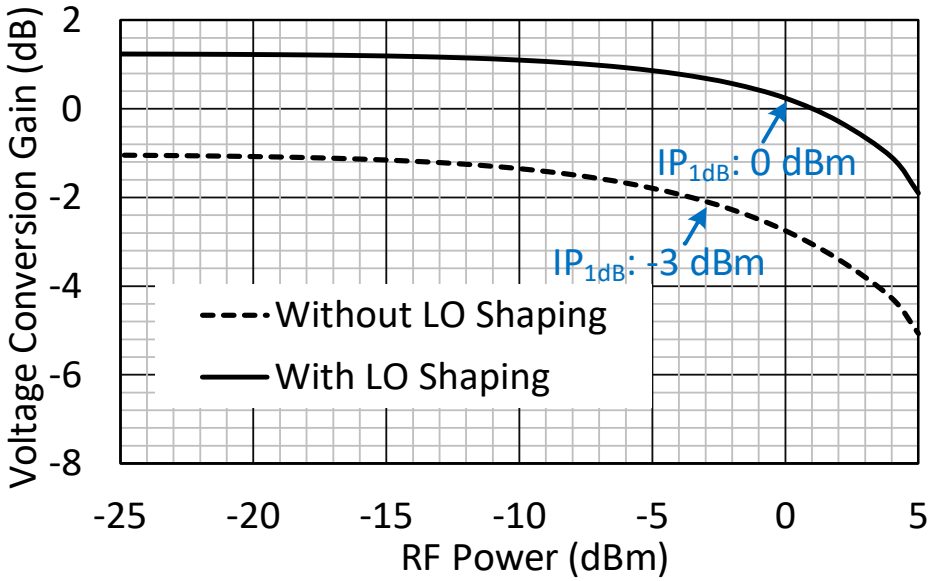

Figure 88. Voltage conversion gain comparison

Figure 89 plots the SSB NF versus frequency of the mixers with and without the NLTL structure. As can be seen, the NF is improved by around 1.2 dB, from 6.7 dB to 5.5 dB. This improvement is due to the narrower pulses of the LO waveform. The NF is flat before it starts increasing significantly at around 7 GHz. This wide bandwidth feature of the mixers is highly desirable in mm-Wave communications systems. At 1 GHz IF output frequency, the SSB NF is 5.5 dB with an LO power of 0 dBm.

Table 9 summarizes the performance comparison between the conventional mixer and the mixer with NLTL structure.

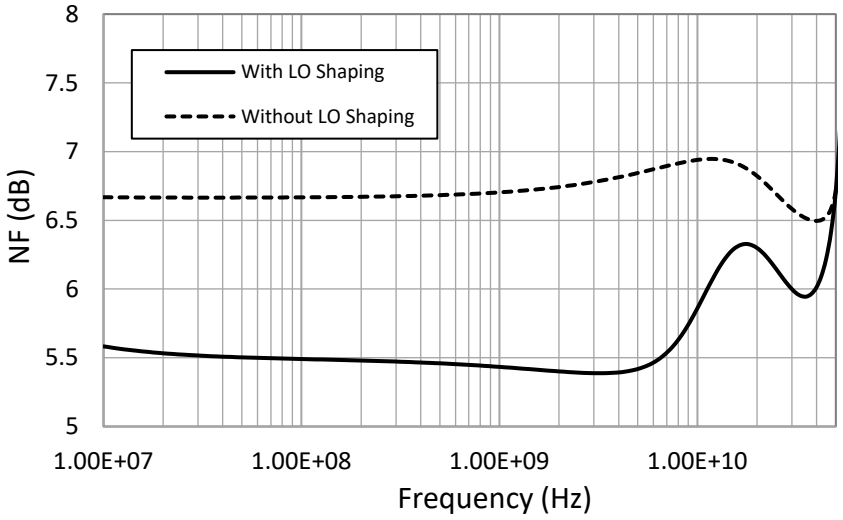

Figure 89. Noise figure comparison

Table 9. Performance Comparison between Two Mixers

	Conventional mixer	Mixer with NLTL	Improvement
NF (dB)	6.7	5.5	1.2 dB
Voltage conversion gain (dB)	-1	1.2	2.2 dB
IP_{1dB} (dBm)	-3	0	3 dB

CHAPTER 6: CONCLUSIONS AND FUTURE WORK

6.1 Conclusions

In this work, the following areas were explored and designed:

i. The landscape of wireless communication systems is studied. With ever increasing wireless communication data rate, conventional existing systems and standards facing ever increasing challenges due to the crowed spectrum.

ii. In particular, CMOS wireless communication systems in mm-Wave frequencies are studied. Exploring mm-Wave communications systems and sensing technologies draw substantial interests in both academia and industries because of its huge bandwidth. With high integration level capability and cost effectiveness, CMOS technologies have gained interests. Currently, OFDM is the most widely used scheme to transmit data. The high PAPR of OFDM signals requires the PA in the transmitter to have high linearity, and the trend in modern wireless designs of battery-operated devices requires the PA to have high PAE.

iii. Previous researches on improving the performance of PAE and linearity have been studied. A dilemma of improving both linearity and PAE is discovered. Doherty amplifiers improve PAE by turning on an additional PA when the input power level is high but suffer from poor IIP_3 performance. Outphasing PAs, on the other hand, enhance PAE by decomposing signal into two constant envelopes. But it is difficult to control the phase modulation precisely in mm-Wave frequencies. Envelope tracking improves the PAE by adjusting the supply voltage to closely track the amplitude of the signal's envelope. However, due to the long feedback loop and PA memory effect,

envelope tracking methods are limited in narrow bandwidth applications. Linearity can also be improved by adjusting the threshold voltage of the transistor.

iv. The application of parametric amplification using non-linear varactors onto mm-Wave PA designs is proposed. Its application to the PA design addresses the issue of improving both linearity and PAE at the same time. In parametric amplification, a pump waveform, which is twice the frequency of the signal waveform, is applied to the signal waveform to amplify it. The phases of the two waveforms must be aligned such that when the signal is rising, the pump also rises, and when the signal is falling, the pump also falls. To address the difficulty of generating the 2x-frequency pump signal, the design proposes a new method to utilize the nonlinearity of the differential PA itself. The second-harmonic tone the virtual ground is first boosted by a high impedance filter circuit, and then aligned in phase with the PA fundament signal through an LC phase shifter. In addition, the varactors at the output of the PA are introduced to compensate the non-linearity of the output capacitance of the PA.

v. A reference conventional PA and a parametric PA, both around 60 GHz, are designed and compared. The 2x-frequency pump waveform is generated at the virtual ground node of the PA itself, eliminating the need of an external pump signal. The reference PA achieves a peak PAE of 28%, and the linear PAE of 10% at an IMD_3 level of -33 dBc at 62 GHz, respectively, which are among the best of the same type PAs. For the parametric PA, the PAE at -6 dB back-off is increased from 8.8% to 15.4% (improved by 75%), the PAE at -8 dB is increased from 6.1% to 11.2% (improved by 84%), and the peak PAE is improved to 32%.

vi. The design requirements of mixers are studied. In order to improve the conversion gain and linearity, and reduce noise figure, it is crucial for mixers not to let both sides of transistors (or both I and Q channels of I-Q mixers) to turn on at the same time. Generating an LO waveform of 25% duty-cycle is previously introduced for I-Q mixers. However, this 25% duty-cycle LO signal generation is not practical at mm-Wave range.

vii. The application of the non-linear transmission line (NLTL) to address the LO overlap issue in mm-Wave mixers is proposed. The NLTL utilizes the non-linear varactor to re-shape the pulses to be taller and narrower. A conventional single-balanced passive mixer and a mixer with NLTL structure, both at 60 GHz, are designed and compared. The noise figure (NF), linearity, and conversion gain are improved. At 1 GHz IF output frequency, with 0 dBm LO power, the single-side-band NF is improved from 6.7 dB to 5.5 dB. The input P_{1dB} is improved from -3 dBm to 0 dBm. The voltage conversion gain is improved from -1 dB (which is loss instead of gain) to 1.2 dB.

6.2 Future work

After exploring the non-linear varactors used in parametric amplification for PA designs and used in non-linear transmission lines for mixer designs, other applications can be considered. The voltage-controlled oscillators (VCO) can be studied to see if the parametric amplification is applicable. Figure 90 shows a possible application of parametric amplification on a typical cross-coupled VCO.

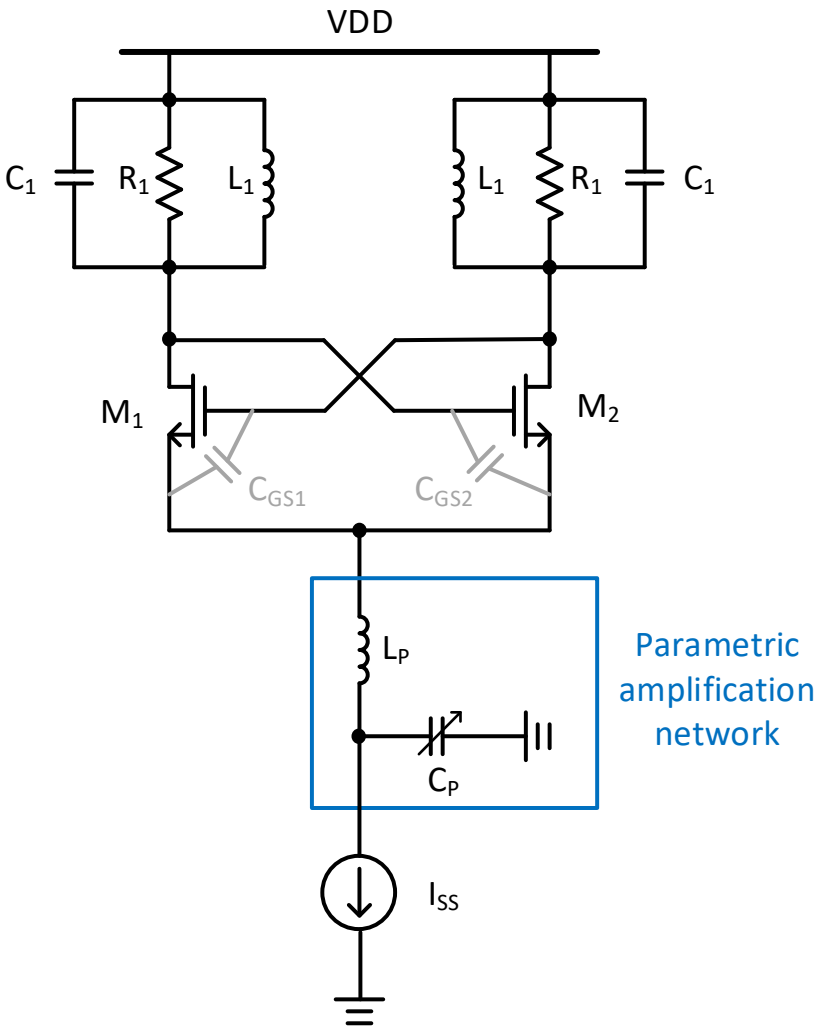

Figure 90. Possible implementation of parametric amplification on VCO

In transceiver designs, the VCO provides the LO signal to mixers, as shown in Figure 5. In many applications that require power consumption to be low, the supply voltage of the VCO is usually low. This may lead to that the output swing of the VCO is small too. These applications include many battery-powered hand-held devices, such as cellphones.

By applying parametric amplification, the output swing may be improved. The cross-couple structure of VCO is the most commonly used structure in mm-Wave VCO designs. It has a differential structure, and, similar to the differential PA, the second harmonic tone at the virtual ground node can be utilized as the pump waveform. As shown in Figure 90, L_P and C_P tunes the second harmonic tone, which combines with the gate-source capacitance (C_{GS}) of M_1 and M_2 to boost the output swing.

BIBLIOGRAPHY

[1] H. F. Arrano and C. A. Azurdia-Meza, "OFDM: today and in the future of next generation wireless communications," 2016 IEEE Central America and Panama Student Conference (CONESCAPAN), Guatemala City, 2016

[2] A. M. Niknejad and H. Hashemi, *mm-Wave Silicon Technology 60 GHz and Beyond*, 1st ed, Chapter 1, Section 1.3 “The Birth of Silicon mm-Wave”

[3] P. M. O’Neill, “CMOS Technology & Business Trends”, http://ewh.ieee.org/r5/denver/sscs/Presentations/2002_12_ONeill.pdf

[4] A. M. Niknejad, D. Chowdhury, and J. Chen, "Design of CMOS Power Amplifiers," IEEE Transactions on Microwave Theory and Techniques, vol. 60, no. 6, pp. 1784-1796, June 2012.

[5] B. Razavi, *Design of Microelectronic RF Circuit*, 2nd ed, Chapter 3, Section 3.3 “Digital Modulations”

[6] W. H. Doherty, “A new high efficiency power amplifier for modulated waves”, Proc. IRE 1936

[7] M. Yahyavi, *On the Design of High-Efficiency RF Doherty Power Amplifiers*, PhD thesis, Technical University of Catalonia

[8] D. Zhao, S. Kulkarni, and P. Reynaert, “A 60-GHz Outphasing Transmitter in 40-nm CMOS”, Journal of Solid-State Circuits, 2012

[9] B. Razavi, *RF Microelectronics*, 2nd ed, Chapter 12, Section 12.2 “Classification of power

amplifiers”

[10] A. Larie, E. Kerhervé, B. Martineau, L. Vogt, and D. Belot, “A 60GHz 28nm UTBB FD-SOI CMOS Reconfigurable Power Amplifier with 21% PAE, 18.2dBm P1dB and 74mW PDC”, IEEE International Solid-State Circuits Conference Digest of Technical Papers, 2015

[11] Southeastern Universities Research Association

[12] R. W. Heath Jr., lecture slides, “Vehicular Millimeter Wave Communications: Opportunities and Challenges”, University of Texas, Austin

[13] L. Frenzel, “Millimeter Waves Will Expand The Wireless Future” http://www.electronicdesign.com/communications/mm-Waves-will-expand-wireless-future

[14] Everything RF, “What is the Impact of the Atmosphere on RF Signal Propagation?” https://www.everythingrf.com/community/what-is-the-impact-of-the-earths-atmosphere-on-rf-signal-propagation, Aug. 17, 2017

[15] Office of Wireless Telecommunications, Federal Communications Commission, “Millimeter Wave 70/80/90 GHz Service”, March 24th, 2017, https://www.fcc.gov/wireless/bureau-divisions/broadband-division/mm-Wave-708090-ghz-service

[16] André Bourdoux, “Project: IEEE P802.15 Working Group for Wireless Specialty Networks (WSNs)”, IEEE Mentor program, May 7, 2018

[17] A. Grebennikov, RF and Microwave Power Amplifier Design, Boston: McGraw-Hill, 2005

[18] “LTE System Specifications and Their Impact on RF & Base Band Circuits”

[19] F. M. Ghannouchi and A. Ghazel, "AM-AM and AM-PM distortion characterization of satellite transponders/base station transmitters using spectrum measurements," *International Conference on Recent Advances in Space Technologies*, 2003. RAST '03. Proceedings of, Istanbul, Turkey, 2003, pp. 141-144

[20] H. L. Krauss, C. W. Bostian, and F. H. Raab, *Solid State Radio Engineering*. New York: Wiley, 1980

[21] S.A. Zainol Murad et. Al., "A 2.4-GHz 0.18-µm CMOS Class E single-ended switching power amplifier with a self-biased cascode", *International Journal of Electronics and Communications*, Volume 64, Issue 9, September 2010, Pages 813-818

[22] T. Mury and V. F. Fusco, "Sensitivity Characteristics of Inverse Class-E Power Amplifier," in *IEEE Transactions on Circuits and Systems I: Regular Papers*, vol. 54, no. 4, pp. 768-778, April 2007

[23] R. A. Beltran, "Class-F and inverse class-F power amplifier loading networks design based upon transmission zeros," 2014 *IEEE MTT-S International Microwave Symposium (IMS2014)*, Tampa, FL, 2014, pp. 1-4

[24] Young Yun Woo, Youngoo Yang and Bumman Kim, "Analysis and experiments for high-efficiency class-F and inverse class-F power amplifiers," in *IEEE Transactions on Microwave Theory and Techniques*, vol. 54, no. 5, pp. 1969-1974, May 2006

[25] Keysight Technologies, Inc., "Concepts of Orthogonal Frequency Division Multiplexing (OFDM) and 802.11 WLAN", http://rfmw.em.keysight.com/wireless/helpfiles/89600b/webhelp/subsystems/wlan-ofdm/content/ofdm_basicprinciplesoverview.htm

[26] David Tse and Pramod Viswanath, *Fundamentals of Wireless Communication*,

Chapter 3: “Point-to-point communication: detection, diversity and channel uncertainty”, Cambridge University Press; 1 edition, July 11, 2005

[27] Ramjee Prasad, *OFDM for Wireless Communications Systems*, Chapter 5: “Basics of OFDM and Synchronization”, Artech House, August 31, 2004

[28] B. Park, Daechul Jeong, J. Kim, Y. Cho, Kyunghoon Moon and B. Kim, "Highly linear CMOS power amplifier for mm-wave applications," *IEEE MTT-S International Microwave Symposium (IMS)*, San Francisco, CA, 2016

[29] E. Kerherve, D. Belot, *Linearization and Efficiency Enhancement Techniques for Silicon Power Amplifiers*, Academic Press, 2015

[30] F. Giannini, P. Colantonio and R. Giofré, “The Doherty Amplifier: Past, present & future”, 2015 *Integrated Nonlinear Microwave and Millimetre-wave Circuits Workshop* (INMMiC), Taormina, 2015, pp. 1-6

[31] Mike Roberts, “Understanding the 3 Level Doherty Power Amplifier”, white paper

[32] M. Kwak et al., "High efficiency wideband envelope tracking power amplifier with direct current sensing for LTE applications," *2012 IEEE Topical Conference on Power Amplifiers for Wireless and Radio Applications*, Santa Clara, CA, 2012, pp. 41-44

[33] J. Buckwalter, “Outphasing PA”, Lecture Slides, University of California, Berkeley, https://www.ece.ucsb.edu/Faculty/rodwell/Classes/ece218c/notes/Lecture12_OutphasingPowerAmplifiers.pdf

[34] B. Razavi, *Design of Analog CMOS Integrated Circuits*, Chapter 2, Section 2.3, “Second-Order Effects”, McGraw-Hill: 2003

[35] D. Zhao and P. Reynaert, “A 60-GHz Dual-Mode Class AB Power Amplifier in 40-

nm CMOS", Journal of Solid-State Circuits, 2013

[36] Y. Yamamoto, Fundamentals of Noise Processes, Chapter 11, "Parametric amplifiers and oscillators".

[37] FCC Rules for 60 GHz operation: CFR 47 Part 15.255

[38] R. Wu et al., "64-QAM 60-GHz CMOS Transceivers for IEEE 802.11ad/ay," *IEEE Journal of Solid-State Circuits*, vol. 52, no. 11, pp. 2871-2891, Nov. 2017

[39] H. Kuo, H. Wang, P. Wang, H. Chuang, and F. Lin, "60-GHz millimeter-wave life detection system with clutter canceller for remote human vital-signal sensing," IEEE MTT-S International Microwave Workshop Series on Millimeter Wave Integration Technologies, Sitges, 2011

[40] R. Wu, Q. Bu, W. Deng, K. Okada and A. Matsuzawa, "A 0.015-mm2 60-GHz reconfigurable wake-up receiver by reusing multi-stage LNAs," IEEE Asian Solid-State Circuits Conference (A-SSCC), KaoHsiung, 2014

[41] T. Wada, M. Ikebe and E. Sano, "60-GHz, 9-µW wake-up receiver for short-range wireless communications," Proceedings of the European Solid-State Circuit Conference (ESSCIRC), Bucharest, 2013

[42] S. Yoshida, K. Maruyama, D. Matsushita and K. Nishikawa, "UHF-band meander line antenna and 60-GHz-band patch antenna with single feed structure for 5G terminal application," International Symposium on Antennas and Propagation (ISAP), Okinawa, 2016, pp. 1044-1045

[43] Y. Li and K. Luk, "A 60-GHz Dense Dielectric Patch Antenna Array," IEEE Transactions on Antennas and Propagation, vol. 62, no. 2, pp. 960-963, Feb. 2014

[44] H. Vettikalladi, O. Lafond and M. Himdi, "High-Efficient and High-Gain

Superstrate Antenna for 60-GHz Indoor Communication," IEEE Antennas and Wireless Propagation Letters, vol. 8, pp. 1422-1425, 2009

[45] Jeong-Geun Kim, Hyung Suk Lee, Ho-Seon Lee, Jun-Bo Yoon and S. Hong, "60-GHz CPW-fed post-supported patch antenna using micromachining technology," IEEE Microwave and Wireless Components Letters, vol. 15, no. 10

[46] Jichao Zhan, Jincai Wen, Lingling Sun and Xiongjun Shu, "Design of 60 GHz mm-wave patch antenna arrays," 2015 IEEE 16th International Conference on Communication Technology (ICCT), Hangzhou, 2015, pp. 262-265

[47] CertifyTech, "Impedance Matching" http://certifytech.tripod.com/references/electronic/electronics/impedance.html

[48] A. Larie, E. Kerhervé, B. Martineau, L. Vogt and D. Belot, "A 60GHz 28nm UTBB FD-SOI CMOS reconfigurable power amplifier with 21% PAE, 18.2dBm P1dBand 74mW PDC," IEEE International Solid-State Circuits Conference (ISSCC), 2015

[49] J. Zhao, M. Bassi, A. Bevilacqua, A. Ghilioni, A. Mazzanti and F. Svelto, "A 40–67GHz power amplifier with 13dBm P_{SAT} and 16% PAE in 28 nm CMOS LP," *ESSCIRC 2014 - 40th European Solid-State Circuits Conference (ESSCIRC)*, 2014

[50] M. Babaie, R. B. Staszewski, L. Galatro and M. Spirito, "A wideband 60 GHz class-E/F2 power amplifier in 40nm CMOS," IEEE Radio Frequency Integrated Circuits Symposium (RFIC), 2015

[51] S. Kulkarni and P. Reynaert, "A Push-Pull mm-Wave power amplifier with <0.8° AM-PM distortion in 40nm CMOS," IEEE International Solid-State Circuits Conference Digest of Technical Papers (ISSCC), 2014

[52] A. L. Swindlehurst, E. Ayanoglu, P. Heydari and F. Capolino, "Millimeter-wave

massive MIMO: the next wireless revolution?", IEEE Communications Magazine, vol. 52, no. 9, pp. 56-62, September 2014.

[53] B. Razavi, *RF Microelectronics*, 2nd ed, Chapter 6 “Mixers”, Section 6.1 “General Considerations”

[54] A. Mirzaei, H. Darabi, J. C. Leete and Y. Chang, "Analysis and Optimization of Direct-Conversion Receivers With 25% Duty-Cycle Current-Driven Passive Mixers," in *IEEE Transactions on Circuits and Systems I: Regular Papers*, vol. 57, no. 9, pp. 2353-2366, Sept. 2010.

[55] D. Kaczman et al., "A Single–Chip 10-Band WCDMA/HSDPA 4-Band GSM/EDGE SAW-less CMOS Receiver with DigRF 3G Interface and +90 dBm IIP2," in *IEEE Journal of Solid-State Circuits*, vol. 44, no. 3, pp. 718-739, March 2009.

[56] W. Redman-White and D. M. W. Leenaerts, "1/f noise in passive CMOS mixers for low and zero IF integrated receivers," *Proceedings of the 27th European Solid-State Circuits Conference*, Villach, Austria, 2001, pp. 41-44.

[57] E. Afshari, A. Hajimiri, "Nonlinear transmission lines for pulse shaping in silicon," *IEEE Journal of Solid-State Circuits*, vol.40, no.3, pp.744-752, March 2005

[58] T. Xi, S. Huang, S. Guo, D. Huang, S. Chakraborty and P. Gui, "A New Passive CMOS Mixer with LO Shaping Technique for mm-Wave Applications," in *IEEE Microwave and Wireless Components Letters*, vol. 26, no. 6, pp. 455-457, June 2016.

[59] S. Magierowski, J. Bousquet, Z. Zhao, T. Zourntos, "RF CMOS Parametric Downconverters," *IEEE Transactions on Microwave Theory and Techniques*, vol.58, no.3, pp.518-528, March 2010